The Effects of Processing Conditions on Thermoplastic Prototypes Reinforced with Thermotropic Liquid Crystalline Polymers

Robert W. Gray IV

Thesis submitted to the Faculty of the Virginia Polytechnic Institute and State University in partial fulfillment of the requirements for the degree of

Master of Science
in
Chemical Engineering

Dr. Donald G. Baird, Chairman

Dr. Jan Helge Bøhn Dr. Richey M. Davis

July 30, 1997
Blacksburg, Virginia

Keywords: Polymer, Composite, TLCP, Prototype, and FDM

The Effects of Processing Conditions on Thermoplastic Prototypes Reinforced with Thermotropic Liquid Crystalline Polymers

Robert W. Gray IV

This work is concerned with preliminary studies on developing thermoplastic composite materials suitable for use in fused deposition modeling (FDM). Polypropylene (PP) strands reinforced with continuous thermotropic liquid crystalline polymer (TLCP) fibrils were generated in a novel dual extruder process. Strands were then re-extruded to form short fiber composite monofilaments that were used as feed stock in the FDM 1600 rapid prototyping system. Prototypes containing 40 wt% Vectra A were shown to have tensile properties twice those of parts built using acrylonitrile butadiene styrene copolymer (ABS), a commercially available material used in the FDM 1600 rapid prototyping system. It was also shown that the final mechanical properties of a composite prototype can be tailored to a specific application by adjusting the lay-down pattern, increasing the functionality of the prototype. In order to obtain the maximum tensile properties in these composite prototype, additional studies were performed to determine the effects of thermal and deformation histories on the mechanical properties of monofilaments that were re-extruded from long fiber TLCP reinforced strands. Strands were consolidated uniaxially at temperatures just above the melting point of the matrix in order to determine the effects of thermal history, and an approximate 20% reduction in tensile modulus relative to the modulus of the strands was observed. Monofilaments that could be used as feed stock in FDM were extruded from long fiber TLCP reinforced strands using a capillary rheometer in order to study the effects of capillary diameter, capillary L/D, and apparent shear rate on the tensile properties.

This work was supported by the Army Research Office (Grant No. DAAH04-94-G-0282), the Naval Surface Warfare Center, Dahlgren Division and Armstrong Laboratory, Brooks AFB under contract N60921-89-D-A239, Order 0059, and Stratasys, Inc.

Acknowledgments

The author wishes to thank Prof. Baird for his advice and support resulting in the completion of this work. Also, the author would like to thank the members of the research committee: Prof. Bøhn and Prof. Davis.

The author wishes to acknowledge:

- My family and fiancée, for the support and motivation to complete this degree.
- To Prof. R. E. Cohen and his graduate students who encouraged me to pursue an advanced degree.
- Prof. Wilkes for the use of the WAXS and SEM.
- Mike McLeod for operating the SEM.
- Bryan Kaushiva for operating the WAXS.
- Robert Young and Thomas Xue, who always offered assistance and advice.
- Raj Krishnaswamy who offered a wealth of knowledge.
- Wendell Brown for machining many little widgets.

Original Contributions

The author regards the following as significant original contributions in this work.

• Two processes were developed to produce pregenerated composite monofilaments with well controlled diameters for fused deposition modeling (FDM). In the first process, continuous monofilaments were extruded with short fiber thermotropic liquid crystalline polymer (TLCP) reinforcement, less than 6 mm. In the second process, monofilaments were generated with long fiber TLCP reinforcement, approximately 10 cm in length, via a piston actuated extrusion system.

• Software was developed that is able to generate the computer file necessary to control the fabrication of a plaque via fused deposition modeling where the prototype was built from a single continuous road. This allows parts to be fabricated from materials that do not cleave easily from the extrusion head upon the completion of a road.

• The feasibility of the use of TLCP and TLCP composites was shown in fused deposition modeling. Prototypes made from these materials were shown to have tensile properties far superior to those of the commercial FDM materials, and it was shown that there is potential for improved properties of TLCP and TLCP composite prototypes over those reported in the work.

Table of Contents

List of Figures

List of Tables

1.0 Introduction and Literature Review

1.1 Rapid Prototyping

1.1.1 Introduction

A common step in the production of a part is to build a prototype which has the dimensions and the functionality of the proposed part. The method used to build the prototype may not be commercially viable but only serves to manufacture the prototype or a limited number of final parts. For example, the part may be machined from a block of metal, or a temporary mold may be constructed for producing a single part only. In any event the process of building the initial functioning part or prototype is time consuming and costly.

Over the last few years there has been considerable interest in developing techniques for accelerating the production of prototypes. In essence, these techniques consist of using a procedure for precisely laying down, or fusing, material in a controlled fashion in order to build a prototype, or a replica of a prototype, rather than, for example, milling the part from a block of material. The part or the mold for producing the part is fabricated in a manner analogous to a computer controlled "spider" which is required to lay down its web in a precise three dimensional pattern. The spider's coordinates typically come from a computer aided drawing of the desired object.

There are four primary "rapid prototyping" technologies in use today. These are stereolithography (SLA), selective laser sintering (SLS), layered object manufacturing (LOM), and fused deposition modeling (FDM), and they all construct a part or a mold for a part in layer fashion. SLA constructs a part using photoreactive polymers, usually ones that react to ultraviolet (UV) light. A layer is built by selectively exposing resin to sufficient UV light to polymerize it. This is performed by using a precisely directed laser beam or, in the case of solid

ground curing, by a floodlight that is directed through an optical mask. Once the layer is polymerized, liquid resin is placed on top of a part, or the part is lowered in a vat of resin so that the top of the part is covered. This new layer of resin is then polymerized, along with subsequent layers to construct the final part. When using SLS, a layer of powder is distributed across the part that is in a chamber heated to a temperature just below the T_m of the powder. A laser is then passed across the powder, selectively melting only the material desired in the particular layer so that it bonds with previously melted material. Subsequent layers are then added to construct the final part. LOM laminates a thin sheet to the top of the part before using a laser to cut the outline of the layer. Subsequent sheets are then added in order to fabricate the final part. FDM systems fabricate a layer by extruding a small bead of material, or road, in a particular "lay-down" pattern, such that the layer is covered with the adjacent roads. After a layer is completed, the height of the ram extrusion head is raised and subsequent layers are built to construct a part[1, 2, 3].

The use of these systems has altered the definition of a prototype. The traditional view of a prototype is a fully functional model that is identical to the product to be manufactured. Now it also includes replicas and models that may only resemble the proposed product and that can aid in the product's design. The above systems are able to produce parts and molds for parts that are replicas. Due to material limitations, these systems are unable to fabricate parts and molds that have the mechanical properties necessary to be functional in many applications. Most of the materials used in these processes have tensile moduli of about 1 GPa or less. Therefore, it is of considerable interest to develop high performance materials for these applications, so that functional prototypes can be constructed[1, 2, 3].

The following work will focus on developing high performance materials for use in a FDM system, so that functional prototypes can be fabricated. The purpose of this chapter is to introduce the reader to rapid prototyping and to inform the reader of a class of composite materials that may be used to build functional parts. The remainder of this section will explain in greater detail FDM and review previous research on composite materials that have been used with this system. The second part (Section 1.2) introduces the reader to a new class of reinforcing materials, thermotropic liquid crystalline polymers (TLCPs), and demonstrates their reinforcing potential. Processing considerations concerning the development of TLCP reinforcement in thermoplastics are discussed in Section 1.3. In the final section (1.4), the research objectives are enumerated.

1.1.2 Lay-Down Pattern

The FDM is a unique processing method because of its ability to build a layer by laying a polymer line, or road, down in three different ways. First, a contour pattern can be used, where the first road is laid around the perimeter of the layer, and then subsequent roads of the layer are laid adjacent to the previous road (Figure 1.1). A second pattern, raster, has a specified direction and the material is laid in a series of parallel straight lines in that one direction to build the entire

layer. Finally, a combination of the two is used where the perimeter is several contour roads and the core of the layer is filled with the raster.

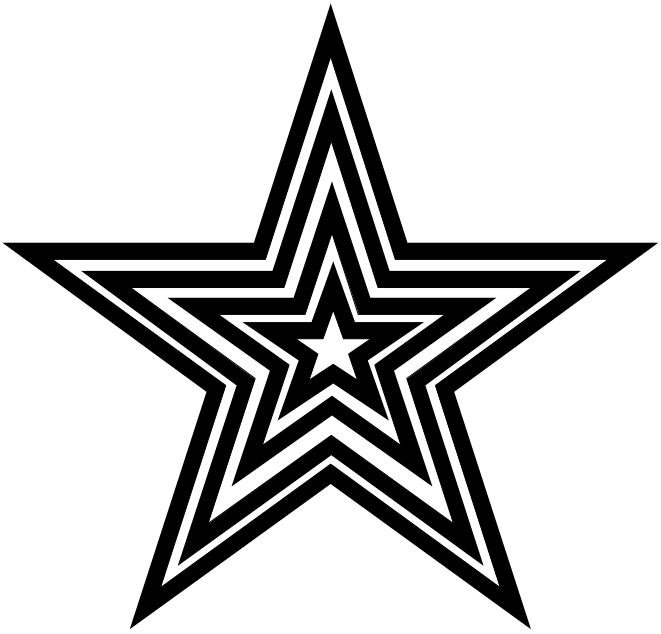

a: contour

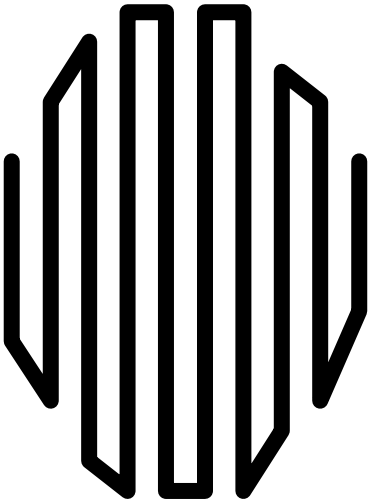

b: raster

c: combination

Figure 1.1 : Lay-down patterns for fused depostion modeling.
a: contour, b: raster, and c: combination.

The advantage of the different lay-down patterns is that the part can be customized according to the surface appearance and mechanical properties that are desired. The contour produces smoother surfaces because the outside edge is a continuous road. However, the orientation of the material is dependent on the perimeter, and complex geometries may cause irregular road patterns and voids to be built into the part. The rastering scheme does not produce as good of surface on the final part as the contour. However, it does generate a very regular and oriented core with a more controlled packing of adjacent roads with less voids, resulting in a stronger part. Therefore, for applications where a good surface and mechanical properties are desired, a combination scheme is used.

Another key advantage to the raster lay-down pattern is the ability to customize mechanical properties for the specific application envisioned for the part. This is especially important when using a polymer melt which readily produces anisotropic parts. Polycarbonate filled with 30 wt% glass was laid down in a uniaxial pattern [4]. The tensile modulus and strength in the direction of the lay-down pattern were 3.04 GPa and 106 MPa, respectively. The properties perpendicular to the lay-down pattern were 1.46 GPa and 61 MPa, respectively. Therefore, the final mechanical properties of the part are dependent on the lay-down pattern.

The dependence of mechanical properties on the lay-down pattern can be used to engineer the final mechanical properties of the part. If a potential part is being designed and if the mechanical properties in the machine direction need to be three times those of the transverse direction, the build pattern can be adjusted to account for the required anisotropy. Three times as many layers would be oriented in the machine direction than in the transverse direction. Therefore, by using this build scheme instead of a uniaxial or 0-90 lay-down pattern, the total volume of the part is smaller, less material is needed, and the build time of the part is decreased. Therefore, fused deposition modeling is a useful processing technique because it has the potential to easily change both the mechanical properties and the part geometry.

1.1.3 Previous FDM Work with Thermoplastics

Rapid prototyping, and FDM in particular, is a relatively new field and studies of mechanical properties are limited. Only three studies concerned with mechanical properties of polymers were found in the literature using varied materials: filled and unfilled engineering thermoplastics, acrylonitrile butadiene styrene copolymer (ABS)/adhesive blends, and a carbon filled acrylic resin. These studies are limited in scope as well as quality of research.

Work has been done using the Stratasys' fused deposition modeling process with several filled and unfilled engineering thermoplastics [4]. Parts were made using a uniaxial lay-down pattern, and the tensile modulus and strength were measured in both the machine and transverse directions. This was done for polyetheretherketone (PEEK), 30 wt% carbon filled PEEK, polycarbonate (PC), 30 wt% glass filled PC, and polymethyl methacrylate (PMMA). Neither the grades of material nor the processing procedures are detailed. In several of the cases, the

mechanical properties were obtained from less than five samples, and only one 30 wt% carbon filled PEEK sample was tested, (tensile modulus 9.4 GPa and tensile strength 256 MPa) which was the maximum value reported in the study. It was found that in all cases, the experimental tensile moduli were 13%-70% (average approximately 50%) less than those supplied by the manufacturer, and the PEEK and PC samples had similar properties in the machine and the transverse directions. It was stated without further evidence, that lubricants and degradation of the products from processing were the reasons for the dramatic decreases in mechanical properties reported by the manufacturer. It was also stated that porosity and reduced adhesion between lines were not factors in the unfilled PEEK and PC systems because the parts were isotropic. However, from a polymer processing perspective, the porosity appears to be the more probable reason for the dramatic decrease in properties, and the isotropy of the unfilled PEEK and PC systems was probably due to a lack of a preferred molecular orientation.

Two other studies concerned with mechanical property enhancement were reported with marginal success. ABS parts were made by rastering adjacent layers at 45° and -45° [5]. There were no gaps between the 15 mil (0.38 mm) wide roads. The modulus and peak stress were found to be 1.02 GPa and 19.42 MPa, respectively. Then parts were made with gaps between the roads and the voids were filled with various adhesives, with the belief that the ABS would act as fiber reinforcement. It was found that only a slight increase in properties could be obtained. The maximum modulus and peak strength reported of all the adhesives was 1.20 GPa and 19.82 MPa, respectively. This small increase is probably due to the assumption that ABS is a fiber reinforcement. Because it has elastomeric units, it does not act as a good reinforcement. Another study noted the difference between carbon filled and unfilled acrylic resin [6]. The flexural modulus and strength of the unfilled resin were 0.96 GPa and 38.3 MPa, respectively. The resin was filled with 5 vol. % carbon fibers which were 100 microns long. The aspect ratio was calculated to be between 10 to 15 using typical carbon fiber diameters [18]. The flexural modulus increased to 1.24 GPa while the strength decreased to 27.0 MPa, which was attributed to poor adhesion between the matrix and reinforcement.

A review of the literature indicates that there has been little published success in making complex geometries using high performance polymeric materials from a polymer processing perspective. Also, previous research was unable to obtain manufacturers' mechanical properties specifications for PC and PEEK. The research has been limited in scope.

1.2 Liquid Crystalline Polymer Systems

1.2.1 Molecular Structure of LCP Systems

Liquid crystalline polymers (LCPs) are a novel form of thermoplastic. They are known for excellent mechanical properties, good chemical and thermal residence, low dielectric constants, excellent dimensional stability, and exceptional barrier properties [7, 8]. LCPs are highly aromatic

materials with rigid and semi-rigid backbone structures. Thus, excluded volume imparts order to the rigid rod molecules with minimal entanglements, unlike other thermoplastics. Upon cooling from the melt they form an intermediate phase, or mesophase, which consists of one and two dimensional order. This order allows for excellent tensile properties in the direction of flow and lower properties in the perpendicular direction. LCPs also are shear thinning and hence the viscosity can be more sensitive to shear than ordinary polymers [9].

There are three primary types of liquid crystalline mesophases: nematic, cholesteric, and smectic [10]. The nematic phase is the most common for polymer systems (Figure 1.2). The rod-like molecules are aligned in a common direction in which the average orientation of the molecules is represented by the unit vector $\vec{n}$. The center of gravity of each molecule is positioned randomly throughout the system. Therefore, there is no long-range positional order [11 - 14]. The cholesteric mesophase is a variation of the nematic phase. Similar to the nematic phase, the cholesteric phase has no long-range position order. Also, the molecules are oriented in a common direction, represented by the unit vector $\vec{n}$. However in a direction perpendicular to $\vec{n}$, $\vec{n}$ rotates in a helical fashion [11, 12, 14]. The smectic mesophase has long-range position order, thus the molecules are arranged into planes perpendicular to the direction of the molecules. The molecules are positioned differently, so $\vec{n}$ must be redefined where $\vec{n}$ is the average direction of the molecules within each layer. $\vec{n}$ is either parallel to the normal of each layer or at an angle to the normal [11 - 14].

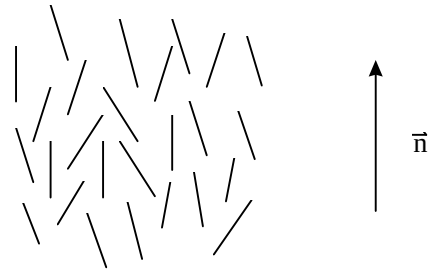

a: nematic

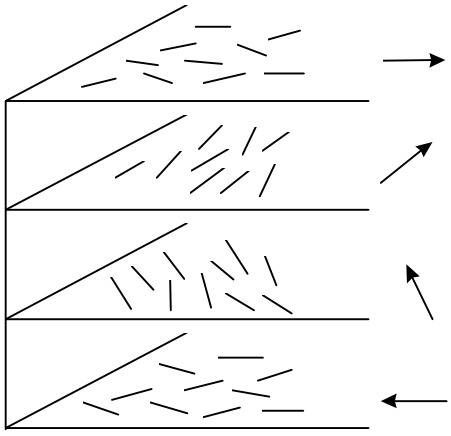

b: cholesteric

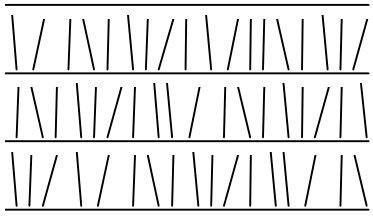

c: smectic

Figure 1.2 : Order of Liquid Crystal Structures. a: nematic, b: cholesteric, and c: smectic.

There are two classifications of LCPs: lyotropic and thermotropic liquid crystalline polymers (LLCPs and TLCPs). Because the LLCP polymer chain is very rigid, the material will degrade at a temperature below its melting temperature. LLCPs undergo the mesophase transition at a certain concentration of polymer in solution and at a certain temperature, and exhibit phase transitions with changing concentration and temperature. LLCPs typically do not dissolve in common solvents, and processing via hazardous solvents is undesirable. TLCPs, though rigid, have enough chain mobility to melt at temperatures below the degradation temperature. TLCPs undergo the mesophase transition in a certain temperature range and are thus melt processed similarly to commodity thermoplastic resins [10 - 13].

1.2.2 Mechanical Properties of Thermotropic Liquid Crystalline Polymers

TLCPs typically exhibit tensile properties that greatly exceed those of traditional thermoplastics. They are able to readily obtain high degrees of molecular orientation, resulting in their excellent tensile properties. Thus, TLCPs have the potential to be a reinforcing material for commodity resins. In order to achieve these mechanical properties, the TLCPs must be processed properly. They orient far more easily in extensional flow than shear flow [15 - 17]. Fiber spinning is very efficient in orienting the molecules and obtaining high mechanical properties. Similar to traditional thermoplastic fiber spinning, draw down, thermal history, and post-processing are all important in determining final properties of TLCP systems.

TLCPs have mechanical properties comparable to those of other reinforcing materials for commodity resins. As shown in Table 1.1 [18], the tensile modulus and strength of TLCP fiber and annealed TLCP fiber are similar to those of glass fiber, and the specific tensile modulus and strength are above those of glass fibers. The specific tensile properties of annealed TLCP fibers are comparable to aramid fibers. The range of prices for TLCPs ($26/kg. to $48/kg.) is at the lower end of the price range for the aramid fibers ($22/kg. to $220/kg.). Thus, TLCPs have the potential to reinforce commodity materials because TLCPs are competitive in both properties and cost when compared to other reinforcing materials [18].

Table 1.1: Neat Fiber Reinforcement Characteristics [18].

	Glass Fiber	Carbon Fiber	Aramid Fiber	TLCP Fiber	Annealed TLCP Fiber (Vectra Series)
Range of Cost/unit weight ($/kg)	1.65	22 to 2200	22 to 220	26 to 48	26 to 48
Average Unit Cost ($/kg)	1.65	46	33	37	37
Tensile Modulus (GPa)	69 to 83	207 to 637 (around 230 is typical)	128	40 to 100	40 to 100
Specific Tensile Modulus (GPa•cm^3/g)	28 to 33	109 to 302 (around 130 is typical)	88.9	31 to 77	31 to 77
Tensile Strength (GPa)	1.72 to 2.07	2.24 to 2.65	3.79	0.5 to 1.0	0.5 to 2.0
Specific Tensile Strength (GPa•cm^3/g)	0.69 to 0.83	1.17 to 1.30	2.63	0.7	1.4
Density (g/cm^3)	2.52 to 2.61	1.73 to 2.11	1.44	1.2 to 1.4	1.2 to 1.4
Fiber Diameter (μm)	0.5 to 14	7 to 10	12	Less than 1 to greater than 10	Less than 1 to greater than 10
Typical Diameter	10 to 13	7	12	2	2

The tensile properties of TLCPs are dependent on molecular orientation. The Herman's orientation factor, $<P_2>$, is used to quantify the molecular orientation of TLCP fibers and parts:

$$< P_2 >= \frac{3 < \cos f > -1}{2} \qquad (1)$$

where f is the angle between the unit vector $\vec{n}$ and the direction of the fiber or the machine direction of the part. A systematic increase in orientation and tensile modulus has been observed with increasing draw ratios before becoming independent of draw ratio at high draw downs (>30) where the orientation factor is approximately 0.90 [19 - 22, 23] (Figure 1.3). Other work, however, has shown a maximum orientation (~0.85) at low draw ratios (<5), while the modulus did not reach a maximum until higher draw ratios (~30) [20]. It was speculated that the increase in properties at high draw ratios was due to an increase in aspect ratio and that only at low strains does the molecular orientation increase. There is a clear dependence of tensile modulus on molecular orientation at low draw ratios. At higher draw ratios there is an increase in properties which is probably due to a slight increase in molecular orientation.

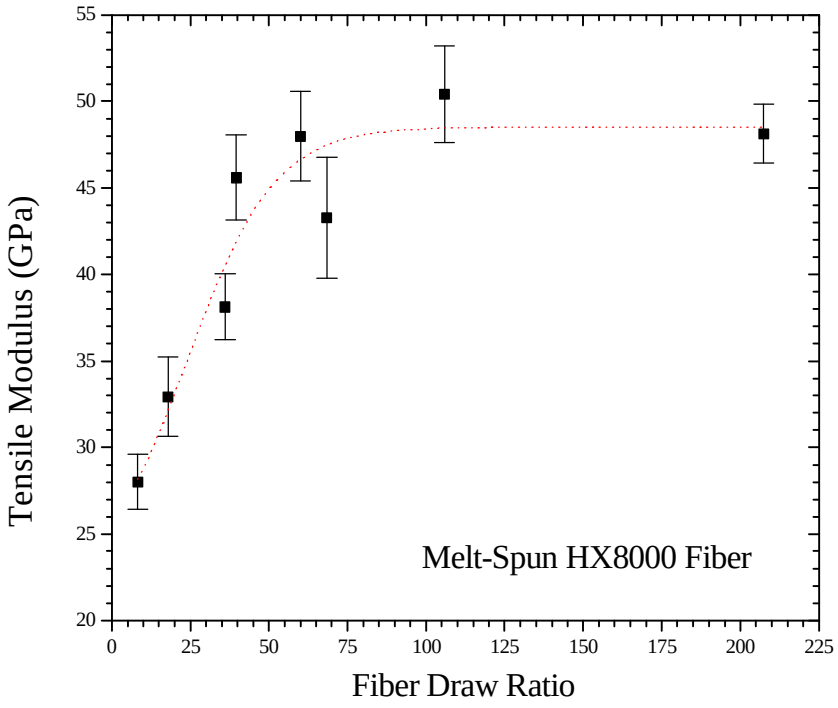

Figure 1.3 : Modulus as a function of draw ratio of neat HX8000. At higher draw ratios the modulus becomes independent of draw ratio [23].

The thermal history during processing is also important in order to obtain the optimal mechanical properties of neat TLCPs. Sarlin and Tormala [24] demonstrated that the spinning temperature can affect the final characteristics of neat Vectra A900 (TLCP). They extruded fibers with a die temperature of 287°C, 307°C, and 327°C (calorimetric melting point ~280°C). For a given draw ratio, the mechanical properties decreased at higher processing temperatures, with a maximum modulus of 60 GPa and strength of 1.2 GPa. They also demonstrated that spinning at higher temperatures resulted in increased fiber diameter fluctuation and increased surface defects. The fluctuations were attributed to three possibilities: inhomogeneity of the melt, inhomogeneity in the raw material, or draw line resonance. Vectra A, however, does not fully melt at these temperatures. It has been shown that it must be heated to 320°C in order to fully melt all of the crystallites [25]. Therefore, the material needs to be exposed to these temperatures to fully melt out the crystallites and then cooled somewhat before being spun at high draw ratios so that the optimal mechanical properties can be obtained.

The die design is critical to enhancing the final tensile properties at low draw ratios. Turek and Simon [26] extruded Vectra A950 though a capillary rheometer with a 0.76 mm diameter die while varying the L/D (length/width). Samples were produced at both 290°C and 300°C with a draw ratio of 4, and the molecular orientation was observed using wide angle x-ray scattering, WAXS. At a L/D of 2.5 and temperatures of 290°C and 300°C the maximum tensile moduli (56 GPa and 55 GPa, respectively) and orientation ($<P_2>$ equals 0.98) were observed. A minimum L/D is required in order to develop the flow fields necessary that result in molecular orientation. However, longer L/Ds and high temperatures result in a relaxation of the morphology developed in the contraction. The relaxation yielded lower tensile properties.

Post-processing of TLCPs can affect the orientation. Kaito et al. [19] annealed a TLCP composed of 73 mol% 4-hydroxybenzoic acid, HBA, and 27 mol% 6-hydroxy-2-naphthoic acid, HNA, (calorimetric melting point ~274°C). Annealing below 230°C had no effect on orientation, while annealing at 250°C increased orientation and 270°C decreased orientation. Annealing caused a partial melting and resulted in a structural reorganization of the crystallites. Annealing at too low of a temperature, 230°C, would not melt the low melting crystals and too great of a temperature, 270°C, would allow relaxation of the molecular orientation. Winter and coworkers [27, 28] also attributed an increase in storage modulus and loss modulus to crystallization. Similarly, Sarlin and Tormala [29, 30] annealed Vectra A900 and observed an increase in tensile modulus and strength to approximately 70 GPa and 2.5 GPa, respectively. Studies have indicated that Vectran M increases in molecular weight when annealed and this manifested itself as an increase in tenacity [31].

In summary, TLCPs, when processed properly, have excellent mechanical properties that are comparable to composite reinforcing materials and have the potential to reinforce materials themselves. The mechanical properties are very sensitive to shear forces, extensional forces, and temperature profiles during processing. Also orientation and mechanical properties are sensitive to the effects of thermal treatment in post-processing.

1.2.3 Composite Theory of Fiber Reinforced Systems

The tensile properties of TLCP thermoplastic blends have been analyzed as a fiber reinforced system, where the TLCP is the reinforcing phase. The Halpin-Tsai equation is used to predict the tensile modulus of the composite from the tensile modulus of the individual components [32, 33]. It assumes a uniform aspect ratio (length divided by diameter) of the reinforcing TLCP in the matrix and assumes constant stress is applied across the whole of the composite. The tensile modulus along the fiber axis of a composite reinforced with uniaxial fibers is given as:

$$E_{comp} = E_m \frac{1 + 2\eta(L/D)\phi_f}{1 - \eta\phi_f} \tag{2}$$

$$\eta = \frac{\frac{E_f}{E_m} - 1}{\frac{E_f}{E_m} + 2\frac{L}{D}} \tag{3}$$

where E_f, E_m, and E_{comp} are the tensile moduli of the fiber, the matrix and the composite, respectively, taken in the direction of uniaxially oriented reinforcement. L and D are the length and diameter, respectively, and ϕ_f is the volume fraction of the reinforcement. Longer aspect ratios result in a greater tensile modulus. The effect of aspect ratio is evident in Figure 1.4 where the modulus of the matrix is 1 GPa and the fiber is 70 GPa. As the aspect ratio approaches 100, optimal properties are observed and the above equations simplify to the "rule of mixtures":

$$E_{comp} = \phi_f E_f + (1 - \phi_f) E_m \tag{4}$$

The predictions of the "rule of mixtures" are consistent with experimental data for uniaxially reinforced thermoplastics.

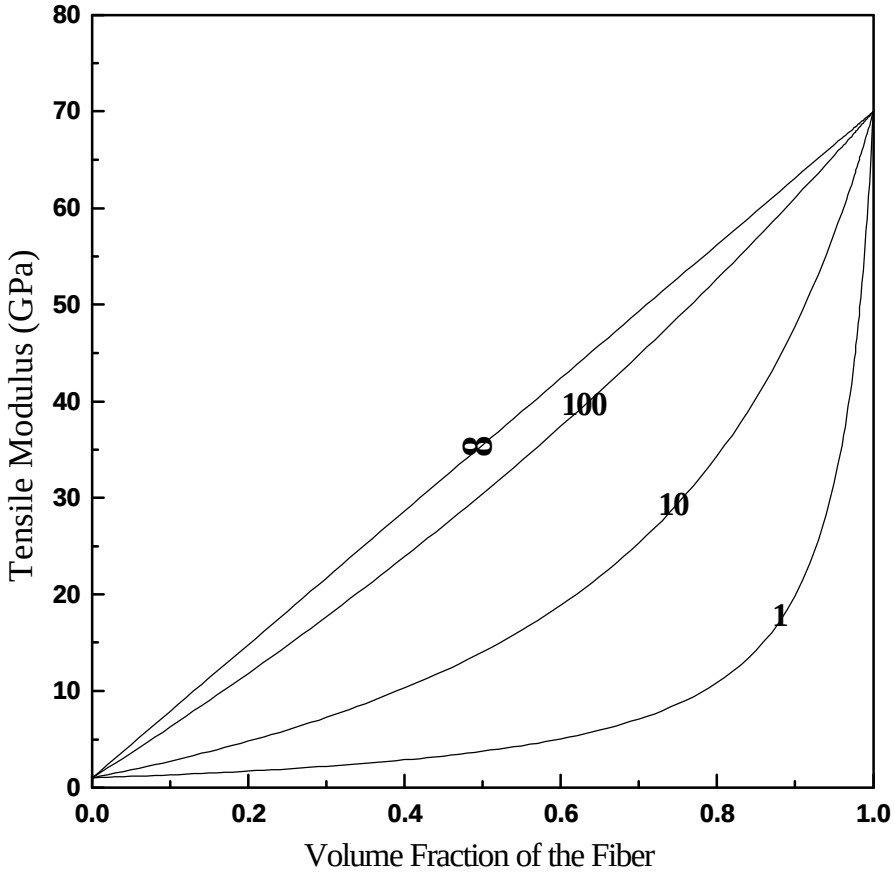

Figure 1.4 : Modulus as a function of volume fraction of fiber, where the aspect ratio of the fiber is indicated and the modulus of the fiber was taken as 70 GPa. At an aspect ratio of 100 the maximum reinforcement is obtained.

The properties of a randomly aligned fiber reinforced system is similarly analized. The Halpin-Tsai equation for randomly oriented fibers in the plane with an L/D greater than 100 reduces to:

$$E_{random} = \frac{3}{8} E_{machine} + \frac{5}{8} E_{transverse} \quad (5)$$

$E_{machine}$ and $E_{transverse}$ are the modulus of the uniaxially composite parallel and transverse to fiber direction, respectively. This also assumes that there is uniform aspect ratio and that stress is evenly applied across the composite. Using these tools, realistic estimates of the maximum reinforcement can be determined [34, 35].

1.3 In Situ TLCP Composites

TLCPs can be used as a reinforcing material, because they have excellent mechanical properties and easily form fibril morphologies, which is the optimal geometry for composite reinforcement. Because some TLCPs are processable at reasonable temperatures (>240°C), they can be processed in situ as melts with some thermoplastic resins. Traditional in situ processing imparts a single thermal history to the blend. In situ processing of TLCP thermoplastic systems has several advantages over glass reinforced systems. The matrix fully wets the TLCP fibrils, and no additional compounding or curing is required. Also traditional in situ processing is easily performed via dry blending the two resins and then processing them using conventional processing techniques. In general TLCP reinforcement has several other advantages over glass reinforcement: light weight, small diameter fibrils, melt process at temperatures slightly higher than those of commodity thermoplastics, less wear on processing equipment, interfacial agents are easily added, and the potential for recycling of blends.

In situ injection molding of TLCP reinforced composites leads to materials with mechanical properties that are similar to glass filled systems of the same weight percent (Table 1.2) [36-38]. Polyetherimide (PEI), polypropylene (PP), and polyethylene terephthalate (PET) matrices were used with several different TLCP reinforcements. The glass reinforced system, only in the case of the PP matrix, has a significantly higher tensile strength than the TLCP systems. Of the examples of the tensile and flexural moduli for each matrix in Table 1.2, at least one of the TLCP blends had comparable properties to the glass reinforced systems. The PET/60 PHB (para-hydroxy-benzoic-acid) composite, however, is significantly more anisotropic than the PET/glass composite. The PET/60 PHB sample has a modulus 13 times greater in the machine direction than in the transverse direction. Thus, TLCPs are effective reinforcing materials in the machine direction, but they are not effective in reinforcing the transverse direction.

Table 1.2 : Comparison of properties of glass reinforced composites to in situ composites of the same matrix and wt% reinforcement [36-38].

Thermoplastic/ Reinforcement	Tensile Strength MPa	Flex Modulus Machine Direction GPa	Tensile Modulus Machine Direction GPa	Elongation %
Polyetherimide (PEI)	91.0	3.34	3.0	59
PEI/30% HX4000	152	7.00	9.8	2.28
PEI/30% HX1000	129	7.27	8.7	1.94
PEI/30% Glass	170	9.0	8.9-11	3
Polypropylene (PP)	31.24		1.37	>10
PP/20% Vectra B	36.85		3.30	2.0
PP/20% 60% HBA/PET	41.19		2.90	
PP/20% Glass	80		3.66	
Poly(ethylene terephthlate)	58.3	3.79	2.69	
PET/20% HX1000	96.6	11.66	8.87	
PET/20% Vectra A	103.7		3.42	
PET/60% PHB		24		
PET/20% Glass	107.8	10.34	7.02	
PET/30% Glass		9.2		

PP/20% Vectra B and PP/20% 60% HBA/PET is compatibilized with maleic anhydride modified PP.

1.3.1 In Situ Processing

TLCP thermoplastic composites, where reinforcement is generated in situ, can be processed using conventional thermoplastic processing equipment. The proper processing conditions must be used in order to achieve the optimal mechanical properties from the TLCP reinforcement. The final properties of a TLCP reinforced system increase with increasing molecular orientation and aspect ratio. In the melt, the TLCP forms into droplets. In order to obtain optimal tensile properties, the flow history and processing conditions must deform the TLCP droplets into fibrils and orient the rigid backbone. Hence, the final tensile properties of the blend are directly dependent on the processing conditions. When injection molding parts, the

mechanical properties are affected by viscosity, temperature, mold thickness and injection speed. When extruding fibers and films in a single extruder, the tensile properties are similarly affected via temperature and draw down, and the effects of these conditions will be detailed.

The generation of reinforcing fibrils through droplet deformation in an injection molder is very complex. In order to understand the effect of processing conditions on final part properties, it is first important to understand the flow field during the mold filling step. In any mold, the flow field is very complex with many stages, and the flow field will vary between different mold geometries. During mold filling there are two primary flow stages which determine the final mechanical properties: fountain flow at the free surface of the advancing front, and shear flow behind the melt front (Figure 1.5) [39]. The material that enters the mold cavity after the initial material, flows faster than the advancing front. After a given time, the material will reach the advancing front and experience fountain flow, or extensional flow, and flow outward from the center to the surface. In fountain flow, high degrees of orientation occur in the TLCP phase of the blends. The orientation is frozen when the material comes in contact with the cooler wall, thus leaving a highly oriented skin. Material that does not reach the front is only oriented by shear flow which is not as effective as extensional flow in orienting the material. In an injection molder, the shear rates in the core are not effective in deforming droplets into fibrils. It has been shown that with injection molded PEI/Vectra A (10/90 wt%) there are clear skin and core regions [40]. The Herman's orientation factors of the skin, the core, and the entire plaque were determined to be 0.82, 0.65, and 0.75, respectively. Therefore, the flow field during mold filling produces a skin-core morphology where the skin is highly oriented and the core is somewhat oriented, resulting in inefficient reinforcement [39 - 42].

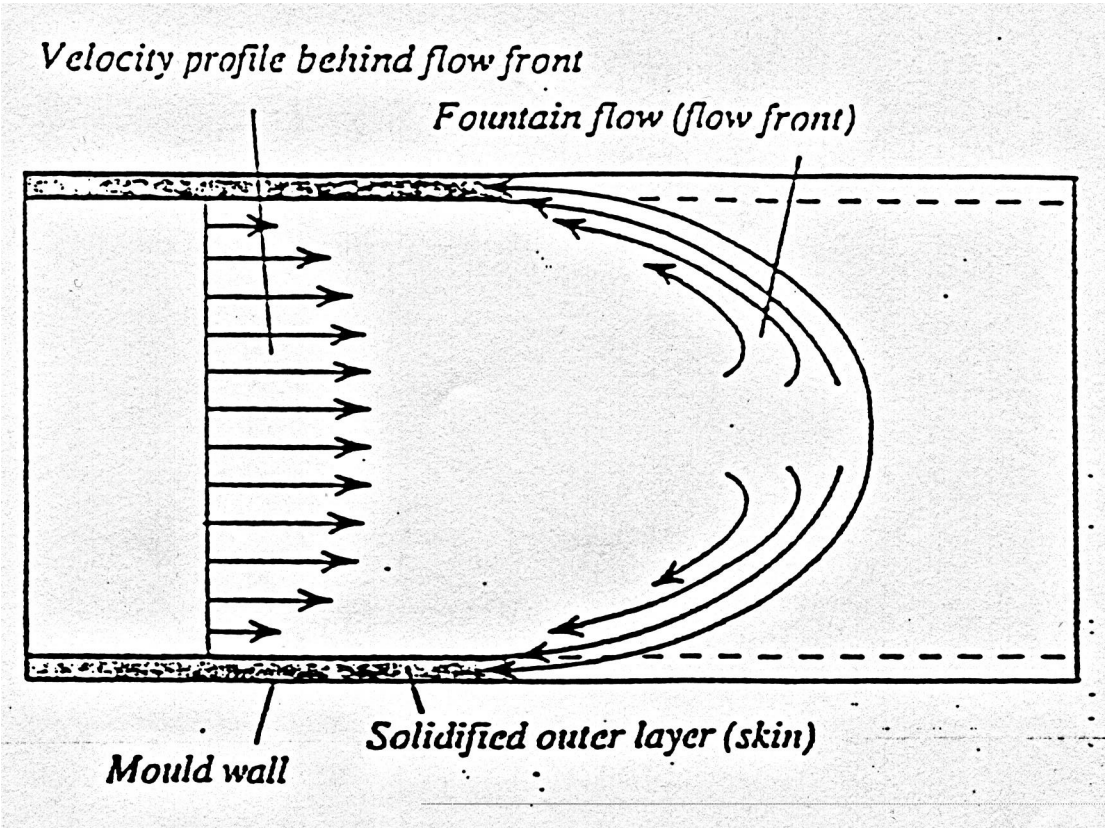

Figure 1.5 : Flow scheme inside of an injection mold. There is fountain flow at the advancing front and shear flow behind the advancing front [39].

The mechanical properties of injection molded blends are dependent on the viscosity ratio between the TLCP and the matrix and on the melt temperature. O'Donnell [41, 43, 44] injection molded LC3000 (poly-ethylene-terephthalate 40 wt% modified with para-hydroxy-benzoic-acid 60 wt%) with two grades of PP (PP/MAP/TLCP 63/7/30 wt%) with differing viscosities. The viscosity ratio between PP_1 (MFI = 0.4) and the TLCP and between PP_2 (MFI = 45) and the TLCP were 0.008 and 0.04, respectively. In all cases the tensile and flexural moduli were higher for the blend with the greater viscosity ratio, and it was suggested that this was a result of increased deformation of the TLCP droplets. Using a 1 mm end-gated mold and processing at a temperature of 250°C, the flexural moduli for PP_2 and PP_1 blends were 5.2 GPa versus 3.6 GPa, respectively. The processing temperature is also critical. When the PP_2/LC3000 was processed at 230°C using similar processing conditions as those at 250°C, the flexural modulus was only 3.6 GPa. It was shown by rheological data that when the TLCP was heated to 250°C and cooled at a rate of 5°C /min the loss modulus was greater than the storage modulus until cooled below

240°C. However, when similarly cooled from 230°C, the storage modulus was greater than the loss modulus. Thus, when processed at 230°C the TLCP was behaving more as a solid making it more difficult to deform the TLCP fibrils [41, 43, 44].

Injection molding speed and mold thickness affect the mechanical properties of the final part. O'Donnell [41, 43, 44] determined that injection speed was critical to mechanical properties. However, the correlation between mechanical properties and injection speed was inconsistent. When injection molding LC3000/PP/MAP (30/63/7 wt%), where MAP means maleated PP, using a 1 mm thick end-gated mold using short fill times, the greatest flexural modulus was 5.2 GPa. While at long injection times, the modulus was 4.0 GPa. 1.5 mm and 2.3 mm thick molds resulted in a maximum modulus of 3.6 GPa in both cases. Also when comparing the maximum properties of samples generated from differing mold thickness, the thinner mold resulted in higher mechanical properties [41, 43, 44].

The generation of in situ reinforced fibers and films via extrusion increases the mechanical properties of the reinforcement using different flow kinematics than injection molding, but both processes rely on extensional flow [45 - 57]. When extruding the TLCP blends, droplets are formed in the screw. The droplets enter the die assembly, and undergo extensional flow in the contraction before the die exit, developing low aspect ratio fibrils. Upon exiting the die, the extensional flow of high drawdowns effectively orients the TLCP forming reinforcing fibrils. Effective reinforcement is dependent upon the processing temperatures, draw ratio, and die design, which has already been discussed with respect to neat TLCPs fibers.

Blizard and coworkers [49] studied the effect of processing temperatures on tensile properties of Vectra A950/PC strands produced by means of a single extruder in order to determine the optimal processing range. Holding all other variables constant, three temperature profiles were employed with a systematic increase in temperature in each zone. The maximum temperature for each profile was 300°C, 320°C, and 340°C, and the percent of Vectra A in fibril form in each composite processed at these temperatures was 95, 90, and 30, respectively. This decrease in percent of Vectra A in fibril form correlates with the decrease in tensile moduli, 8.1 GPa, 7.3 GPa, and 3.0 GPa, respectively. Hence, higher processing temperatures result in lower mechanical properties, and this is attributed to TLCP domain relaxation as a result of shortened relaxation time scales. There is the potential for degradation of the Vectra A at higher temperatures. However, a minimum temperature is required to fully melt out the crystallites [49, 50]. Thus, there is an optimal thermal processing range to maximize mechanical properties.

The drawing of in situ TLCP/thermoplastic fibers increases the mechanical properties analogously to neat TLCPs. Kytani and coworkers [47] extruded strands of Vectra A/PET (20/80 wt%) blends at increasing draw ratios. The modulus increased from 4 GPa to 10 GPa at draw ratios 10 and 40, respectively, due to increasing strain and strain rate. However, at sufficiently high extension rates, draw ratios of at least 80, the modulus reaches a plateau of 12 GPa. Work was also done to couple relationships between the aspect ratio of the reinforcement and the draw ratio, using the Halpin-Tsai equation, and between the tensile modulus of the

reinforcement and the draw ratio [46]. For Vectra B/PC systems the fiber modulus was predicted to increase with draw ratio and TLCP composition, and higher draw ratios are required to obtain the maximum properties with increasing TLCP reinforcement.

Similar to fiber spinning, the drawing of films will alter the tensile properties [56, 58 - 61]. Dutta and Weiss [56] extruded Vectra A 950/PC (10/90) films at varying draw ratios. At a draw ratio of 2 and 7 the modulus in the machine direction was 1.5 GPa and 2.5 GPa, respectively, while the transverse direction decreased slightly from 1.3 GPa to 1.2 GPa due to the preferred alignment in the machine direction. Baird and coworkers [59], using an Ultem/Vectra A900 (70/30 wt%) blend, demonstrated a systematic increase in machine tensile modulus with increasing draw ratio, and this was attributed to an increase in molecular orientation as determined by means of WAXS. There is a clear relationship between the strain and strain rate and the final mechanical properties of in situ reinforced TLCP/ thermoplastic blends.

In order to obtain maximum mechanical properties of TLCP in situ reinforced composites using conventional processing techniques, the proper conditions must be used. There is an optimal extrusion temperature in order to ensure full melting of the crystallites and to avoid molecular relaxation in the draw line. Higher properties are obtained from extensional flow than from shear flow, and greater strains and strain rates increase properties in the flow direction.

TLCP in situ reinforced composites, where the matrix and the reinforcement are plasticated with the same thermal history, have several advantages over glass as a reinforcement. TLCPs are lighter weight than glass and have smaller reinforcing fibril diameters than glass. Interfacial agents or compatiblizers can be used to increase adhesion between the two immiscible phases. Finally, there is the potential to recycle TLCPs and TLCP thermoplastic blends [32, 33, 41, 48, 62 - 68].

TLCPs are relatively light weight materials with a density of 1.2 g/cm^3 to 1.4 g/cm^3, while glasses range from 2.52g/cm^3 to 2.61 g/cm^3 [18]. For similar volume fractions, TLCP blends weigh less. This is very attractive to the auto and aviation industries, who want light weight, high performance materials.

TLCPs typically exist in fibers of diameters (submicron to 5μms) smaller than those of glass fibers (order of 10μms) (Figure 1.6) [69]. The Halpin-Tsai equation for composite theory indicates that an aspect ratio of 100 is necessary to obtain optimal reinforcement. Thus, with smaller diameters, higher aspect ratios are obtainable with similar fiber lengths, and thus greater tensile properties [32, 33].

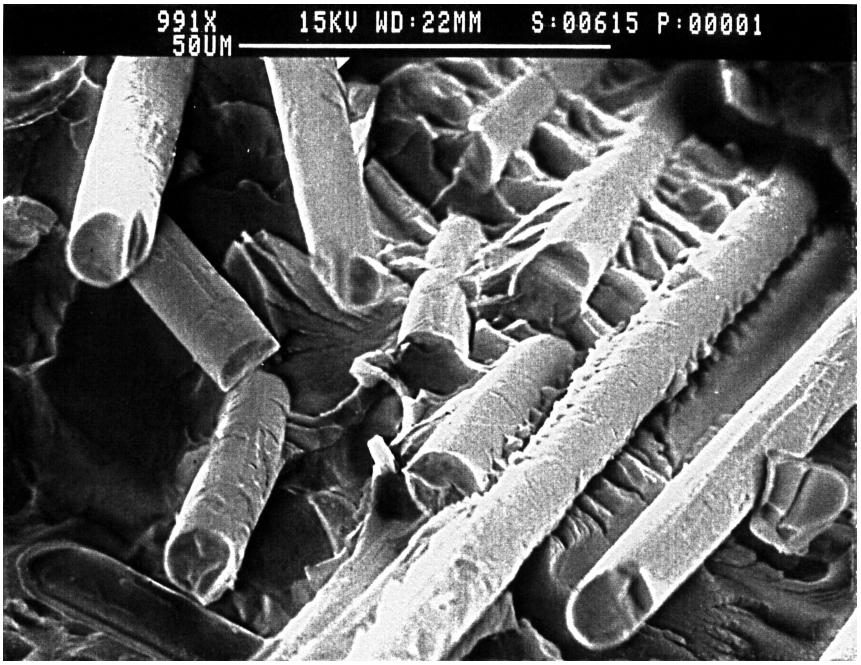

a)

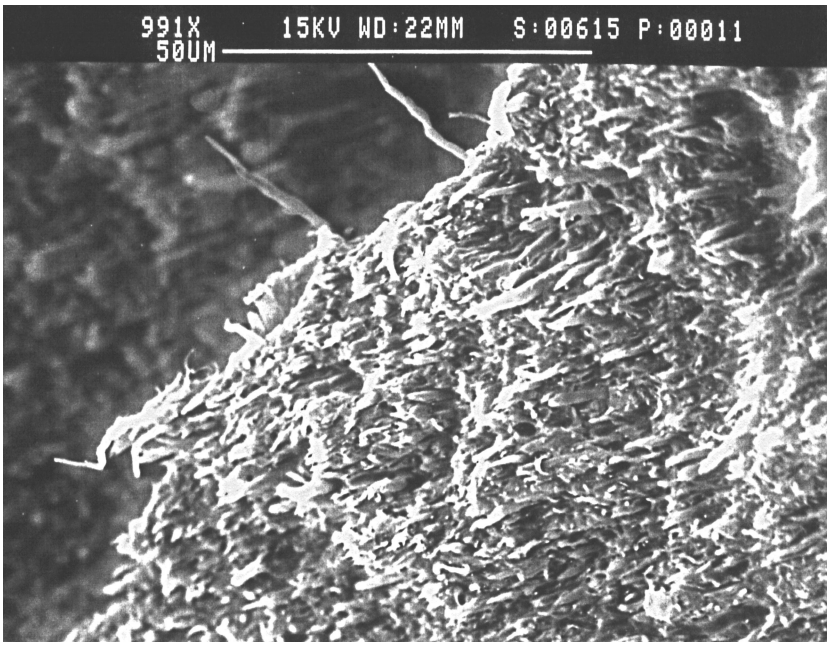

b)

Figure 1.6 : Difference in diameter of the reinforcing phase. a) SEM of PET with 30 weight percent loading of glass fiber. Fiber diameter about 12um. b) SEM of pregenerated microcomposite plaque of PT X267/HX1000/Rynite (30/30/40 wt%) from a fiber draw ratio of 40. Fiber diameter ranges from 3μm to under 1μm [69].

The use of interfacial agents or compatiblizers can improve mechanical properties of TLCP thermoplastic blends [41, 62 - 64, 68]. An interfacial agent is a material with two distinct phases that are immiscible with each other, but each phase is miscible or has secondary bonding with one of the two distinct phases in the blend. The interface between these two phases acts as a stress concentrator, resulting in the point of failure. Interfacial agents act as a link or bridge to increase adhesion between the two phases which in turn leads to an increase in tensile properties. It is also easily added as a third component to a dry blend. Baird et al. [41, 62 - 64, 68] reported that maleic anhydride grafted polypropylene (MAP) increases the mechanical properties of PP/TLCP (Vectra A900, Vectra B950, and LC3000) blends and that tensile properties of nylon 11/HX8000 blends were also increased through the use of an interfacial agent. The increase in properties was speculated to be due to an increased dispersion of the TLCP phase and improved adhesion between the two phases.

Finally, there is the potential to recycle TLCP reinforced thermoplastic parts. Granulated TLCP reinforced thermoplastic parts can be used as feed stock in an injection molder or extruder. The TLCP fibril is remelted into droplets, and the reinforcing fibrils are regenerated by droplet deformation in the flow field. This can be repeated many times because the TLCP is melt processed, and relies on the process flow and thermal history to produce the reinforcing morphology. With glass filled systems, however, the shear stresses of reprocessing break the solid glass reinforcement [66, 67]. Therefore, each time the glass is reprocessed the aspect ratio decreases along with mechanical properties and the glass fibrils cannot be regenerated as in the TLCP system.

There are many advantages of TLCP in situ reinforcement composites over glass reinforcement. TLCPs are lighter weight and form smaller diameter fibrils. Blend properties can easily be enhanced by adding an interfacial agent to the blend. The final parts have the potential to be recycled.

Some TLCPs also have the advantage of being able to supercool to temperatures below their melting point (T_m) [70 - 72]. HX8000 was cooled from 310°C at a rate of 5°C/min [72]. After cooling below it's melting point of 277°C, the complex viscosity began to increase significantly when the temperature of the melt approached 250°C. The degree of supercooling is usually increased with an increasing difference between the highest processing temperature and the T_m. This can be exploited in order to prevent premature solidification to ensure that optimal orientation can be imparted in the spinline during fiber spinning. When the matrix and the TLCP are plasticated using a single thermal history, the supercooling nature of TLCPs may be difficult to exploit because the maximum processing temperature may be limited by the maximum possible processing temperature of the matrix.

The use of TLCP reinforcement via in situ processing, where the matrix and the reinforcement are plasticated together with the same thermal history, has several disadvantages. First, in situ processing develops anisotropic reinforcement. Second, it is difficult to reach the optimal mechanical properties of the TLCP phase. Third, in general TLCPs require a matrix with

high processing temperatures. Baird and coworkers [73] injection molded end-gated plaques of Ultem/HX4000 (50/50 wt%). The flexural modulus in the machine direction was approximately 12 GPa, and the modulus in the transverse direction was approximately 3 GPa, indicating anisotropic reinforcement of the plaque. Second, the properties of the injection molded samples are low due to the difficulty in obtaining the optimal mechanical properties of the TLCPs. In order to obtain these properties, extensional flow, as found in fiber spinning, is required. At high draw ratios Vectra B has a tensile modulus of 75 GPa [74]. Therefore, only certain processes can be employed to obtain optimal mechanical properties of TLCPs and TLCP blends. Finally, because many of the TLCPs that exhibit excellent tensile properties process at temperatures close to the degradation temperature of commodity thermoplastics, higher melting point thermoplastic resins are required as a matrix for in situ processing with a single thermal history. Although one can use commodity resins with TLCPs that process at lower temperatures, higher processing range TLCPs require more costly resins for a matrix, making them cost prohibitive. Thus, TLCP reinforcement has distinct disadvantages.

In order to capitalize on the advantages and overcome the disadvantages of traditional in situ TLCP reinforcement, Baird and Sukhadia patented [75] a novel dual extrusion process, which was further improved by Sabol [34, 35]. The process consists of two separate extruders, allowing the matrix and TLCP to be plasticated separately. The TLCP is then injected into the matrix using a multiple-port injection nozzle and then the melt passes through a series of static mixers, before being drawn to high draw ratios in order to fully orient the TLCP reinforcement.

The dual extrusion process has three advantages over traditional in situ processing. First, because the materials are plasticated in separate extruders, the TLCP can be processed at temperatures above the processing range of the matrix. The TLCP is supercooled and injected into a matrix with a thermal processing range lower than that of the TLCP's melting point. The separate thermal histories imposed on the TLCP and the matrix along with the supercooling of the TLCP decrease the degradation of the matrix and allow for the processing of two materials with differing thermal processing ranges. The injection of the TLCP into the matrix yields continuous streams of TLCP reinforcement encapsulated in the thermoplastic matrix. Because the streams are continuous, fibril formation does not rely on drop deformation as in traditional in situ processing. The melt then passes through a series of static mixers which serve to divide the TLCP reinforcing streams. The strand is then drawn to obtain the optimal level of molecular orientation of the reinforcing TLCP phase. Finally, composite strands can be post-processed as a solid filled system, where the matrix is processed above the T_m of the matrix and below the T_m of the TLCP. Therefore, this system is able to overcome the afore-mentioned disadvantages of requiring high melting point thermoplastic resins as a matrix and the difficulty of obtaining the optimal mechanical properties of the strand.

Using the dual extrusion process, continuously reinforced composite strands have been produced with optimal tensile properties. Sabol and Handlos [34, 35] showed that the tensile modulus of the strands corresponded with the rule of mixtures. Vectra B950/PP (30/70) strands were extruded, and their tensile modulus and strength were 17 GPa and 160 MPa, respectively, at

draw ratios greater than 60. The experimental values were the same as the those predicted by the rules of mixtures, where the modulus of Vectra B950 was taken as 75 GPa [74]. Baird and Robertson [76] showed that higher draw ratios resulted in synergistic effects upon the strand modulus. Vectra B950/PP (50/50) strands were spun with draw ratios in excess of 100 and the tensile modulus was approximately 42 GPa. The modulus of the Vectra B reinforcing fibrils was calculated to be 110 GPa, which is well above the 75 GPa reported for pure Vectra B [74]. Other work with nylon-11 and HX8000 has also shown similar synergistic results at high draw ratios [72]. 13 wt% and 22 wt% TLCP strands had fibril moduli of approximately 80 GPa, and 35 wt% TLCP strands had a fibril modulus of approximately 70 GPa. However, neat HX8000 strands had a modulus of only 48 GPa. The increase in TLCP fibril modulus was attributed to greater fibril orientation, which was obtained by encapsulating the TLCP fibrils with in a matrix. It was suggested that the thermal insulation provided by the matrix prevents premature solidification of the TLCP fibrils in the spinline, and the matrix allows the fibrils to reorganize more freely as a result of extensional flow. Neat material would be too constrained to reorganize and would solidify before being fully oriented. Hence, the 35 wt% TLCP blend had a lower fibril modulus than that of lower TLCP concentrations. Therefore, strands from the dual extruder have moduli equal to or greater than that predicted by the rule of mixtures.

Using a similar extrusion assembly, Boer et al. [77, 78] were unable to extrude strands with tensile properties similar to the afore-mentioned composite strands. Vectra A950/PP (52 vol% TLCP) strands were extruded at a draw ratio of 15, and the maximum extrusion temperature was 300°C. The strands had a modulus of 15.8 GPa. Using this value, the modulus of the Vectra A fibrils was calculated to be 30.1 GPa, which was approximately 40% of the modulus of neat Vectra A reported in other studies [24, 29, 36]. The authors attributed the low tensile properties to two reasons. First, there probably was slippage between the Vectra A and the matrix, resulting in less than affine fibril deformation during drawing. Second, the temperature of the spinline may have been such that the Vectra A was too viscous (or even solidifer) to elongate in the extensional flow field. The properties may also be low due to several other factors. Guskey and Winter [25] showed that Vectra A needs to be heated to 320°C to melt out the residual crystallites. At 300°C the reinforcement was not fully melted, making it impossible to obtain the optimal orientation or tensile properties. Baird and Handlos [36,79] also proved, if taken to 330°C, Vectra A950 will supercool 30°C below its melting point, creating a larger overlapping processing window between the TLCP and the matrix. This allows the Vectra A to be deformable at lower temperatures. Also, the poor properties were probably a result of low draw ratios. Thus, if a maximum temperature of 330°C was used in the Vectra A extruder, then there would have been full melting of the crystallites, and the TLCP would have remained deformable at lower temperatures, resulting in higher draw ratios and tensile properties.

In summary, a dual extrusion process was developed to overcome the disadvantages of traditional single thermal history in situ processing by taking advantage of supercooling and continuous TLCP reinforcing streams. The system has shown synergistic effects with properties 60% greater than those predicted by the rules of mixtures, and the system enables a new resin to be reprocessed as a solid filled system, while retaining the TLCP orientation.

1.3.2 Post-Processing of TLCP/PP Strands from the Dual Extruder

Composite strands from the dual extruder can be post-processed in ordered to produce many final parts with varying geometries. As a final product, the strands are somewhat limited in use due to their geometry. In order to construct other useful parts, the strands need to undergo a post-processing step. They can be post-processed as a solid filled system, where the composite is processed just above the T_m of the matrix and below the T_m of the TLCP reinforcement. Thus, the excellent orientation of the TLCP can be retained in the final part geometry because the reinforcement is not melted.

The TLCP/PP strands were reprocessed using compression molding, injection molding, and film extrusion. Sabol [34, 35] consolidated HX1000/PP (29/71 wt%) strands into uniaxial plaques at 190°C. The tensile modulus and strength of the strands were 12.6 GPa and 62.2 MPa, respectively. After consolidation, the properties were similar, 13.6 GPa and 67 MPa, respectively. Robertson [76] performed a similar study with Vectra B950/PP. The T_g and T_m of Vectra B are 110°C and 280°C, respectively. There was no loss in properties when consolidated just above the T_m of PP and above the T_g of Vectra B. Therefore, HX1000 and Vectra B do not undergo significant molecular relaxation when exposed to temperatures that are needed to consolidate the PP matrix.

Handlos injection molded pelletized Vectra A950/PP/MAP (20/72/8) microcomposites at 190°C [80]. The mechanical properties in the machine and transverse directions were found to be similar. The machine direction modulus and strength were 2.31 GPa and 37.6 MPa, respectively, and the transverse properties were 2.18 GPa and 21.6 MPa, respectively. However, the modulus of the injection molded plaques was less than that predicted theoretically (Table 1.3) [36]. It was found that pregenerated strands with increasing TLCP concentration after injection molding exhibited greater deviations from theoretical predictions as calculated from equation 5. Pregenerated strands produced at increasing draw ratios from the dual extruder after injection molding also exhibited greater deviations from the theoretical properties. These deviations from ideality were attributed to three possibilities: The aspect ratio of the reinforcement may have been less than 100; poor fibril distribution was observed in the plaques and may have resulted in agglomeration of the fibrils or may have lead to a reduction in the effective aspect ratio; and there may have been a loss in molecular orientation in the TLCP fibrils.

Table 1.3 : Comparison of the tensile modulus of injection molded PP (10 wt% MAP)/Vectra A and PP (10 wt% MAP)/HX6000 composites versus the calculated values provided by composite theory [36].

		Theoretical Modulus (GPa) PP/VA	Theoretical Modulus (GPa) PP/HX	VA Machine Direction Modulus (GPa)	HX Machine Direction Modulus (GPa)
10 wt% TLCP	LDR	1.53	1.92	1.47 (0.066)	2.06 (0.10)
	MDR	2.04	2.11	1.97 (0.082)	2.22 (0.11)
	HDR	2.21	2.25	2.11 (0.11)	2.45 (0.25)
20 wt% TLCP	LDR	2.45	3.13	2.07 (0.22)	2.43 (0.16)
	MDR	3.43	3.61	2.29 (0.21)	2.89 (0.073)
	HDR	3.85	4.08	2.31 (0.18)	3.23 (0.26)
30 wt% TLCP	LDR	2.50	3.89	2.59 (0.21)	3.20 (0.21)
	MDR	4.31	4.56	2.79 (0.30)	3.78 (0.21)
	HDR	4.89	5.20	3.18 (0.37)	3.98 (0.25)

For Vectra A (VA) composites: LDR = 4.7, MDR = 20, and HDR = 30
For HX6000 (HX) composites: LDR = 4, MDR = 13.5, and HDR = 25
Standard deviations given in parentheses.

Krishnaswamy and Xue [23] similarly injection molded pregenerated microcomposites of HX8000/PP (60/40). Strands were pelletized at a draw ratio of 3, and injected into an end-gated mold. It was determined, when processed at temperatures (temperature settings 150°C/ 170°C/ 175°C/ 180°C) just above the melting point of the matrix, the moduli in the machine and in the transverse direction were 3.7 GPa and 3.5 GPa, respectively. These values were within experimental error of the theoretical modulus (4.0 GPa) predicted by the rule of mixtures for

random orientation in the plane (Equation 5). The strengths in the machine and transverse direction were 36 MPa and 30 MPa, respectively. At slightly higher temperatures (160°C/ 175°C/ 185°C/ 195°C) the moduli for the machine (3.8 GPa) and transverse direction (3.0 GPa) were comparable to those above. The strengths in the machine and transverse direction were 39 MPa and 27 MPa, respectively. Thus slightly higher temperatures resulted in increases in anisotropy. At higher temperature settings (160°C/ 220°C/ 220°C/ 220°C and higher) both the strengths and moduli in the machine and transverse direction decreased. These results are probably due to molecular relaxation and greater fibril deformation. Microcomposites were also pelletized from strands of higher draw ratios (20 and 47) which had greater tensile properties. The moduli of the pregenerated plaques decreased in both the machine and the transverse direction when using these high draw ratio microcomposites. The tensile strength remained constant in the machine direction, while increasing in the transverse directions. The reason for these trends from the higher draw ratio pelletized microcomposites is not clear.

Pregenerated microcomposite pellets generated from the dual extruder were re-extruded as films. The properties were similar to those reported by Handlos [36, 79] for pregenerated injection molded plaques. The moduli were found to increase with increasing composition and draw ratio, and they were found to have similar properties in the machine and transverse direction. However, their properties were less than the properties predicted by theory for random orientation in the plane. 20 wt% and 30 wt% TLCP blends were extruded with two different TLCPs. The experimental moduli of the Vectra A/PP blends were 25%-40% less than the theoretical results, and the theoretical moduli of the HX6000/PP blends were 175%-200% of the actual results. The poor properties were attributed to an uneven distribution of the TLCP reinforcement in the film as a result of insufficient mixing and to agglormeration of the reinforcing fibrils.

Strands from the dual extruder have been post-processed with reasonable success. Some TLCP/PP systems have excellent retention of properties during compression molding. The microcomposite resins are also able to overcome the anisotropy of traditional in situ injection molding and film extrusion. However, there is difficulty in obtaining the theoretical mechanical properties after post-processing of high draw ratio strands.

1.4 Research Objectives

1.4.1 Research Objective #1

The TLCP/thermoplastic strands generated by means of the dual extrusion process have demonstrated excellent mechanical properties. In order to obtain more useful geometries, there has been interest in a post-processing step to reform the strands into other final products. This post-processing step has included compression molding, injection molding, and extrusion. These steps have had difficulty in obtaining the optimal reinforcement, which has been attributed to

agglomeration, fibril break, and insufficient mixing. Due to the complexity of post-processing pregenerated composites, it is difficult to know what processing parameters cause a reduction in mechanical properties. In order to isolate the effects of differing parameters, the first objective is:

a) to determine the effects of thermal history on the tensile properties of Vectra A/PP pregenerated composite strands in the absence of a flow field, and to discern the reason for a reduction in tensile properties.
b) to determine the effects of the flow field through a capillary die on the tensile properties of Vectra A/PP pregenerated composite strands, and to discern the reason for a reduction in tensile properties.

1.4.2 Research Objective #2

In order to have a commercially viable resin, it must be able to be readily processed into well controlled parts, with consistent mechanical and dimensional properties. One of the most common processes is the extrusion of continuous parts. Materials for this process should produce complex cross-sections with limited die swell to insure dimensional precision, form a smooth surface, and consistently produce the same part. This criterion is dependent on the resin and the processing conditions. With these considerations, the second objective is:

to develop a process to produce well controlled continuous cross-sections from pregenerated microcomposite resins from the dual extrusion assembly, and to determine the effects of the processing conditions on the final properties of the cross-section.

1.4.3 Research Objective #3

When developing new equipment it is often beneficial to build a working model before the product is mass produced. In order to learn as much as possible, prototypes are often constructed. However, they are only replicas of the final product and are not fully functional models. The mechanical properties of the materials used to construct these replicas are not acceptable for a functional model. Presently there are a limited number of polymeric materials that are used in rapid prototyping applications, and they were developed for this use due to their ease of processing, not for their mechanical performance. Hence, few high performance polymeric materials have been studied to date. The third objective is:

to determine the feasibility of using Vectra A and Vectra A/PP pregenerated composite strands from the dual extrusion assembly in a fused deposition modeling process (FDM 1600 rapid prototyping system), and to determine the effects of processing temperature, Vectra A concentration, and lay-down pattern on the tensile properties of the final parts

The subsequent two chapters of this thesis will be presented in manuscript form and will contain the results of the research that was necessary to complete the above objectives.

---

1 M. Burns, Automated Fabrication, P T R Prince Hall, New Jersey 1993.
2 L. Wood, Rapid Automated Prototyping: An Introduction, Industrial Press Inc., New York 1993.
3 J. L. Johnson, Principles of Computer Automated Fabrication, Palatino Press, Inc., Irvine 1994.
4 R. S. Crockett, J. O'Kelly, P. D. Calvert, B. D. Fabes, K. Stuffle, P. Creegaan, and R. Hoffman, Solid Freeform Fabrication Symposium, 1995.
5 E. Fordan, M. Koch, and U. Menon, Solid Freeform Fabrication Symposium, 1996.
6 P. Calvert, R. Crockett, J. Lombardi, J. O'Kelly, K. Stuffle, Solid Freeform Fabrication Symposium, 1994.
7 A. I. Isayev, in Liquid-Crystalline Polymer Systems Technological Advances, ed. A. I. Isayev, T. Kyu, and S. Z. D. Cheng, American Chmical Society, Washington D.C. 1996.
8 R. R. Luise, in Polymer Materials Encyclopedia, Ed. J. C. Salamone, CRC Press, Boca Raton 1996.
9 G. Marrucci, Thermotropic Liquid Crystal Polymer Blends, Ed. F. P. La Mantia, Technomic Publishing Co., Inc., Lancaster PA 1993.
10 G. Vertogen and W. H. deJeu, Thermotropic Liquid Crystals, Fundamentals, Springer-Verlag, New York 1988.
11 J. H. Wendorff, Liquid Crystalline Order in Polymer, ed. Alexandre and Blumstein, Academic Press, Inc., New York 1978.
12 A. A. Sonin, The Surface Physics of Liquid Crystals, Gordon and Breach, United States, (1995).
13 D. S. Kalika, PhD Dissertation, University of California at Berkley, Berkley (CA) 1988.
14 Tai-Shung Chung, *Polym. Eng. and Sci.*, 26, 901 (1986).
15 K. G. Blizard and D. G. Baird, *Polym. Eng. and Sci.*, 27, 653, (1987).
16 Y. Ide and Z. Ophir, *Polym. Eng. and Sci.*, 23, 261 (1983).
17 A. Kohli, N. Chung, and R. A. Weiss, *Polym. Eng. and Sci.*, 29, 573 (1989).
18 M. A. McLeod, PhD Dissertation, Virginia Polytechnic Institute and State University, Blacksburg (VA) 1997.
19 A. Kaito, M. Kyatani, and K. Nakayama, *J. Macromol. Sci. - Phy.*, B34, 105 (1995).
20 W.- C. Lee, A. T. Dibenedetto, and J. M. Gromek, *Polym. Eng. and Sci.*, 33, 156 (1993).
21 H.- S. Moon, J.- K. Park, J.- H. Liu, *J. Appl. Polym. Sci.*, 59, 489 (1996).
22 C. Carfagna, E. Amendola, L. Nicolais, D. Acierno, O. Francesangeli, B. Yang, and F. Rustichelli, *J. Appl. Polym. Sci.*, 43, 839 (1991).
23 R. Krishnaswamy, T. Xue, and D. G. Baird, *In Preparation* (1997).
24 J. Sarlin and P. Tormala, *J. Appl. Polym. Sci.*, 40, 453 (1990).
25 S. M. Guskey and H. H. Winter, *J. Rheol.*, 35, 1191 (1991).
26 D. E. Turek and G. P. Simon, *Polymer*, 34, 2750 (1993).

27 Y. G. Lin and H. H. Winter, *Macromol.*, 24, 2877 (1991).
28 Y. G. Lin and H. H. Winter, *Macromol.*, 21, 2439 (1988).
29 J. Sarlin and P. Tormala, *J. Appl. Polym. Sci.*, 50, 1225 (1993).
30 J. Sarlin and P. Tormala, *J. Polym. Sci. Part B*, 29, 395 (1991).
31 S. B. Warner and J. Lee, *J. Polym. Sci. Part B*, 32, 1759 (1994).
32 G. Crevecoeur and G. Groeninckx, *Polym. Eng. and Sci.*, 30, 532 (1990).
33 J. C. Halpin, *Polym. Eng. and Sci.*, 16, 344 (1976).
34 E. A. Sabol, M. S. Thesis, Virginia Polytechnic Institute and State University, Blacksburg (VA) 1994.
35 E. A. Sabol, A. A. Handlos, and D. G. Baird, *Polym. Comp.*, 16, 330 (1995).
36 A. A. Handlos, PhD Dissertation, Virginia Polytechnic Institute and State University, Blacksburg (VA) 1994.
37 M. A. McLeod and D. G. Baird, *SPE ANTEC Tech. Papers*, 43, Paper #248 (1997).
38 W. J. Jackson and H. F. Kuhfuss, *J. Ploym. Sci., Polym. Chem. Ed.*, 14, 2043 (1976).
39 J.G. Plummer, in Advanced Thermoplastic Composites: Characterization and Processing, Hanser Publishers, New York 1993.
40 J. P. de Souza and D. G. Baird, *Polym.*, 37, 1985 (1996).
41 H. J. O'Donnell, PhD Dissertation, Virginia Polytechnic Institute and State University, Blacksburg (VA) 1993.
42 Y. Ide and Z. Ophir, *Polym. Eng. and Sci.*, 23, 261 (1983).
43 H. J. O'Donnell and D. G. Baird, *Polym. Eng. and Sci.*, 36, 963 (1996).
44 H. J. O'Donnell and D. G. Baird, *Inter. J. Polym. Proc.*, XI (1996).
45 M. T. Heino and J. V. Seppala, *J. Appl. Polym. Sci.*, 44, 2185 (1992).
46 Q. Lin and A. F. Yee, *Polym. Comp.*, 15, 156 (1994).
47 M. Kytani, A. Katio, and K. Nakayama, *Polymer*, 33, 4757 (1992).
48 G. Kiss, *Polym. Eng. and Sci.*, 27, 410 (1987).
49 K. G. Blizard, C. Federici, O. Federico, and L. L. Chapoy, *Polym. Eng. and Sci.*, 30, 1442 (1990).
50 Z. S. Petrovic and R. Farris, *J. Appl. Polym. Sci.*, 58, 1349 (1995).
51 J. He, W. Bu, and H. Zhang, *Polym. Eng. and Sci.*, 35, 1695 (1995).
52 A. I. Isayev and M. Modic, *Polym. Comp.*, 8, 158 (1987).
53 D. Beery, S. Kenig, and A. Siegmann, *Polym. Eng. and Sci.*, 33, 1548 (1993).
54 C. L. Choy, K. W. E. Lau, and Y. W. Wong, *Polym. Eng. and Sci.*, 36, 1256 (1996).
55 S. Metha and B. L. Deopura, *J. Appl. Polym. Sci.*, 56, 169 (1995).
56 R. A. Weiss, W. Huh, and L. Nicolas, *Polym. Eng. and Sci.*, 27, 684 (1987).
57 F. P. La Mantia, F. Cangialosi, U. Pedretti, and A. Roggero, *Eur. Polym. J.*, 29, 671 (1993).
58 D. Dutta and R. A. Weiss, *Polym. Comp.*, 13, 394 (1992).
59 T. Sun, D. G. Baird, H. H. Huang, D. S. Done, and G. L. Wilkes, *J. Comp. Mat.*, 25, 788 (1991).
60 A. M. Sukhadia, D. Done, and D. G. Baird, *Polym. Eng. and Sci.*, 30, 519 (1990).

61 F. P. La Mantia, A. Valenza, M. Paci, and P. L. Magagnini, *Polym. Eng. and Sci.*, 30, 7 (1990).
62 A. Datta, H. H. Chen, and D. G. Baird, *Polymer*, 34, 759 (1993).
63 H. J. O'Donnell, A. Datta, and D. G. Baird, SPE ANTEC Tech. Papers, 38, 2248 (1992).
64 H. J. O'Donnell and D. G. Baird, *Polymer*, 36, 3113 (1995).
65 A. Datta and D. G. Baird, *Polymer*, 36, 505 (1995).
66 B. Frazen, C. Klason, J. Kubat, and T. Kitano, *Composites*, 20, 65 (1989).
67 S. Kessler, in Plastics Additives and Modifiers Handbook (Chap. 48), ed J. Edenbaum, Van Nostrand Reinhold, New York 1992.
68 R. K. Krishnaswamy, S. E. Bin Wadud, and D. G. Baird, submitted to *Polymer*.
69 M. A. McLeod, unpublished data.
70 D. Done and D. G. Baird, *Polym. Eng. and Sci.*, 27, 816 (1987).
71 D. Done and D. G. Baird, *Polym. Eng. and Sci.*, 30, 989 (1990).
72 R. K. Krishnaswamy and D. G. Baird, *Polym. Comp.*, 17, 1 (1997).
73 S. S. Bafna, J. P. De Souza, T. Sun , and D. G. Baird, *Polym. Eng. And Sci*, 33, 808 (1993).
74 Product Literature from Hoechst Celanese.
75 D. G. Baird and A. M. Sukhadia, U.S. Patent 5,225,488 (1993).
76 C. G. Robertson, M. S. Thesis, Virginia Polytechnic Institute and State University, Blacksburg (VA) 1995.
77 A. G. C. Machiels, K. F. J. Denys, J. Van Dam, and A. Posthuma De Boer, *Polym. Eng. and Sci.*, 36, 2451 (1996).
78 A. G. C. Machiels, K. F. J. Denys, J. Van Dam, and A. Posthuma De Boer, *Polym. Eng. and Sci.*, 37, 59 (1997).
79 A. A. Handlos and D. G. Baird, *Polym. Comp.*, 17, 73 (1996).
80 A. A. Handlos and D. G. Baird, *Inter. J. Polym. Proc.*, XI, 82 (1996).

2.0 Effects of Processing Conditions on Prototypes Fabricated by FDM

This chapter focuses on the second and third objective of this thesis. Composite monofilaments were generated and used as feedstock in order fabricated parts using the FDM 1600 rapid prototyping system. This chapter is organized as a manuscript and will be submitted to *Rapid Prototyping Journal*

Effects of Processing Conditions on Prototypes Reinforced with Short Fiber Thermotropic Liquid Crystalline Polymers Fabricated via Fused Deposition Modeling

R. W. Gray IV, D. G. Baird, and J. H. Bøhn
Department of Chemical Engineering,
Department of Mechanical Engineering,
Rapid Prototyping Laboratory, and
Polymer Materials and Interfaces Laboratory
Virginia Polytechnic Institute and State University

Abstract

This work is concerned with preliminary studies on developing thermoplastic composite materials suitable for use in fused deposition modeling (FDM). Polypropylene (PP) strands reinforced with thermotropic liquid crystalline polymer (TLCP) fibrils are generated in a novel dual extruder process. The process allows one to combine PP having a melting point (T_m) equal to 165°C with a TLCP (Vectra A950) of T_m equal to 283°C to form strands with continuous TLCP fibrils. The strands were then re-extruded to form composite monofilaments that were used as feedstock in the FDM 1600 rapid prototyping system. The effects of prototype fabrication temperature, Vectra A concentration, and lay-down pattern were studied. It was found that prototypes fabricated below the melting point of the reinforcement as a solid filled system had greater tensile properties than those of prototypes fabricated above the melting point of the reinforcement. Increased Vectra A concentration was shown to increase the tensile properties of the prototypes. Prototypes containing 40 wt% Vectra A had tensile properties twice those of parts built using acrylonitrile butadiene styrene copolymer (ABS), a commercially available material used in the FDM 1600 rapid prototyping system. Pure Vectra A parts were also fabricated and shown to have tensile properties four times those of parts fabricated with ABS. It was shown that the final mechanical properties of a composite prototype can be tailored to a specific application by adjusting the lay-down pattern, increasing the functionality of the prototype and these properties could be predicted by composite theory.

2.1 Introduction

Fused deposition modeling (FDM) is one of several different rapid prototyping fabrication technologies that are being studied at present. The FDM 1600 rapid prototyping system by Stratasys, Inc. consists of an extrusion system that is able to precisely control where the extrudate is laid in three dimensional space in order to build a complex geometry prototype. Parts are fabricated in layers, where a layer is built by extruding a small bead of material, or road, in a particular lay-down pattern, such that the layer is covered with the adjacent roads. After a layer is completed, the height of the extrusion head is increased and the subsequent layers are built to construct the part.

At present, only a few polymeric materials with limited mechanical properties are used in the FDM 1600 rapid prototyping system. Many of the prototypes fabricated can only serve as geometric replicas of the proposed production part because of the inherently poor mechanical properties. The materials that are commercially available for the FDM 1600 rapid prototyping system are acrylonitrile butadiene styrene copolymer (ABS), a nylon copolymer, and investment casting wax, and of the three commercially available materials, ABS has the highest tensile modulus and strength. Therefore, there is interest in developing materials that can be used to fabricate prototypes with higher mechanical properties which give the parts greater functionality.

Thermotropic liquid crystalline polymers (TLCPs) are a novel class of materials that have potential for use in FDM applications for several reasons. First, it has been shown that TLCPs have excellent tensile properties with moduli ranging from 50 GPa to 100 GPa for neat fibers. It has also been shown that due to their excellent tensile properties and due to their fibril forming nature, TLCPs have been used to reinforce thermoplastics [1 - 3]. The diameter of the reinforcing TLCP fibrils are typically one order of magnitude smaller than those of typical glass and carbon fiber. Whereas, it may be not possible to extrude glass and carbon fibers through the die head and still maintain high aspect ratio fibers (i. e. L/D > 100) due to the small diameter capillary die used in order to fabricate dimensionally precise prototypes, this may be possible for the TLCP systems.

The final mechanical properties of TLCP based composites, where the reinforcing fibrilar morphology is developed during the processing step on an in situ basis, are directly dependent upon the processing conditions [3 - 6]. Shear and extensional flow fields during processing serve to deform dispersed TLCP droplets into reinforcing fibrils and impart molecular orientation to the fibril, which results in increased tensile properties in the direction of the flow field. This preferred orientation, of both the molecules and the fibrils, results in anisotropic mechanical properties. It is generally known that extensional flow fields develop higher aspect ratio fibrils and greater molecular orientation, and hence extensional flow yields higher tensile properties than strong shear flow. For example, 20 wt% Vectra A, a commercial TLCP marketed and sold by Hoechst Celanese, was used to reinforce polypropylene (PP), and composites that were generated via fiber spinning and injection molding had tensile moduli of 9.6 GPa and 2.6 GPa, respectively [4, 7, 8].

Therefore, in order to obtain the optimal reinforcement, strong extensional forces, such as those present in fiber spinning, are necessary.

There are two disadvantages with TLCP/thermoplastic composites where the TLCP reinforcement is generated during prototype fabrication relative to glass fiber reinforced composites: degradation and shear dominated fibril formation. Most commercial TLCPs are processed at temperatures near or above the degradation temperature of many commodity resins which precludes their reinforcement. Vectra B, for example, has a melting point of 280°C and processes at approximately 320°C [9]. PP can be processed above 260°C, but this can lead to increased degradation [10]. Engineering thermoplastics can be used as matrix, but they are generally much more expensive. Secondly, in the case of the FDM 1600 extrusion head, the flow field present during fabrication is similar to that of extrusion without draw down which is dominated by shear flow. The tensile properties of TLCP reinforced prototypes are expected to be similar to those of extruded TLCP reinforced composites and less than those of injection molded TLCP reinforced composite because some extensional stresses are present during injection molding.

In order to overcome the problems associated with processing the blends directly, the formation of pregenerated microfibrils was considered using a novel dual extrusion process [9, 11, 12]. In the dual extrusion process, the thermoplastic and TLCP are plasticated in separate extruders so that independent thermal histories are imposed on the two materials. TLCP is heated to sufficiently high temperatures to fully melt all of the crystallites. For example, the melting point of Vectra A is 283ºC, but it needs to be heated to 320ºC in order to fully melt all the residual crystallites [13]. Vectra A is then supercooled to the temperature at which the matrix is processed and using a multiple-port injection nozzle, is then injected into the matrix stream which results in continuous TLCP streams encapsulated within the matrix. The melt is passed through a series of static mixers which serve to divide the TLCP into fine streams before being extruded through a capillary die and drawn in the spinline to high draw ratios. The high draw ratios lead to high levels of molecular orientation in the TLCP fibrils.

There are several advantages of the dual extrusion process over generating TLCP fibrils in situ during FDM. Processing the TLCP in a separate extruder minimizes degradation of the matrix because the matrix is not exposed to the high temperatures that are necessary to fully melt the TLCP. The TLCP is supercooled before being injected into the matrix minimizing the degradation of the matrix. The dual extrusion process does not rely on droplet deformation because the multiple-port injection nozzle introduces continuous TLCP streams into the matrix, resulting in high aspect ratio fibrils. Finally, the composite strands can be post-processed above the melting point of the matrix and below the melting point of the TLCP using a variety of conventional processing techniques (e.g., FDM) which allow for the retention of the TLCP reinforcing fibrils generated during the dual extrusion process in the final part [7 - 9, 12, 14 - 20].

Post-processing of composite strands above the melting temperature of the matrix and below the melting temperature of the TLCP is critical to transforming the composite strands into

final parts while retaining the reinforcement achieved in the original strands. The strands have been post-processed using several conventional processing techniques: compression molding, injection molding, film extrusion, and blow molding. Composite strands have been uniaxially compression molded, and tensile properties of the consolidated plaques have been shown to agree with those predicted by composite theory [9, 12, 14, 15, 17]. The mechanical properties of the injection molded plaques, films, and bottles were lower than those calculated by composite theory, but the properties had greater isotropy in the plane than those of parts where the reinforcement was generated in situ [18 - 20]. The deviations from composite theory were attributed to three possibilities. The aspect ratio of the reinforcement may have been less than 100 due to agglomeration of the fibrils or fibril breakage in the screw extrusion process. Poor fibril distribution was observed in the plaques and may have been the result of agglomeration of the fibrils or insufficient mixing. There may have been a loss in molecular orientation in the TLCP fibrils.

The purpose of this work is to determine the feasibility of using TLCP reinforced thermoplastics in FDM. More specifically, it is our goal to determine the feasibility of post-processing TLCP composite strands generated by means of the dual extrusion process using FDM for the purpose of enhancing the tensile properties and the functionality of prototypes. Composite strands spun using the dual extrusion process are re-extruded via a second novel process to generate monofilament feedstock necessary for the FDM 1600 rapid prototyping system. During this second process, the strands are extruded at temperatures just above the melting point of the matrix and below the melting point of the reinforcement, in order to retain the tensile properties generated in the dual extrusion process. The effects of TLCP concentration, prototype fabrication temperature, and lay-down pattern on the tensile properties and on the morphology of the prototypes are evaluated. The tensile properties of the composite prototypes are compared to those of ABS, the commercially available feedstock with the greatest mechanical properties. Pure TLCP parts are also fabricated, and the effects of lay-down pattern on the tensile properties are discussed.

2.2 Experimental

2.2.1 Materials

Three polymeric materials were is this work. The TLCP used was Vectra A950 (Hoechst Celanese). It is a random copolyester based on hydrobenzoic acid (73% mole) and 2-hydroxy-6-napthoic acid (27% mole). It has a glass transition temperature of 108°C and a melting point of 283°C [21]. However, Vectra A needs to be heated to 320°C to melt out all of the residual crystallites [13]. Prior to spinning, the Vectra A was dried at least 18 hours in a forced convection oven set at 150°C. The matrix material used was the 4018 grade of Amoco polypropylene (PP). It has a melting point of 160ºC and a melt flow index (MFI) of 13.5 [22].

P400 grade of acrylonitrile butadiene styrene copolymer (ABS) monofilaments were obtained from Stratasys, Inc., and they were dried by storing with desiccate for several weeks prior to use.

2.2.2 Spinning of TLCP/PP Composite Strands

The novel dual extrusion process was used to spin self-reinforced composite strands. The dual extrusion process has been described in detail elsewhere [11, 12]. Vectra A and PP were plasticated separately in two Killion KL-100 extruders (1 inch single screw extruders with L/D=24) where the metering zone temperatures of the TLCP and PP extruders were set at 325°C and 245°C, respectively. The TLCP mass flow rate was controlled by metering it into the PP stream using a Zenith gear pump (model number 6135419-001 and 1.725 cc/rev). The TLCP was injected into the matrix as continuous streams via a multiple-port injection nozzle. The melt passed through a series of three Kenics and four Koch mixing elements that served to split the TLCP streams. The melt was then extruded through a capillary die with a diameter of 1.8 mm and a L/D of 1. The filaments were drawn through a 3.7 m long drawing chimney before being quenched in water and taken up on a constant speed godet. The draw ratio, estimated as the ratio of cross-sectional area of the capillary to that of the fiber, was greater than 70. The composition was determined from the total mass flow rate and the Vectra A mass flow rate.

2.2.3 Monofilament Feedstock Production

In order to generate monofilaments for use in the FDM 1600 rapid prototyping system, the composite strands had to be re-extruded because the diameter of the monofilament needed to be 1.7 mm. The pelletized strands, however, would not feed directly into the extruder. Therefore, the composite strands from the dual extrusion process were consolidated into plaques using a Carver hot press (model number 2696) with the temperature set at 180°C. The strands, cut to approximately 6 cm in length, were laid randomly into a preheated picture frame mold (228 mm by 228 mm), and the mold was placed in the press for 6 minutes and subjected to 1 MPa of pressure. The sample was then quenched in a water-cooled press where the cooling rate was determined to be approximately 20°C per minute. The plaques were then granulated using a Cumberland 6x8 granulator, with a screen having 6.3 mm diameter holes. The granules were fed into a Killion KL-100 extruder (1 inch single screw extruder with L/D=24) and extruded through a capillary die with a diameter of 1.6 mm and a L/D of 4 with no draw imposed. The screw speed was less than 10 RPM, and the melt temperature was 177°C.

Pure Vectra A monofilaments with the similar diameters were also extruded for FDM applications. They were similarly generated using a Killion KL-100 extruder, where the screw speed was approximately 3 RPM, and the melt temperature was 317°C.

2.2.4 Part Production using FDM

The FDM 1600 rapid prototyping system from Stratasys, Inc. was used to extrude monofilament feedstock in order to fabricate parts (Figure 2.1). Solid monofilament feedstock was forced into the ram extruder using drive motors located at the rear of the head at an approximate mass rate of 3.0 mg/sec. Once in the ram extruder (diameter approximately 1.8 mm and length 105 mm), the feedstock was immediately heated to the temperature of the ram extruder. The resonance time of the material in the ram extruder was approximately 90 seconds if the drive motors were constantly feeding material. However, if the second extruder was being used to generate support structures for the model material, the resonance time of the model material could be up to an hour depending on the amount of the support material that was required. In the case of this research the resonance time of the modeling material was less than five minutes.

Parts were fabricated using the FDM 1600 rapid prototyping system. Monofilaments generated by the afore-mentioned procedure were used as feedstock and were extruded through a 0.6 mm capillary die with a L/D of 2 (apparent shear rate = 111 1/sec) laying a road approximately 0.25 mm high and 0.76 mm wide. Plaques were constructed in the shape of a rectangular prism with an approximate height of 2.0 mm, width of 7.6 mm, and length of 76 mm. Due to the excellent melt strength of the TLCP reinforced materials, the extrudate would not easily cleave from the die of the FDM 1600 rapid prototyping system upon the completion of a road. To avoid this problem, software was developed to generate a tool path for the FDM 1600 rapid prototyping system in which the entire part was generated from a single continuous road. Each of the parts in this investigation was fabricated using one continuous path.

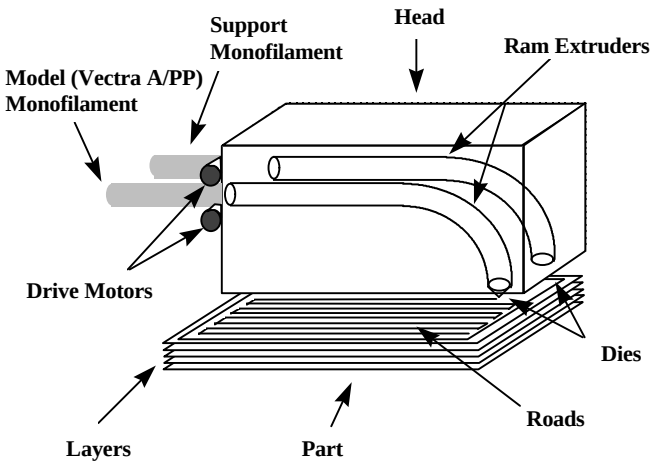

Figure 2.1 : The Extrusion Assembly of the FDM 1600 Rapid Prototyping System.

Plaques were fabricated using three different lay-down patterns: uniaxial in the machine direction, uniaxial in the transverse direction, and in a 0-90 lay-down pattern (Figure 2.2). The machine direction will be referred to as the direction of the length dimension. When fabricating parts that were generated uniaxially in the machine direction, the roads were laid parallel to the length direction. When fabricating plaques uniaxially in the transverse direction, the material was laid perpendicular to the length direction. When generating parts using the 0-90 lay-down pattern, the above two patterns were both employed, and they were alternated every second layer.

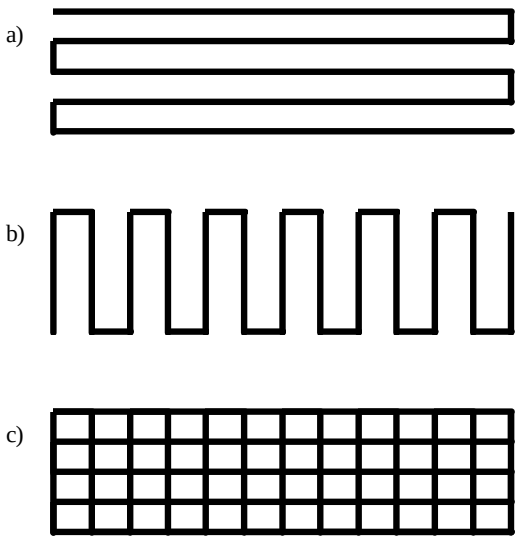

Figure 2.2 : Plaques were fabricated using three different lay-down patterns: a) uniaxial in the machine direction b) uniaxial in the transverse direction, and c) 0-90 lay-down pattern.

2.2.5 Mechanical Properties

The tensile modulus and strength were measured using an Instron Mechanical Tester (model 4204) following the ASTM standard D 638-87b. The test samples were approximately 7.6 mm wide, 2.0 mm thick, and the gage length was 30.5 mm. The load was measured with a 5 kN load cell, and the strain was measured using an extensiometer (Instron model 2630-25), while the crosshead speed was kept at 1.27 mm/min. For all tests, the average and the standard deviation were calculated from at least five samples, and data points greater than 2 standard deviations from the mean were removed.

2.2.6 Scanning Electron Microscope

Cross sections of plaques were fractured after being placed in liquid nitrogen for 5 minutes. The surfaces were gold coated using an Edwards sputter coater (model S150B). Micrographs were then taken using a Cambridge Stereoscan Model 100 scanning electron microscope operating at 20 kV.

2.3 Results and Discussion

The results of this research are arranged as follows. The tensile properties of ABS plaques fabricated from commercially supplied feedstock are reported in order to indicate the maximum tensile properties of prototypes fabricated from commercially available materials and to establish a basis for comparison with the tensile properties of Vectra A composite prototypes. A novel process is introduced for the generation of Vectra A reinforced composite monofilaments for use in the FDM 1600 rapid prototyping system. The effects of Vectra A concentration, fabrication temperature, and lay-down pattern on the tensile properties of the composite plaques are evaluated, and these properties are then compared to those of ABS plaques.

2.3.1 Fabrication of ABS Parts

In order to establish a basis of comparison and determine the maximum tensile properties of prototypes that can presently be fabricated via the FDM 1600 rapid prototyping system, plaques are fabricated from commercially supplied ABS feedstock. Specifically, the effects of the lay-down pattern on the tensile properties of ABS prototypes are evaluated.

ABS plaques were fabricated via the FDM 1600 rapid prototyping system using three different lay-down patterns: uniaxial in the machine direction, uniaxial in the transverse direction, and in a 0-90 pattern. When building plaques using the 0-90 lay-down pattern, the direction in which the road was laid was alternated every second layer. The temperature of the extrusion head was set to the recommended fabrication temperature of 270°C. In Figure 2.3, the tensile modulus and strength if ABS are shown as a function of lay-down pattern. The abscissa is defined as the volume percent of material laid in the machine direction. Thus, plaques fabricated entirely in the transverse direction had 0 vol% laid in the machine direction, and parts with 0-90 lay-down patterns had 50 vol% laid in the machine direction, and parts built uniaxially in the machine direction had 100 vol% of the material laid in the machine direction. The moduli of the ABS plaques were approximately 1.5 GPa and showed no clear dependence on the lay-down pattern, indicating that the tensile properties of the plaque were isotropic. This would be expected for parts fabricated from ABS because the material does not readily orient during processing. The strength of the plaques increased monotonically from 17.0 MPa to 22.4 MPa with increasing volume percent of material laid in the machine direction. The lower properties were observed when layers were laid in the transverse direction and were attributed to the weld lines between adjacent roads laid in the transverse direction.

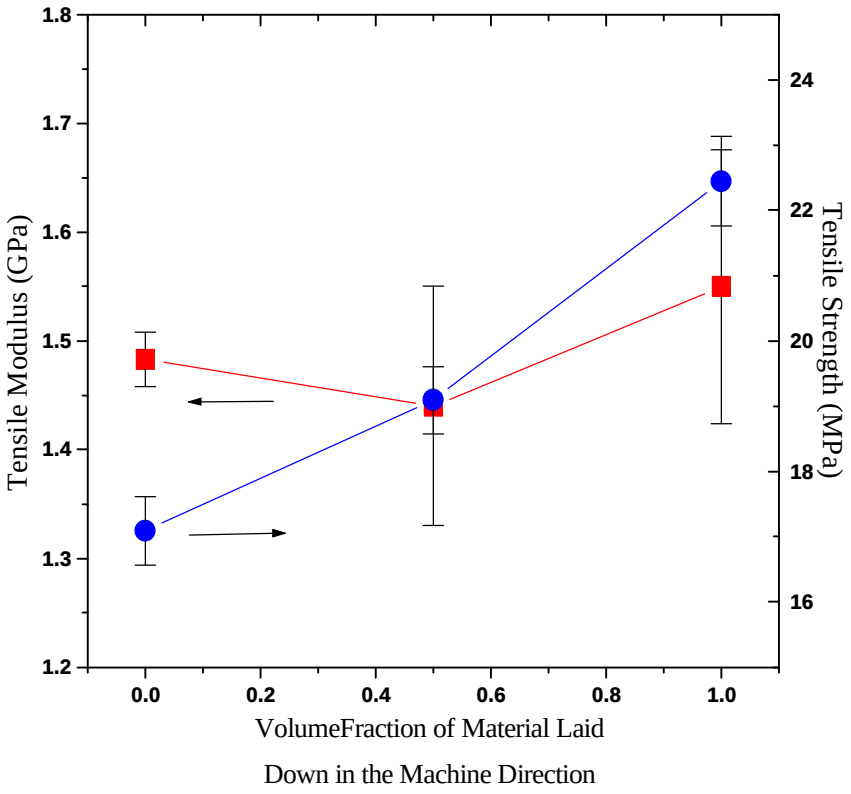

Figure 3 : Tensile modulus (– ■ –) and strength (– ● –) of ABS plaques as a function of lay-down pattern.

In Figures 2.4a and 2.4b cross sections are shown of an ABS plaque fabricated uniaxially in the machine direction and of an ABS plaque fabricated in the 0-90 lay-down pattern, respectively. The roads in the uniaxially aligned plaque were packed in a square array, and incomplete packing resulted in voids between the adjacent roads and adjacent layers. These voids were attributed to premature solidification of the material during fabrication. ABS plaques built using the 0-90 lay-down pattern had voids similar to those present in plaques built in a uniaxial lay-down pattern, where the voids were parallel to the roads of that particular layer.

a)

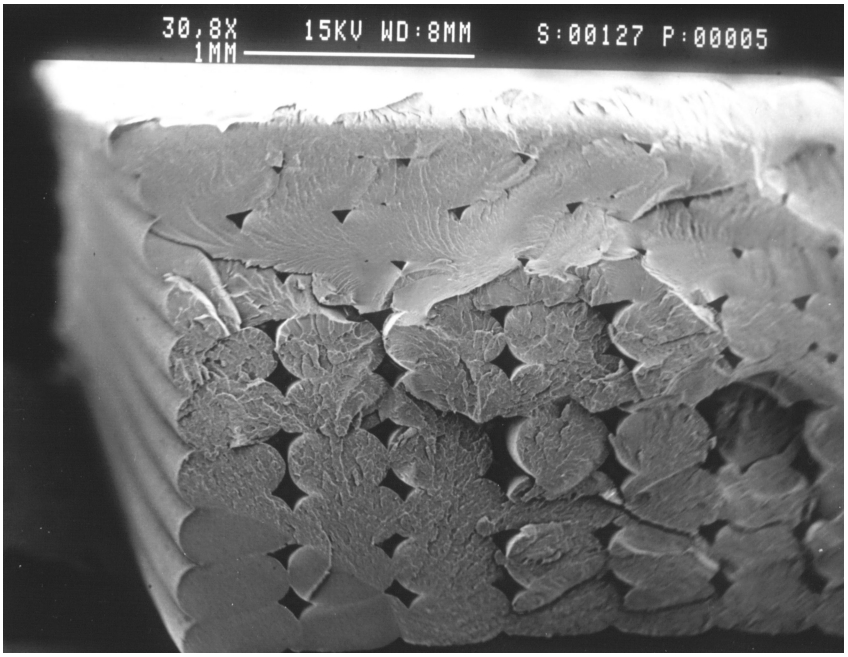

b)

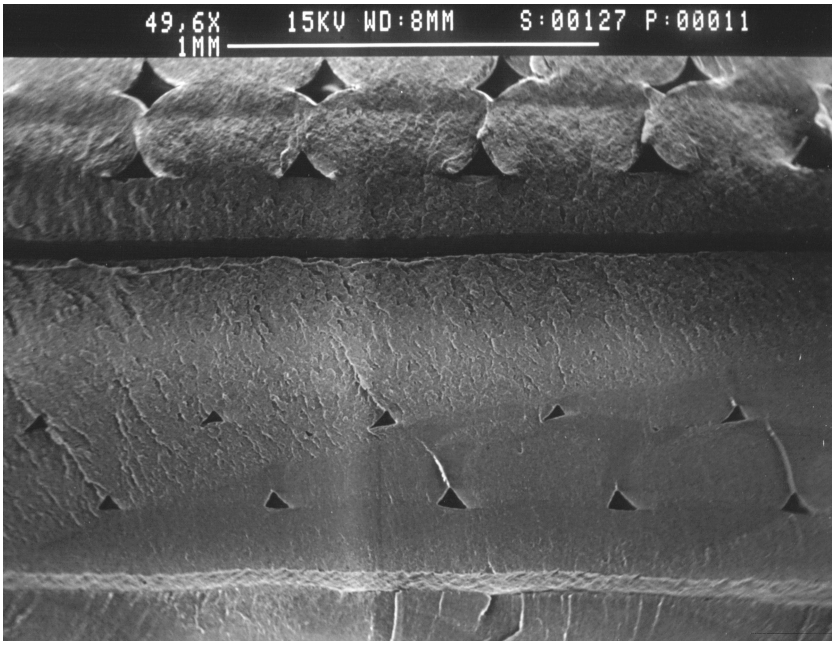

Figure 2.4 : Micrographs of ABS plaques fabricated via the FDM 1600 rapid prototyping system using two different lay-down patterns, a) uniaxial in the machine direction and b) in a 0-90 lay-down pattern.

The tensile properties of the ABS plaques were compared to the tensile properties of the ABS monofilament feedstock. ABS monofilament used in the FDM 1600 rapid prototyping system was found to have a tensile modulus and strength of 2.07 GPa and 25.3 MPa, respectively. The tensile modulus and strength of the ABS plaques fabricated uniaxially in the machine direction were 1.55 GPa and 22.4 MPa, respectively, which were 75% and 88%, respectively, of those of the monofilament. A reason for some of this reduction in properties was the presence of voids in the plaques. The void space determined by density measurements was found to be approximately 13%. Therefore, the tensile properties of the plaques were probably lower than the bulk properties impart due to voids that were formed during part fabrication.

2.3.2 Novel Process for Generation of Composite Feedstock for FDM

In this section, a novel two step process used to generate composite monofilaments for use in the FDM 1600 rapid prototyping system is described. First the generation of composite strands from the dual extrusion process is discussed, and then the process used to extrude composite monofilaments necessary for the FDM 1600 rapid prototyping system is detailed. Finally, the tensile properties of the composites are evaluated.

In order to develop new materials for use in the FDM 1600 rapid prototyping system that could be used to fabricate prototypes with greater mechanical properties and greater functionality than those presently available, self-reinforced thermoplastic composite strands were generated using a novel dual extrusion process. Vectra A, a TLCP know for its exceptional mechanical properties, was used as the reinforcing phase, and PP served as the matrix. Vectra A/PP strands were spun with 20 wt% and 40 wt% TLCP concentrations, and the moduli of the strands were 9.55 GPa and 22.8 GPa, respectively. Further results concerning the properties of these strands are given elsewhere [7, 8].

Strands from the dual extrusion process were then granulated and re-extruded to form monofilaments with a diameter of 1.6 mm for use in the FDM 1600 rapid prototyping system. In Table 2.1, the tensile properties of the composite strands and the re-extruded composite monofilaments are shown. The Vectra A reinforcement in the re-extruded monofilaments resulted in an increase in modulus of approximately 100% over those of neat PP, while having similar strengths. The tensile properties of the monofilaments, however, were significantly lower than those of the strands generated by means of the dual extrusion process. Previous work has shown that these lower properties were probably due to a reduction in aspect ratio, poor fibril distribution, and poor fibril alignment [7, 8, 18].

Table 2.1: Tensile Properties of PP and PP/Vectra A composites.

	Tensile Modulus GPa	Tensile Strength MPa
PP [9]	0.98 (0.18)	23.2 (3.9)
Vectra A/PP (20/80 wt%) Strands from the dual extrusion process	9.55 (0.55)	116 (16)
Vectra A/PP (20/80 wt%) re-extruded monofilaments	1.9 (0.14)	25.6 (1.3)
Vectra A/PP (40/60 wt%) Strands from the dual extrusion process	22.8 (1.6)	321 (39)
Vectra A/PP (40/60 wt%) re-extruded monofilaments	2.2 (0.13)	21.1 (2.3)

(one standard deviation)

2.3.3 Plaque Fabrication via FDM

In this section, processing conditions of composite prototypes generated via the FDM 1600 rapid prototyping system are evaluated in order to discern their effects on the tensile properties of the prototype. First, the dependence of mechanical properties on the processing temperature during part fabrication is examined for composites with varying Vectra A compositions, and the tensile properties of the plaques fabricated above and below the melting point of the reinforcement are compared. Second, the tensile properties of the composite parts fabricated at temperatures below the melting point of the reinforcement are correlated with the lay-down pattern. Finally, the tensile properties of parts that were fabricated using neat Vectra A are related to the lay-down pattern. The effects of these processing conditions on the mechanical properties of the composite prototypes are examined in order to fabricate parts with greater mechanical properties giving them greater functionality.

Vectra A/PP monofilaments were used as feedstock to fabricate plaques via FDM, and the effects of fabrication temperature on the tensile properties of the final part were examined. Monofilaments with 20 wt% and 40 wt% Vectra A were used to build parts with a lay-down pattern aligned uniaxially in the machine direction. In Figure 2.5, the tensile modulus is shown as a function of fabrication temperature for both the 20 wt% and 40 wt% Vectra A composite parts. Plaques with 20 wt% Vectra A reinforcement were fabricated at processing temperatures of 190°C, 240°C, and 290°C. The moduli of these plaques were essentially independent of processing temperatures and were approximately 1.6 GPa, even above the melting point of the reinforcement. The 40 wt% Vectra A monofilaments were processed at 240°C and 290°C, and the moduli of the plaques were 2.7 GPa and 2.4 GPa, respectively. Thus the moduli of the fabricated plaques decreased somewhat when processed above the melting point of the reinforcement. Parts were not fabricated at 190°C for the 40 wt% Vectra A composite because

the FDM 1600 rapid prototyping system was unable to generate the pressure required to extrude the composite.

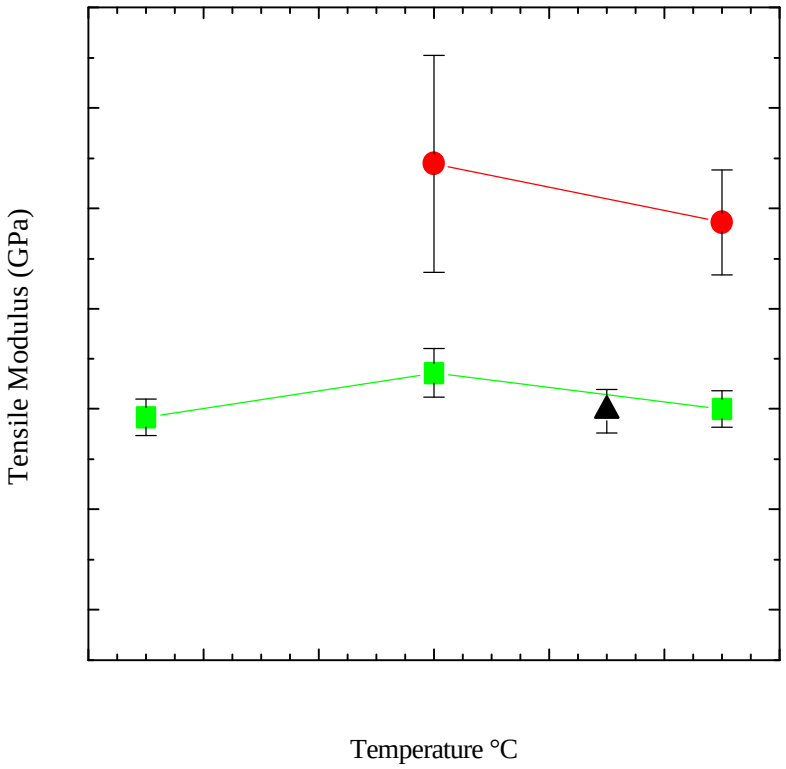

Figure 2.5 : Tensile modulus of Vectra A/PP (20/80 wt%) (—■—) and (40/60 wt%) (—●—) and ABS (—▲—) plaques built uniaxially in the machine direction as a function of fabrication temperature.

In Figure 2.6, the tensile strength is shown as a function of fabrication temperature. The strengths of both the 20 wt% and 40 wt% Vectra A reinforced plaques decreased by approximately one third when processed at 290°C as compared to the strengths of the plaques when processed below the melting point of Vectra A. The strength of the 20 wt% Vectra A plaques decreased from approximately 33 MPa when fabricated below the melting point of the Vectra A to 21 MPa when fabricated above the melting point. Similarly, the strength of the 40 wt% Vectra A plaques decreased from 37 MPa when post-processed at 240°C to 25 MPa when extruded above the melting point of the TLCP. When processed below the melting point of Vectra A, the composite relies on the reinforcement generated in the dual extrusion process. However, when Vectra A/PP composites are processed above the melting point of the TLCP, the reinforcing fibrils are melted and orientation is lost within the TLCP phase. In the melt state, the fibrils form into droplets, and there are minimal extensional forces present in the FDM 1600 rapid prototyping system to develop the fibrilar morphology required for the optimal tensile properties. Thus, tensile properties of Vectra/PP prototypes, where reinforcement was generated in the dual extrusion process, were somewhat better than those where the reinforcement was generated during prototype fabrication.

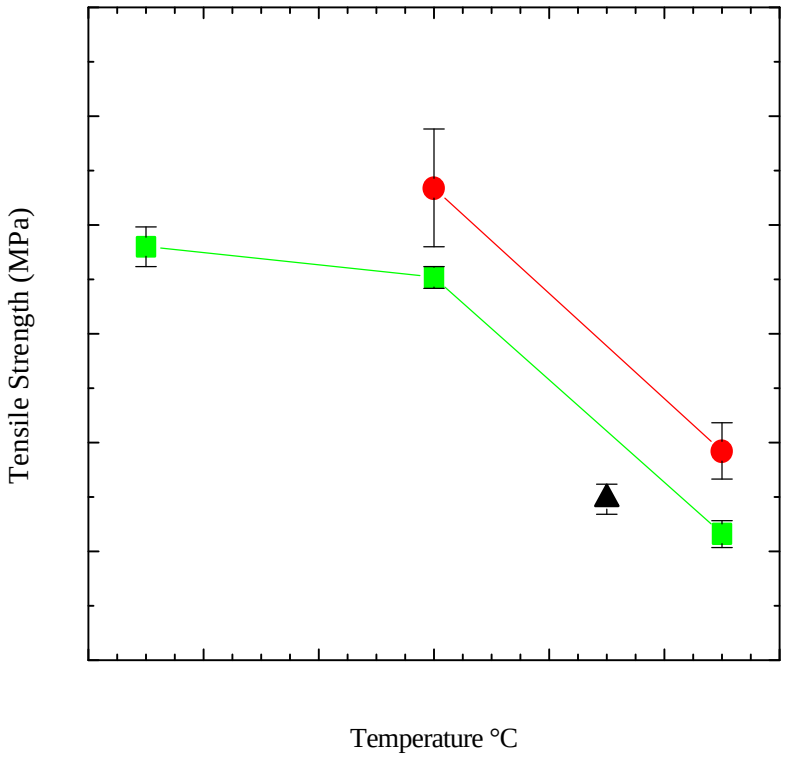

Figure 2.6 : Tensile strength of Vectra A/PP (20/80 wt%) (−■−) and (40/60 wt%) (−●−) and ABS (−▲−) plaques built uniaxially in the machine direction as a function of fabrication temperature.

The morphology of the prototypes fabricated at temperatures above and below the melting point of Vectra A are compared in Figures 2.7a and 2.7b. The cross sections of Vectra A/PP (40/60 wt%) plaques fabricated at 240°C and 290°C, respectively, are shown here and a clear change in morphology is evident. When processed at 240°C, below the melting point of the Vectra A, the fibrilar morphology of the reinforcement is evident and the fibril diameters range from 1 to 5 microns. The aspect ratio of these fibrils were estimated to be 10 from the micrograph. However, when processed above the melting point of the reinforcement, Vectra A ellipsoids, having major and minor axis ranging from 5 to 150 microns, are evident indicating that the TLCP fibrils melted and coalesced. The shear and extensional forces present in the die of the FDM 1600 rapid prototyping system were unable to effectively elongate the Vectra A domains at 290°C. Thus, the aspect ratio of the ellipsoids was less than the aspect ratio of the fibrils generated via the dual extrusion system. As indicated by composite theory, the composites with lower aspect ratios have lower moduli with equal volume percent of reinforcement [23, 24]. Therefore, the composites processed below the melting point of the reinforcement should have had significantly higher tensile properties than those of the composites processed above the melting point of the TLCP. The reason the properties of the plaques fabricated at temperatures below the melting point of the Vectra A were not similar to those of the composite strands generated by means of the dual extrusion process is probably due to fibril breakage and poor fibril alignment, during the re-extrusion of the composite strands into monofilaments [8, 18].

a)

b)

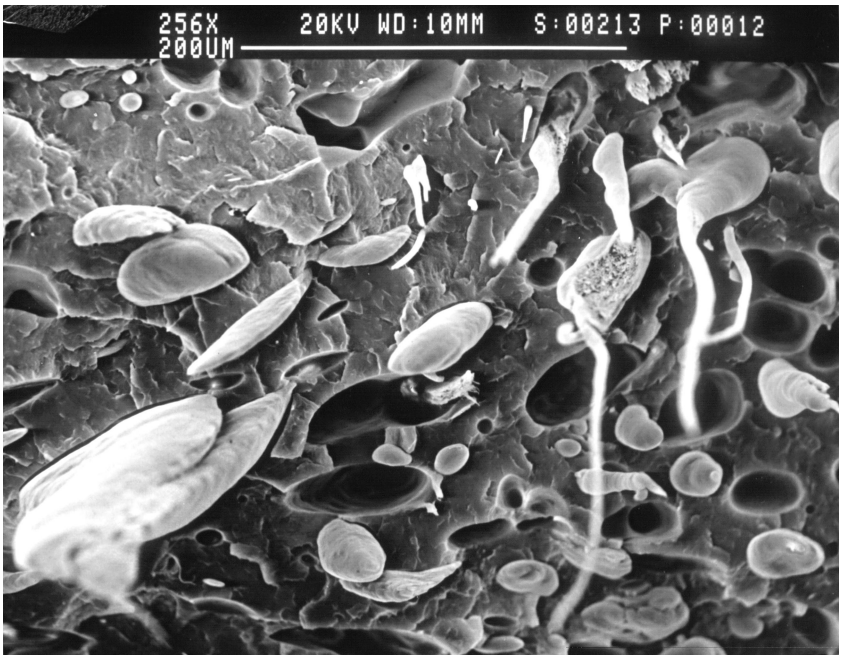

Figure 2.7 : Micrographs of Vectra A/PP (40/60 wt%) plaques fabricated the via FDM 1600 rapid prototyping system with a lay-down patterns uniaxial in the machine direction and fabricated at a processing temperature of a) 240°C and b) 290°C.

The mechanical properties of the Vectra A/PP monofilament feedstock were compared to those of the plaques fabricated via the FDM 1600 rapid prototyping system. The modulus of the 40 wt% Vectra A monofilament was measured to be 2.2 GPa. Plaques fabricated uniaxially in the machine direction at 240°C had a modulus of 2.7 GPa. Similarly, the strength of the composite increased from 21 MPa to 37 MPa in the fabricated plaque. The modulus of the 20 wt% Vectra A monofilaments and plaques was similar before and after fabrication and was approximately 1.8 GPa. The strength of the 20 wt% Vectra A monofilaments increased from 26 MPa to 33 MPa after being fabricated into a plaque. The increase in mechanical properties of the 40 wt% Vectra A composite was probably due to a change in alignment of the reinforcing fibrils as a result of the flow kinematics of the extrusion head of the FDM 1600 rapid prototyping system. It has been shown elsewhere that the tensile properties of post-processed long fiber composite strands are very sensitive to the flow kinematics of the die [7, 8]. It was shown that a critical L/D was necessary in order to obtain the optimal mechanical properties and that the extrusion rate, and die diameter can effect the tensile properties of the extrudate. Vectra A/PP (28/72 wt%) composite strands from the dual extrusion process were post-processed into monofilaments, and the maximum tensile modulus and strength were 4.0 GPa and 45 MPa, respectively. Thus, higher properties can be obtained with lower Vectra A concentrations under the proper post-processing conditions [7, 8].

Plaques were fabricated from composite monofilaments using the same three lay-down patterns used previously to fabricate ABS parts: uniaxial in the machine direction, uniaxial in the transverse direction, and a 0-90 lay-down pattern. The plaques were fabricated from the Vectra A/PP (40/60 wt%) composite monofilaments at 240°C which was the processing temperature that resulted in the greatest tensile properties for plaques fabricated uniaxially in the machine direction. In Figure 2.8, the mechanical properties are shown as a function of lay-down pattern. It is shown that both the tensile modulus and strength increased monotonically with the volume percent laid-down in the machine direction. For parts fabricated uniaxially in the transverse direction and parts fabricated uniaxially in the machine direction, the modulus increased from 1.3 GPa to 2.7 GPa, and the strength increased from 10 MPa to 37 MPa. This dependence of mechanical properties on the lay-down pattern was due to anisotropic reinforcement of the matrix by the TLCP fibrils as was observed in Figure 2.7a, and this reinforcement was aligned in the direction in which the roads were laid. This was why the greatest mechanical properties were observed in the plaques fabricated uniaxially in the machine direction. Plaques fabricated uniaxially in the transverse direction had the lowest properties because the reinforcement was aligned orthogonal to the machine direction. Thus, the bulk properties of these plaques were highly dependent on the tensile properties of the matrix. Also, the mechanical properties of a part built in the transverse direction were probably somewhat lower due to weld lines perpendicular to the machine direction. As predicted by composite theory, there was a monotonic increase in mechanical properties with increasing volume fraction laid-down in the machine direction [24]. Therefore, using composite theory, the mechanical properties of the final part can be engineered to match the requirements of the proposed prototype by adjusting the lay-down pattern.

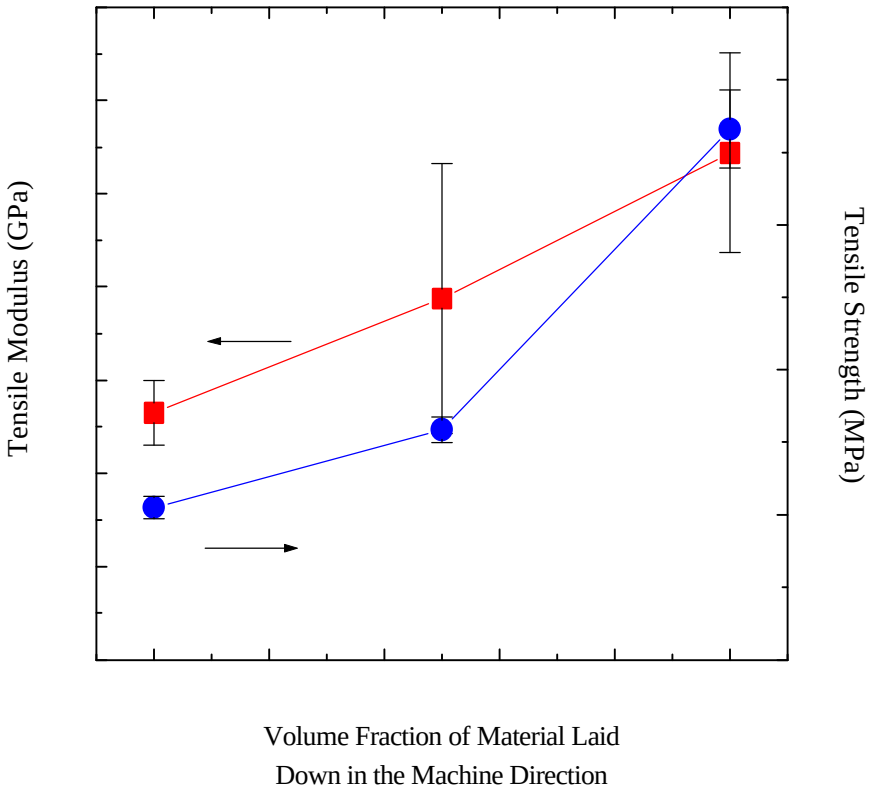

Figure 2.8: Tensile modulus (–■–) and strength (–●–) of Vectra A/PP (40/60 wt %) composite plaques fabricated via FDM as a function of volume fraction laid in the machine direction processed at 240°C.

In order to fabricate prototypes with even greater tensile properties than those of the Vectra A composites, neat Vectra A plaques were fabricated via the FDM 1600 rapid prototyping system using three different lay-down patterns: uniaxial in the machine direction, uniaxial in the transverse direction, and in a 0-90 pattern. Vectra A was processed at 300°C, the maximum temperature of the FDM 1600 rapid prototyping system, which was below the temperature necessary to melt all of the residual crystallites [13]. The tensile properties of the plaques are show in Figure 2.9 as a function of lay-down pattern. Both the tensile modulus and the strength were dependent of the lay-down pattern. The tensile moduli of the plaques with 0%, 50 %, and 100% of the material laid in the machine direction were 1.3 GPa, 6.5 GPa, and 6.1 GPa, respectively, and the strengths were 9 MPa, 66 MPa, and 87 MPa, respectively. The modulus of the samples with 50% of the material laid in the machine direction were greater than those of the samples with 100% of the material laid in the machine direction. Hence, tensile properties of the neat Vectra A parts did not increase linearly with volume percent of TLCP laid in the machine direction as predicted by composite theory and as seen in Vectra A/PP plaques. This deviation from the properties predicted by composite theory was attributed to poor adhesion between adjacent layers and adjacent roads in the plaque. It was observed that roads and layers delaminated in the neat Vectra A plaque. This was probably a result of the high solidification temperature of the Vectra A when compared to both PP and ABS. After the road was laid down, the Vectra A probably quenched to the solid state before adjacent roads and layers could adhere. If the Vectra A could have been processed above 320°C, the time from when the road was laid until the time when the material was no longer deformable, adhesion probably would have increased, due to the supercooling nature of Vectra A [25, 26]. Delamination was not evident with plaques fabricated from the Vectra A/PP, and micrographs indicate that this was due to good adhesion between the PP surface of adjacent roads.

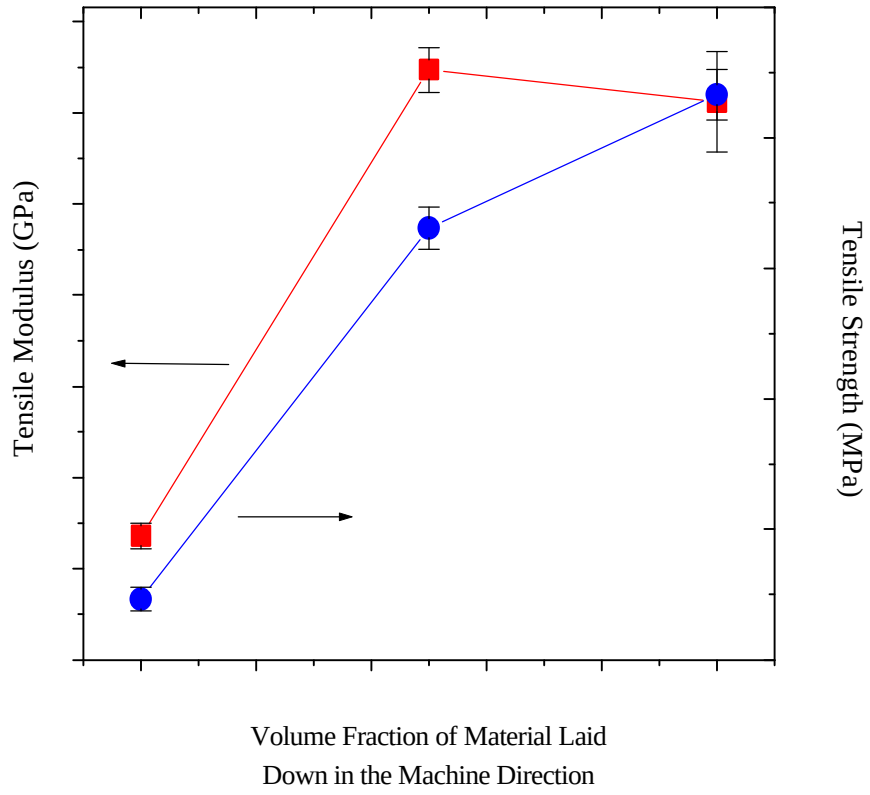

Figure 2.9: Tensile modulus (—■—) and strength (—●—) of neat Vectra A plaques fabricated via FDM as a function of volume fraction laid in the machine direction processed at 240°C.

The tensile properties of pure Vectra A plaques fabricated via FDM were compared to the maximum properties obtained for Vectra A. In order to obtain the maximum tensile properties of TLCP parts, strong extensional forces must be used to obtain high degrees of molecular orientation in the TLCP, and these forces are present during fiber spinning [5, 6]. The maximum reported modulus for pure Vectra A strands was 69 GPa while the modulus of injection molded neat Vectra A plaques was determined to be 14 GPa in the machine direction [7, 8]. The maximum modulus of neat Vectra A prototypes fabricated by FDM was approximately 6 GPa and obtained for samples fabricated using the 0-90 lay-down pattern [7, 8]. Therefore, the properties of fabricated plaques were low compared to those of Vectra A processed using other processing techniques. These results indicate that with the proper flow kinetics and with the increased adhesion between adjacent roads there is potential for the tensile properties of pure Vectra A prototypes fabricated by FDM to approach those of injected molded samples.

2.4 Conclusions

Plaques were fabricated from Vectra A/PP composites and neat Vectra A monofilaments via FDM. Because the composite material flowed readily through the 0.6 mm die on the FDM system during part fabrication with relatively low torque when compared to those ABS, it is believed that parts could be similarly fabricated with a 0.3 mm die. The tensile modulus of Vectra A/PP (40/60 wt%) composite plaques were approximately 100% greater than those of ABS and approximately 150% greater than those of pure PP, and these properties could probably be increased if long fiber reinforced composite monofilaments were used as feedstock. The tensile modulus and strength of the neat Vectra A plaques were approximately four times those of ABS. Therefore, prototypes fabricated with these materials would have greater functionality than those fabricated with ABS.

Due to the anisotropic mechanical properties present in TLCPs and TLCP composites, the lay-down pattern affected the properties of the final part. It was found that the tensile properties of Vectra A/PP composites increased monotonically with roads laid in the machine direction. Thus, the final mechanical properties of a prototype can be tailored to a specific application by adjusting the lay-down pattern, increasing the functionality of the prototype. The mechanical properties of neat Vectra A prototypes with varying lay-down patterns did not agree with the rule of mixtures. This was due to delamination of the plaque as a result of poor adhesion between adjacent roads and layers.

2.5 Acknowledgments

This research was supported by the Army Research Office (Grant No. DAAH04-94-G-0282); the Naval Surface Warfare Center, Dahlgren Division and Armstrong Laboratory, Brooks

AFB under contract N60921-89-D-A239, Order 0059; and Stratasys, Inc. Also, the authors would like to thank Prof. G. L. Wilkes for the use of the SEM and M. A. McLeod for operating it.

---

1 A. I. Isayev, in Liquid-Crystalline Polymer Systems Technological Advances, Ed. A. I. Isayev, T. Kyu, and S. Z. D. Cheng, American Chemical Society, Washington D. C. 1996.
2 D. G. Baird, in Polymeric Materials Encyclopedia, Ed. J. C. Salamone, CRC Press, Boca Raton 1996.
3 A. A. Handlos and D. G. Baird, *J. Macromol. Sci.-Rev. in Macromol. Chem. and Phy.*, C35, 183 (1995).
4 K. G. Blizard and D. G. Baird, *Polym. Eng. and Sci.*, 27, 653 (1987).
5 G. G. Viola, D. G. Baird, and G. L. Wilkes, *Polym. Eng. and Sci.*, 25, 888 (1985).
6 A. Kohli, N. Chung, and R. A. Weiss, *Polym. Eng. and Sci.*, 29, 573 (1985).
7 R. W. Gray IV, M. S. Thesis, Virginia Polytechnic Institute and State University (1997).
8 R. W. Gray IV, D. G. Baird, and J. H. Bøhn, *Polym. Comp.*, in preparation (1997).
9 E. A. Sabol, A. A. Handlos, and D. G. Baird, *Polym. Comp.*, 16, 330 (1995).
10 Himont Profax Bulletin AP-002, Himont U. S. A., Inc. (1990).
11 D. G. Baird and A. Sukhadia, U.S. Patent 5,225,488 (1993).
12 E. A. Sabol, M. S. Thesis, Virginia Polytechnic Institute and State University (1994).
13 S. M. Guskey and H. H. Winter, *J. Rheol.*, 35, 1191 (1991).
14 C. R. Robertson, M. S. Thesis, Virginia Polytechnic Institute and State University (1995).
15 C. G. Robertson and D. G. Baird, *Intern. Polym. Proc.*, in press (1997).
16 R. K. Krishnaswamy and D.G. Baird, *Polym. Comp.*, in press (1997).
17 C. G. Robertson, J. P. de Souza, and D. G. Baird, Recent Advances in Liquid Crystalline Polymers, A. I. Isayev, T. Kyu, and S. Z. D. Cheng eds., ACS Books, Washington D. C. (1996).
18 A. A. Handlos and D. G. Baird, *Intern. Polym. Proc.*, XI, 82 (1996).
19 A. A. Handlos and D. G. Baird, *Polym. Comp.*, 17, 73 (1996).
20 A. A. Handlos and D. G. Baird, *Polym. Eng. and Sci.*, 36, 378 (1996).
21 M. Y. Cao and B. Wunderlich, *J. Polym. Sci.: Polym. Phy. Ed.*, 23, 521 (1985).
22 Amoco Polypropylene Homopolymers Bulletin PP-8, Amoco Polymers, Inc. (1996).
23 G. Crevecoeur and G. Groeninckx, *Polym. Eng. and Sci.*, 30, 52 (1990).
24 J. C. Halpin, *Polym. Eng. and Sci.*, 16, 344 (1976).
25 D. Done and D. G. Baird, *Polym. Eng. And Sci.*, 27, 816 (1987).
26 D. Done and D. G. Baird, *Polym. Eng. And Sci.*, 30, 989 (1990).

3.0 Effects of Processing Conditions on Long Fiber Composites

This chapter focuses on the first objective of this thesis. The effects of thermal and shear history present during FDM are examined on the tensile properties of long fiber composite strands generated using the dual extrusion process. This chapter is organized as a manuscript and will be submitted to *Polymer Composites*.

Effects of Processing Conditions on Thermoplastic Composites Reinforced with Long Fiber Thermotropic Liquid Crystalline Polymers for Fused Deposition Modeling.

R. W. Gray IV, D. G. Baird, and J. H. Bøhn
Department of Chemical Engineering,
Department of Mechanical Engineering,
Rapid Prototyping Laboratory, and
Polymer Materials and Interfaces Laboratory
Virginia Polytechnic Institute and State University
Blacksburg, VA 24061-0211

Abstract

This work is concerned with preliminary studies on developing thermoplastic composite materials suitable for use in fused deposition modeling (FDM). Polypropylene (PP) strands reinforced with thermotropic liquid crystalline polymer (TLCP) fibrils were generated in a novel dual extruder process. The process allowed the reinforcement of PP with a melting point (T_m) equal to 165°C with continuous fibrils of a high melting (283°C) TLCP (Vectra A950). The strands were then re-extruded in a capillary rheometer forming monofilaments to simulate piston actuated FDM. The effects of the thermal and deformation histories on the mechanical properties of the re-extruded strands were evaluated. It was found that tensile properties of the strands improved with draw ratio and that the maximum modulus of the composite strands was similar to that predicted by composite theory. Strands were consolidated uniaxially via compression molding at temperatures just above the melting point of the matrix in order to determine the effect of thermal history. This resulted in approximately a 20% reduction in tensile modulus relative to the modulus of the strands. Monofilaments were extruded from a capillary rheometer in which long fiber strands were used as feedstock in order to study the effects of deformation history on the tensile properties. It was found that the tensile properties of the monofilaments were dependent on capillary diameter, capillary L/D, and apparent shear rate due to fibril alignment.

3.1 Introduction

Fused deposition modeling (FDM) is one of several different rapid prototyping fabrication technologies that are being studied at present. The FDM 1600 rapid prototyping system by Stratasys, Inc. consists of an extrusion system that is able to precisely control where the extrudate is laid in three dimensional space in order to build a prototype with a complex geometry. Using this system, a part is fabricated in layers, where a layer is built by extruding a small bead of material, or road, in a particular lay-down pattern, such that the layer is covered with adjacent roads. After a layer is completed, the height of the extrusion head is increased and subsequent layers are built to construct the part.

At present, only a few polymeric materials with limited mechanical properties are used in this style of rapid prototyping system. Many of the prototypes fabricated can only serve as geometric replicas of the proposed production part because of the inherently poor mechanical properties. The materials that are commercially available for the FDM 1600 rapid prototyping system are acrylonitrile butadiene styrene copolymer (ABS), a nylon copolymer, and investment casting wax. Of the three commercially available materials, ABS has the highest tensile modulus and strength, and the properties of prototypes fabricated using ABS have been determined to be 1.5 GPa and 22 MPa, respectively [1]. Therefore, there is interest in developing materials that can be used to fabricate prototypes with higher mechanical properties which give the parts greater functionality.

Thermotropic liquid crystalline polymers (TLCPs) are a novel class of material that have potential for use in FDM applications for two reasons. First, it has been observed that TLCP fibers have excellent tensile properties with moduli ranging from 50 GPa to 100 GPa in melt-spun fibers. Second, it has also been found that due to their excellent tensile properties and due to their fibril forming nature, TLCPs can be used to reinforce thermoplastics [2 - 4]. The diameter of the reinforcing TLCP fibrils is typically one order of magnitude smaller than that of typical glass and carbon fiber. However, it may be not possible to extrude glass and carbon fibers through the die head and still maintain high aspect ratio fiber (i. e. $L/D > 100$) due to the small diameter capillary die (0.3 mm) used in order to fabricate dimensionally precise prototypes.

It would be desirable to use TLCP/thermoplastic blends to form composites on an in situ basis during prototype fabrication. However, there are two disadvantages with this approach. First, there is potential for degradation of the matrix. Most commercial TLCPs are processed at temperatures near or above the degradation temperature of most commodity resins. Vectra B , for example, has a melting point of 280°C and processes at approximately 320°C [5]. PP can be processed above 260°C, but this can lead to significant degradation [6]. Engineering thermoplastics can be used as matrices, but they are generally much more expensive. Second, in the case of the FDM 1600 extrusion head, the flow field present during fabrication is shear flow, which is known not to be as effective in forming highly oriented fibrils as extensional flow [7,8].

Therefore, tensile properties of in situ reinforced prototypes are expected to be similar to those of extruded TLCP reinforced composites and less than those of injection molded TLCP reinforced composite because some extensional stresses are present during injection molding.

In order to overcome the problems associated with processing the blends directly, the formation of pregenerated microfibrils was considered using a novel dual extrusion process [5, 9, 10]. In the dual extrusion process, the thermoplastic and TLCP are plasticated in separate extruders so that independent thermal histories are imposed to the two materials. TLCP is heated to sufficiently high temperatures to fully melt all of the crystallites. For example, the melting point of Vectra A is 283ºC, but it needs to be heated to 320ºC in order to fully melt all the residual crystallites [11]. Vectra A is then supercooled to the temperature at which the matrix is processed and, using a multiple-port injection nozzle, is then injected into the matrix stream which results in continuous TLCP streams encapsulated within the matrix. The melt is passed through a series of static mixers which serve to divide the TLCP streams, before being extruded through a capillary die and drawn in the spinline to high draw ratios in order to achieve high levels of molecular orientation in the TLCP fibrils.

There are several advantages of the dual extrusion process over generating TLCP fibrils in situ during FDM. Processing the TLCP in a separate extruder minimizes degradation of the matrix because the matrix is not exposed to the high temperatures that are necessary to fully melt the TLCP. The TLCP is supercooled, allowing it to be injected into the matrix. However, some degradation of the matrix is possible upon injection of the TLCP into the matrix. The dual extrusion process does not rely on droplet deformation because the multiple-port injection nozzle introduces continuous TLCP streams into the matrix, resulting in high aspect ratio fibrils. Finally, the composite strands can be post-processed above the melting point of the matrix and below the melting point of the TLCP using a variety of conventional processing techniques (e.g., FDM) which allow for the retention of the TLCP reinforcing fibrils generated during the dual extrusion process in the final part [5, 10, 12 - 21].

Post-processing of composite strands above the melting temperature of the matrix and below the melting temperature of the TLCP is critical to transforming the composite strands into final parts while retaining the reinforcement achieved in the original strands. The strands have been post-processed using conventional processing techniques: compression molding, injection molding, film extrusion, and blow molding. Composite strands have been uniaxially compression molded, and tensile properties of the consolidated plaques have been shown to agree with those predicted by composite theory [5, 10, 12, 14, 16]. The mechanical properties of films and bottles were lower than those calculated by composite theory, but the properties had greater isotropy in the plane than those of parts where the reinforcement was generated in situ [18, 19]. Mixed results have been observed for the mechanical properties of injection molded plaques when compared to those predicted by composite theory [17, 20].

The deviations from composite theory were attributed to three possibilities. The aspect ratio of the reinforcement may have been less than 100 due to agglomeration of the fibrils or fibril

breakage in the screw. Poor fibril distribution was observed in the plaques and may have been the result of agglomeration of the fibrils or insufficient mixing. There may have been a loss in molecular orientation in the TLCP fibrils[17].

Composite strands generated from the dual extrusion system have been used in the FDM 1600 rapid prototyping system in order to fabricate short fiber reinforced composite prototypes with mechanical properties greater than those of the three commercially available materials for the system [12, 21]. Vectra A/polypropylene (PP) strands with 20 wt% and 40 wt% Vectra A generated by means of the dual extrusion system were granulated to lengths less than 6 mm long before being re-extruded into monofilaments for use as feedstock in the FDM 1600 rapid prototyping system. The tensile moduli of Vectra A/PP (40/60 wt%) composite prototypes were shown to surpass those of prototypes fabricated from ABS by nearly 100% and to surpass those of PP by 150%. However, the tensile properties of the composite prototypes were lower than those predicted by composite theory. The reasons for the deviation from ideality were attributed to decreased fibril alignment and decreased aspect ratio due to fibril breakage. It was shown that by taking advantage of the isotropic tensile properties that resulted in the Vectra A/PP beads extruded from the FDM 1600 system, the properties of the composite prototypes could be engineered for specific applications by adjusting the lay-down pattern[12, 21].

The purpose of this work is to demonstrate a new process where TLCP long fiber reinforced monofilaments were generated for use in FDM applications, and to evaluate the effects of processing on the tensile properties of extruded strands. Due to less than optimal tensile properties of short fiber reinforced prototypes discussed above, preliminary studies concerned with TLCP long fiber reinforced composites suitable for use in plunger driven FDM are presented. The composite strands generated from the dual extrusion system were re-extruded at temperatures just above the melting point of the matrix in order to retain the reinforcing fibrils and excellent mechanical properties that were generated via the dual extrusion system. The effects of thermal history on the tensile properties and on the molecular orientation of the reinforcement are studied on the composite strands in a shearfree environment. Also, the effects of temperature coupled with shear flow on the tensile properties of long fiber reinforced composites are determined using a plunger actuated extrusion process. The effects of the post-processing steps on the tensile properties are determined by comparing those of the post-processed composite to those of the composite strands from the dual extrusion process.

3.2 Experimental

3.2.1 Materials

The TLCP used was Vectra A950 (Hoechst Celanese). It is a random copolyester based on hydrobenzoic acid (73% mole) and 2-hydroxy-6-napthoic acid (27% mole). It has a glass transition temperature of 108°C and a melting point of 283°C [22]. However, Vectra A needs to

be heated to 320°C to melt out all of the residual crystallites [11]. Prior to spinning, the Vectra A was dried at least 18 hours in a forced convection oven set at 150°C. The matrix material used was the 4018 grade of Amoco polypropylene (PP). It has a melting point of 160ºC and a melt flow index (MFI) of 13.5 [23].

3.2.2 Spinning of TLCP/PP Composite Strands

The novel dual extrusion process was used to spin self-reinforced composite fibers. The dual extrusion process has been described in detail elsewhere [5, 9, 10]. Vectra A and PP were plasticated separately in two Killion KL-100 extruders (1 inch single screw extruders with L/D=24) where the metering zone temperatures of the TLCP and PP extruders were set at 325°C and 245°C, respectively. The TLCP mass flow rate was controlled by metering it into the PP stream using a Zenith gear pump (model number 6135419-001 and 1.725 cc/rev). The TLCP was injected into the matrix as continuous streams via a multiple-port injection nozzle. The melt passed through a series of three Kenics and four Koch mixing elements that served to split the TLCP streams. The melt was then extruded through a capillary die with a diameter of 1.8 mm and a L/D of 1. The filaments were drawn through a 3.7 m long drawing chimney before being quenched in water and taken up on a constant speed godet. The draw ratio, estimated as the ratio of cross-sectional area of the capillary to that of the fiber, was greater than 70. The composition was determined from the total mass flow rate and the Vectra A mass flow rate.

Pure Vectra A strands were spun using a Killion KL-100 extruder. The metering zone temperature was set at 325°C, and the die diameter was 1.6 mm with a L/D of 4. The extrudate was drawn through a 3.7 m chimney and was taken up on a constant speed godet in a manner similar to that of the dual extrusion process, and the draw ratios were estimated to be greater than 100.

3.2.3 Compression Molding

The composite strands produced by means of the dual extrusion process were consolidated uniaxially using a Carver hot press (model number 2696) with the temperature set at 180°C. The strands were laid into a preheated picture frame mold (89 mm by 89 mm) in a uniaxial fashion, and it was placed in the press for 6 minutes and subjected to 1 MPa of pressure. The sample was then quenched in a water-cooled press where the cooling rate was determined to be approximately 20°C per minute.

3.2.4 Post-Processing Extrusion from the Capillary Rheometer

Composite strands from the dual extrusion process were re-extruded through a capillary die using an Instron Capillary Rheometer (Model 3211). Before being fed into the rheometer barrel, strands were compression molded into cylindrical cartridges that had diameters slightly smaller than that of the barrel. The cartridges were consolidated by uniaxially aligning strands that were approximately 10 cm long in a mold that was 10.5 cm long, and they were compression molded at 180°C using the afore-mentioned procedure for uniaxially aligned plaques. After the strands were consolidated, the composite was quenched in a water-cooled press with an approximate cooling rate of 20°C per minute. The TLCP reinforcement within the cartridges was believed to be continuous, and thus, the aspect ratio of the reinforcement was greater than 100.

The composite cartridges were extruded in a capillary rheometer using the following approach. First, the capillary and barrel temperature of the rheometer was set at temperatures of either 180°C, 210°C, or 240°C. A cartridge was then loaded into the barrel of the capillary rheometer and held at the temperature of the capillary for 6 minutes. The slug containing the unmelted TLCP fibrils was extruded at rates of 0.2 cm^3/min. to 20 cm^3/min. through capillaries of various L/D ratios as listed in Table 3.1 with no draw imposed. The entry angle of the capillaries was 90° while the diameters were 1.8 mm and 0.7 mm.

Table 3.1 : The dimensions of the capillary dies used to post-process the long fiber composites through the capillary rheometer are shown.

Capillary Die Number	Diameter	L/D
1	1.8 mm	7.8
2	1.8 mm	14.2
3	0.7 mm	12.5
4	0.7 mm	18.5
5	0.7 mm	37.1
6	0.7 mm	110

In order to differentiate between composites samples extruded from the dual extruder assembly and those extruded from the capillary rheometer, the former will be referred to as strands and the latter as monofilaments. In the former case, the TLCP fibrils are basically continuous and have not been subjected to an additional thermal or deformation history. In the latter case, the initial strands have been subjected to a thermal history during compression molding and then to an additional thermal history in the barrel of the capillary rheometer as wellas a deformation history.

3.2.5 Mechanical Properties

The tensile modulus and strength were measured using an Instron Mechanical Tester (model 4204) following the ASTM standard D 638-87b. The test samples were approximately 8 mm wide, 1.7 mm thick, and 30.5 mm in length. The load was measured with a 5 kN load cell, and the strain was measured using an extensiometer (Instron model 2630-25), while the cross head speed was kept at 1.27 mm/min.

The modulus and strength of the strands and composite monofilaments were also determined (ASTM D 3376-75). The ends of both the strands and the monofilaments were wrapped with masking tape to ensure uniform gripping of the sample. The length of the strands used in testing was approximately 280 mm long, while the composite monofilaments generated from the capillary rheometer were approximately 180 mm long. A 1 kN load cell was used to measure the load as a function of displacement, while the cross head speed was kept at 1.27 mm/min. For all tests, the average and the standard deviation were calculated from at least five samples, and data points greater than 2 standard deviations from the mean were removed.

3.2.6 Wide Angle X-ray Scattering

A Philips Table-Top X-Ray Generator model PW 1720 with a standard vacuum-sealed Statton Camera was used to produce X-ray diffraction patterns. Strands and plaques were exposed to CuKα radiation with a wave length of 1.54 Å for 6 hours. The distance from the sample to the film was 7.8 cm.

3.2.7 Scanning Electron Microscope

Cross sections of composite fibers, monofilaments, and plaques were fractured after being placed in liquid nitrogen for 5 minutes. The surfaces were gold coated using a n Edwards sputter coater (model S150B). Micrographs were then taken using a Cambridge Stereoscan Model 100 scanning electron microscope operating at 20 kV.

3.3 Results and Discussion

The results of this research are arranged as follows. The tensile properties of the Vectra A/PP strands generated from the dual extrusion system are reported in order to compare experimentally obtained values with those of composite theory and in order to provide a basis of comparison for the tensile properties of the post-processed composite. Thus, the effects of the post-processing step on the tensile properties can be determined. The effects of post-processing on the composite strands are divided into two sections. First, the effects of thermal history in the absence of a flow field on the tensile properties during post-processing are presented. Second, the effects of ram extrusion through a capillary die on the tensile properties are investigated, while varying capillary L/D, capillary diameter, extrusion rate, and post-processing temperature in order to simulate a FDM system for long fiber composite fabrication.

3.3.1 Fiber Spinning using the Dual Extrusion Process

In this section the mechanical properties of the composite strands are evaluated. This provides a basis of comparison for the tensile properties of the post-processed composites allowing for the determination of the effects of the post-processing steps on the tensile properties. First, the effects of draw ratio on the mechanical properties of Vectra A/PP strands that were spun using the dual extrusion process are addressed. Second, to determine the effectiveness of the dual extrusion system at developing the optimal mechanical properties of the composite strands, properties are compared to the rule of mixtures.

In Figure 3.1, the tensile modulus is shown as a function of draw ratio of Vectra A/PP (28/72 wt%) strands that were spun using the dual extrusion process through 1.8 mm capillary with an L/D of 1. The tensile properties of composite strands increased with increasing draw ratio. Between the draw ratios of 12 and 25, the tensile modulus increased from 6 GPa to 9 GPa. The modulus of the strands continued to increase even at very high draw ratios. At draw ratios greater than 100, the modulus increased only slightly, and at the highest attainable draw ratio the modulus was found to be 15 GPa. The strength also increased with draw ratio in a similar fashion reaching an asymptotic value of 160 MPa at high draw ratios. This increase in tensile properties was probably due to greater orientation as a result of increased strain and strain rates in the spinline at higher draw ratios [5, 15].

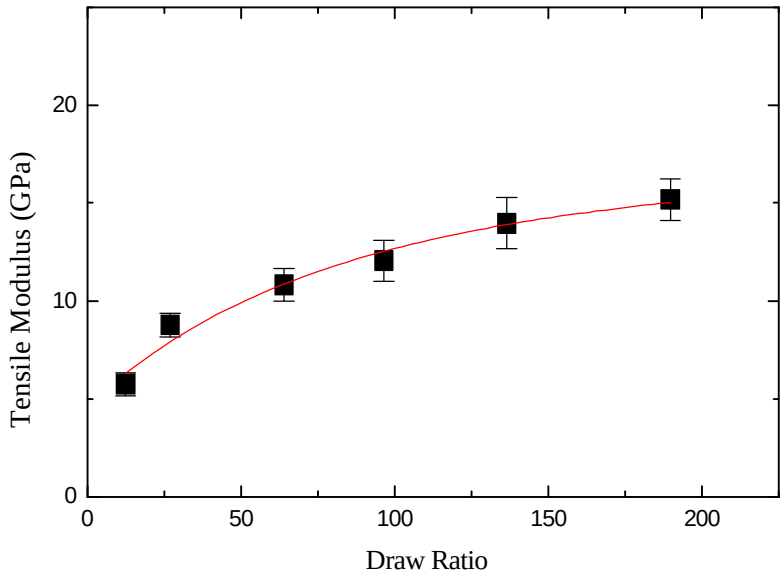

Figure 3.1 : Tensile modulus (■) of Vectra A/PP (28/72 wt%) strands spun using the dual extrusion system as a function of draw ratio.
The capillary die diameter was 1.8 mm, and the L/D was 1.

Vectra A/PP composite strands of three composition levels (20, 28, and 40 wt% Vectra A) were spun using the dual extrusion process, and the tensile properties of strands were compared to those based on composite theory. In Figure 3.2, the modulus of Vectra A/PP strands is shown as a function of composition, and the moduli increased with increasing Vectra A concentration. The moduli were compared to predictions made using the Halpin-Tsai equation, which simplifies to the rule of mixtures for reinforcements for aspect ratios greater than 100 [24, 25]. The rule of mixtures is

$$E_c = E_m\Phi_m + E_f\Phi_f \qquad (1)$$

for uniaxially oriented samples, where E_c, E_m, and E_f are the moduli of the composite fiber, the PP matrix, and the Vectra A reinforcement, respectively, and Φ_m and Φ_f are the volume fractions of the matrix and the reinforcement, respectively. The E_f of the reinforcing fibrils within the composite strands was calculated using the rule of mixtures. The E_m of the PP was taken as 1 GPa, and the volume fraction was calculated from known weight fractions [5]. For 20 wt% (14 vol%), 28 wt% (19 vol%), and 40 wt% (30 vol%) Vectra A composite strands, the moduli of the reinforcing phase of the composite strands, E_f, were calculated to be 63 GPa, 73 GPa, and 74 GPa, respectively. Neat Vectra A strands were spun, and the modulus was found to be approximately 69 GPa at draw ratios in excess of 100. This value is comparable to 65 GPa that has been reported elsewhere for neat Vectra A strands [4]. Therefore, the calculated moduli for the Vectra A reinforcing fibrils within the composite strands were very close to the maximum attainable modulus measured for pure Vectra A, indicating excellent agreement between moduli calculated using the rule of mixtures and those obtained experimentally for the neat strands. This agreement with the rule of mixtures has also been observed with Vectra B/PP (30/70) strands spun using the dual extrusion process when drawn to moderate draw ratios (70-80) [5, 10]. When spun at draw ratios in excess of 100, however, Nylon-11/HX8000 (13, 22, and 35 wt%) and Vectra B/PP (50/50) strands generated by means of the dual extrusion system had tensile properties greater than those predicted by composite theory [12 - 15]. These synergistic properties were attributed to greater TLCP orientation, which was obtained by encapsulating the TLCP fibrils within the matrix. It was speculated that the thermal insulation prevented premature solidification of the TLCP in the spinline, and this may have enhanced molecular orientation because of the ability to impart higher extensional strains to the TLCP fibrils [12 - 15]. Though similar synergistic properties were not observed with the Vectra A/PP composite strands being investigated, the use of others processing conditions (e.g., higher melt temperature for the Vectra A) may have resulted in synergistic effects in these strands.

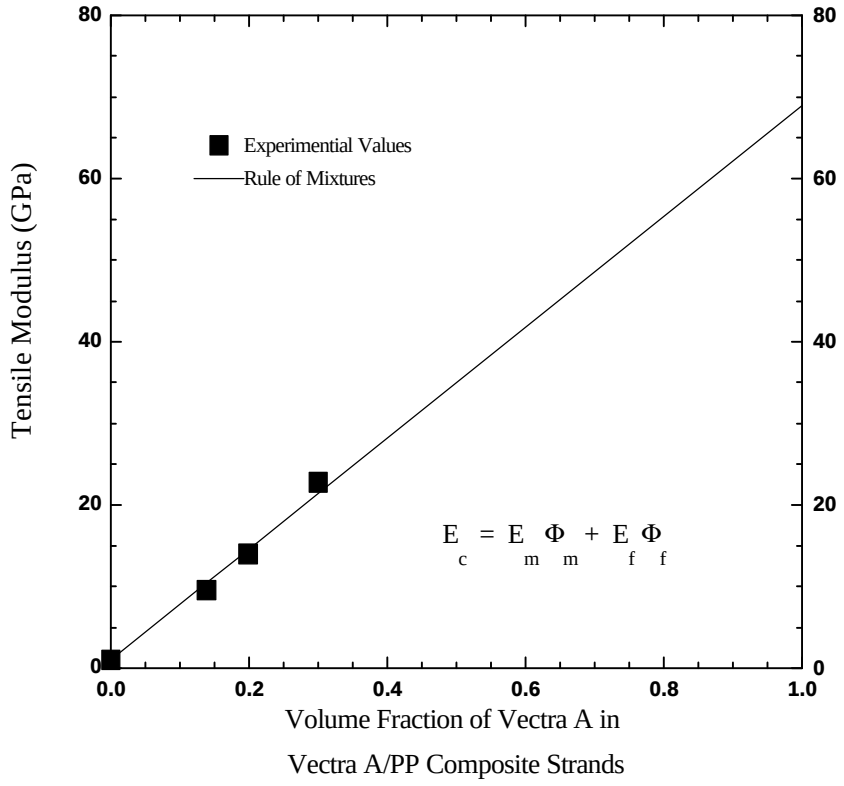

Figure 3.2 : Tensile modulus (■) of Vectra A/PP composite strands as a function of Vectra A volume fraction and as compared to the "rule of mixtures" (———) where the modulus of neat Vectra A was 69 GPa.

3.3.2 The Effects of Post-Processing Thermal History

In this section, the effects of thermal history in the absence of a flow field on mechanical properties of composite strands from the dual extrusion process are discussed. This is done in order to understand more clearly the reasons as to why previously reported experimental properties of composite prototypes fabricated by FDM were not similar to theoretical predictions [12, 21]. Also in this section, a possible reason for an observed decrease in properties as a result of an imposed post-processing thermal history is identified.

In order to isolate the effects of thermal history during post-processing, strands from the dual extrusion process were consolidated uniaxially into plaques using compression molding at 180°C. The mechanical properties of the plaques were then compared to those of the strands. The moduli of the 20 wt% and 40 wt% Vectra A uniaxial plaques were 7.7 GPa and 17.3 GPa, respectively. However, the moduli of the strands were 9.6 GPa and 22.8 GPa, respectively. This approximate 20% reduction in moduli for both samples was probably associated with the TLCP reinforcement. From micrographs, not shown here it was observed that the reduction in tensile properties of the strands was not due to a change in fibril alignment after consolidation or due to fibril deformation [12].

In order to determine if the decrease in tensile properties of the composites was from a reduction in tensile properties of Vectra A fibrils, the effects of post-processing thermal history on the neat TLCP strands were evaluated. In order to emulate the same thermal history on neat Vectra A strands that was present during Vectra A/PP strand consolidation, neat TLCP strands were annealed in a convection oven for 10 minutes and for 2 hours at 180°C, which was the same temperature used to consolidate the composite strands. Before annealing the Vectra A strands, their modulus was 69 GPa. After 10 minutes and 2 hours the moduli of the strands were 61 GPa and 60 GPa, respectively. Annealing of the strands resulted in approximately a 12% loss in moduli. Thus, the loss in modulus during the consolidation of the composite strands was most likely due to the loss in modulus of Vectra A fibrils.

The orientation of the TLCP was examined because the tensile properties of TLCP reinforced composites are dependent to a great extent on the orientation of the TLCP [26]. Wide angle X-ray scattering (WAXS) patterns were employed in order to determine the orientation of the crystalline region of the Vectra A. WAXS patterns of Vectra A/PP strands before and after consolidation were examined, in order to determine the effects of compression molding on the orientation of the TLCP. In order to identify WAXS reflections caused by Vectra A from those caused by PP, WAXS patterns of neat Vectra A were examined. The d spacing of the Vectra A reflections was determined to be 6.9 Å, 4.6 Å, and 3.4 Å, which was also observed by Winter and Lin [27]. Also, an increase in the intensity of the scattering was observed along the equatorial axis indicating that neat Vectra A was oriented parallel to the drawing direction of the strand. In Figure 3.3a, a WAXS pattern of Vectra A/PP (20/80 wt%) composite strands from the dual extrusion process is presented, and it contains several features. The two concentric circles represent reflections which resulted from the crystalline regions of the PP. Focusing on the

Vectra A reflection representing a d spacing of 4.6 Å, the scattering angle of the reflection indicated that the reinforcement was highly oriented in the direction parallel to the spinline. In Figure 3.3b, a WAXS pattern of Vectra A/PP (20/80 wt%) composite strands after being consolidated uniaxially into a plaque is shown, and several features are evident. In this pattern, the four concentric circular reflections resulted from the crystalline regions of the PP. Again focusing on the Vectra A reflection representing a d spacing of 4.6 Å, the scattering angle indicated that Vectra A was highly oriented in the machine direction of the plaque. The scattering angle of this reflection could not be measured accurately from either of the two WAXS patterns due to the diffuse nature of the reflection. The scattering angle of the Vectra A reflection from the consolidated plaques, however, was observed to be broader than that of the Vectra A reflection from the composite strands generated using the dual extrusion process.

a)

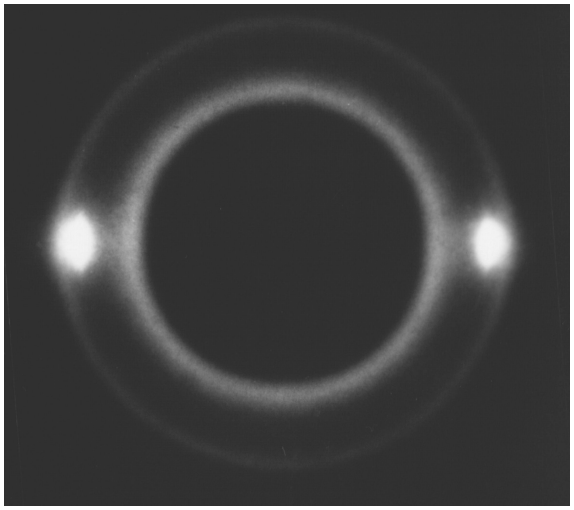

b)

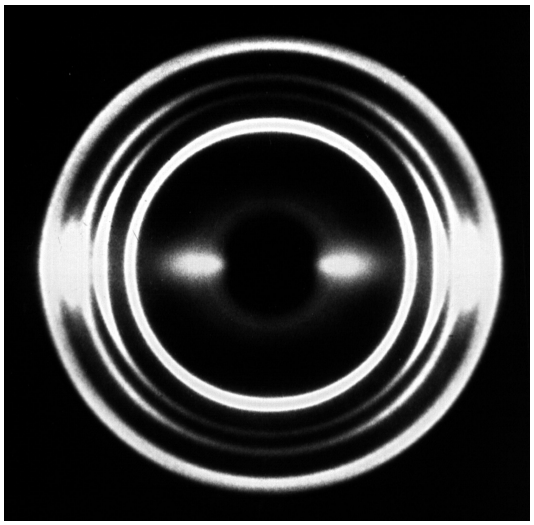

Figure 3.3 : WAXS patterns of a) Vectra A/PP (20/80 wt%) strands from the dual extrusion process and of b) a Vectra A/PP (20/80 wt%) consolidated plaque composed of uniaxially aligned strands from the dual extrusion process.

The increase in the scattering of the Vectra A reflection representing a d spacing of 4.6 Å in the consolidated composite compared to that of the composite strands could be attributed to several reasons. One possible reason for the difference in scattering angle between strands and the consolidated plaque could be due to a decrease in molecular orientation of the TLCP. The reflections indicate the orientation of the crystalline planes which probably did not melt during the consolidation of the strands. The orientation of the crystalline planes may have changed due to mobility in the mesophase during consolidation which would result in a change in the scattering angle. Another possible reason is that during consolidation the fibers may have been slightly misaligned, which would result in a decrease in orientation of the crystalline regions within the plaque. Both reasons would have resulted in an apparent decrease in mechanical properties of the consolidated plaque compared to those of the composite strands. Finally, variations in the thickness of the two samples may have resulted in different scattering angles. The thickness of the test plaque was easily measurable, but the thickness of the bundle of fibers that was used for testing varied across the sample due to voids present between adjacent fibers.

3.3.3 Shear History

The effects of deformation during processing on the tensile properties of the composite were examined under conditions similar to those found in plunger actuated FDM. In order to determine the effects of post-processing flow history on the Vectra A/PP long fiber composite strands, they were re-extruded in a capillary rheometer at temperatures (190°C, 210°C, and 240°C) just above the melting point of the matrix but below the melting point of Vectra A. This was done to simulate the post-processing of long fiber composites via FDM using a plunger actuated extrusion process. This section evaluates the effects of capillary L/D, capillary diameter, extrusion rate, and processing temperature on the mechanical properties of the monofilament.

In Figure 3.4, the tensile modulus and strength of Vectra A/PP monofilaments extruded through a capillary is shown as a function of L/D. Cartridges of Vectra A/PP (28/72 wt%) with continuous TLCP fibrils were extruded through dies 3 - 6 (see Table 3.1) at an apparent shear rate of 67 sec^{-1} and at a constant temperature of 180°C. The entry angle of all of the capillaries used in this research was 90°. The results in Figure 3.4 indicate that a critical L/D of approximately 18 is needed in order to obtain the maximum tensile modulus and strength of 3.5 GPa and 44 MPa, respectively. The tensile properties of the monofilaments decreased slightly when processed through capillaries with a L/D greater than that of the critical L/D. A critical L/D was similarly observed with capillaries having a diameter of 1.8 mm.

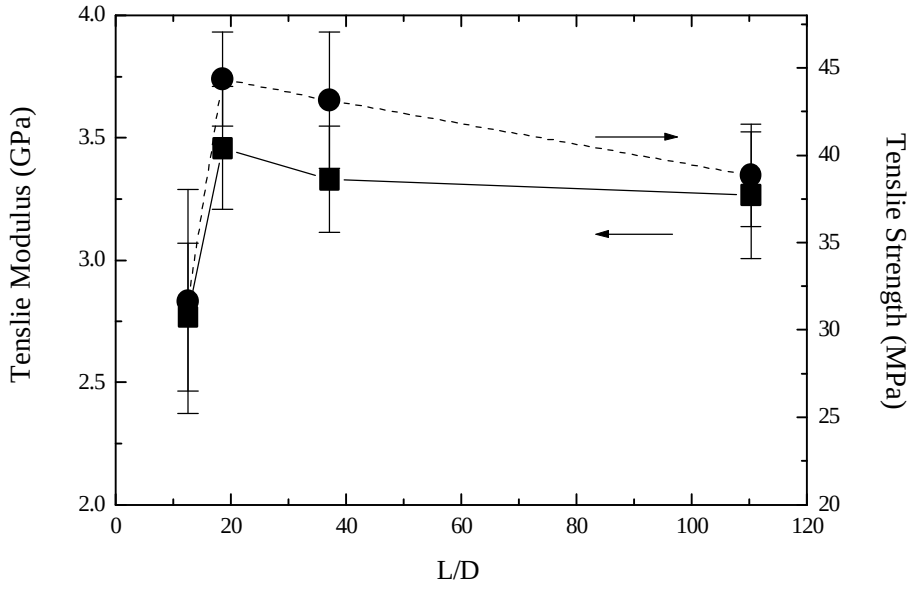

Figure 3.4 : Tensile modulus (—■—) and strength (- · ●- ·) of Vectra A/PP (28/72 wt%) composite monofilaments as a function of L/D extruded through a 0.7 mm diameter capillary at 180 ℃ and at an apparent shear rate of 67 sec^{-1}.

In Figure 3.5a, a micrograph of the end view of a Vectra A/PP (28/72 wt%) composite monofilament extruded through die 3 is presented. It was extruded at 180°C and at an apparent shear rate of 67 sec^{-1}. Many of the fibrils were curved and somewhat twisted. The fibrils were not aligned parallel to the axis of the monofilament or even parallel to themselves. If fibrils were aligned in the direction of the monofilament, only the ends of the fibrils and the matrix would be visible. This would be true for the composites with even higher Vectra A wt% (e.g., 40wt%). A micrograph of an end view of a Vectra A/PP (28/72 wt%) composite monofilament extruded through die 4 using the same processing conditions is shown in Figure 3.5b. In this case the fibrils, though still curved and twisted, appeared to be somewhat straighter. The matrix was also clearly visible indicating the fibrils were not laid over on their side, and fibrils appeared to be somewhat more aligned in the direction of the monofilament, which resulted in the higher tensile properties than those of monofilaments shown in Figure 3.5a.

a)

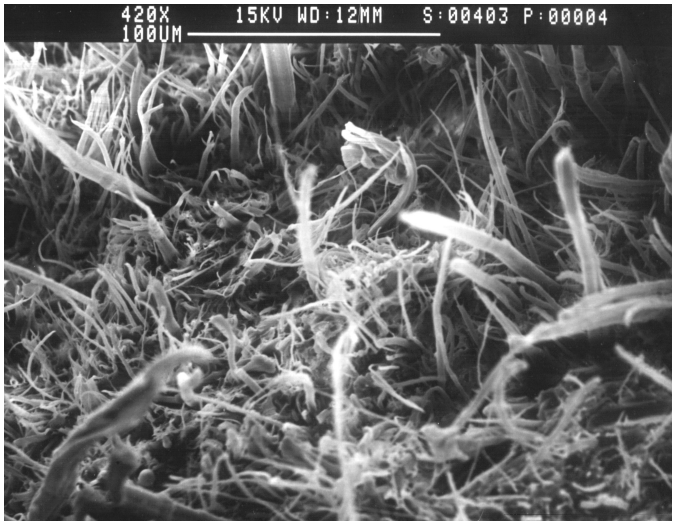

b)

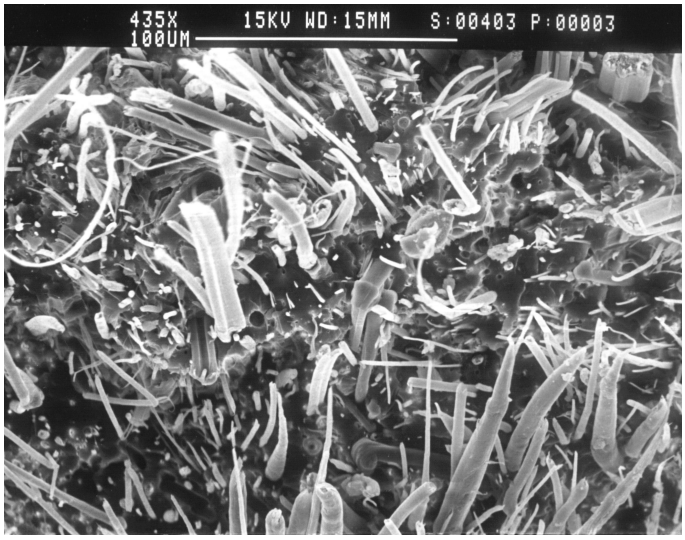

Figure 3.5 : Scanning electron micrographs of the cross section of Vectra A/PP (28/72 wt%) composite monofilaments extruded through the capillary rheometer at 180°C. a) The monofilament was extruded through a capillary die with a diameter of 0.7 mm and L/D of 12.4 at an extrusion rate of 2.3 mg/sec. b) The monofilament was extruded through a capillary die with a diameter of 0.7 mm and L/D of 18.5 at an extrusion rate of 2.3 mg/sec.

The change in tensile properties of the post-processed composites as the result of changing capillary L/D is attributed to TLCP fibril alignment related to increasing strains. A critical L/D was necessary in order to obtain the optimal tensile properties of the monofilament, and micrographs indicated that this was due to bulk fibril alignment. Entering the capillary, extensional flow served to elongate and accelerate the matrix. Because of the ridged nature of the reinforcing fibrils at these temperatures, they were probably unable to align in the matrix under low strains. A critical strain was probably necessary to obtain the maximum alignment of the fibrils in the flow field, and at larger strains the effects of shear probably served to disrupt the alignment of the TLCP fibrils which resulted in the slight decrease in mechanical properties.

The effects of capillary diameter on tensile properties of the Vectra A/PP (28/72 wt%) composite strands were studied next. Monofilaments were extruded through die 4 at 180°C. The extrusion rate was 7.1 mg/sec, and the L/D was 18, which is slightly above the critical L/D that is necessary to obtain the optimal properties of the monofilaments. The tensile modulus and strength were 3.5 GPa and 44.4 MPa, respectively. Monofilaments were also extruded through die 2 at the same temperature and extrusion rate. The L/D of die 2 was greater than the critical L/D necessary to obtain the maximum tensile properties for its diameter. The tensile modulus and the tensile strength were 3.0 GPa and 42.5 MPa, respectively. Thus, the smaller diameter resulted in greater monofilament tensile properties. The difference in tensile properties of the monofilaments extruded through the different dies is believed to be due to fibril alignment as a result of differences in the extension rates. The smaller diameter capillary has a greater contraction ratio of 184, thus larger extension rates which were probably able to better align the solid Vectra A fibrils. Using the larger diameter capillary with a smaller contraction ratio of 28, lower extensional stresses were present which resulted in less fibril alignment within the monofilament and lower mechanical properties of the monofilament.

In Figure 3.6, a micrograph of a monofilament cross section, extruded through die 2, is shown. It indicates that the TLCP fibrils were only slightly curved and were not twisted. The fibrils also appear to have been laid over on their side, covering the view of the matrix, and they were aligned in somewhat of a spiral pattern and not parallel to the monofilament axis. When compared with monofilaments extruded through die 4 (Figure 3.5b), the monofilaments from the die 2 had better retention of the original fibril shape. However, the fibrils within the monofilament extruded from die 2 were not as well aligned along the axial direction of the monofilament as seen in the monofilament extruded from die 4. Thus, the greater fibril alignment along the axis of the monofilament resulted in greater monofilament tensile properties and this probably resulted from differing capillary diameters.

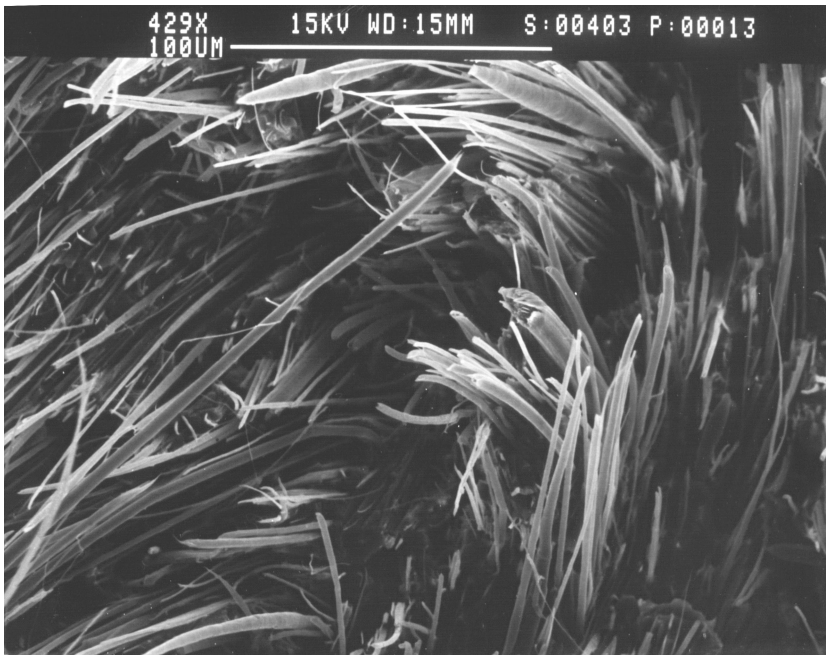

Figure 3.6 : Scanning electron micrograph of the cross section of Vectra A/PP (28/72 wt%) composite monofilaments extruded through the capillary rheometer at 180°C. The monofilament was extruded through a capillary die with a diameter of 1.8 mm and L/D of 14.2 at an extrusion rate of 6.9 mg/sec.

The effects of extrusion rate through a capillary die on the tensile properties of the Vectra A/PP (28/72 wt%) strands was studied next. Increasing extrusion rates resulted in increasing shear rates through the capillary. The apparent shear was used as the control variable, where:

$$\dot{\gamma}_{app} = \frac{4Q}{\pi R^3} \qquad (2)$$

and Q is the volumetric flow rate. The composites were extruded through dies 1 through 4, which had differing diameters and L/Ds. In Figure 3.7, the tensile modulus is shown as a function of apparent shear rate for monofilaments that were extruded through die 3 and die 4, where the latter die had the afore-mentioned critical L/D, and the material was extruded at a constant temperature of 180°C. As the apparent shear rate increased, the moduli of the monofilaments extruded through die 3 decreased from 2.8 GPa to 1.6 GPa. Similarly, the moduli of the monofilaments extruded through die 4 decreased from 3.5 GPa to 1.4 GPa with increasing apparent shear rate. Thus, at the higher shear rates the advantage of extruding through a larger L/D was eliminated because the modulus of the monofilament is less sensitive to the L/D. In the case of both dies, the moduli appear to pass through a sigmoidal transition with increasing shear rate. The moduli at the lower apparent shear rates were somewhat constant. As the shear rate increased, the moduli decreased, and at higher shear rates the moduli appeared again to be somewhat constant.

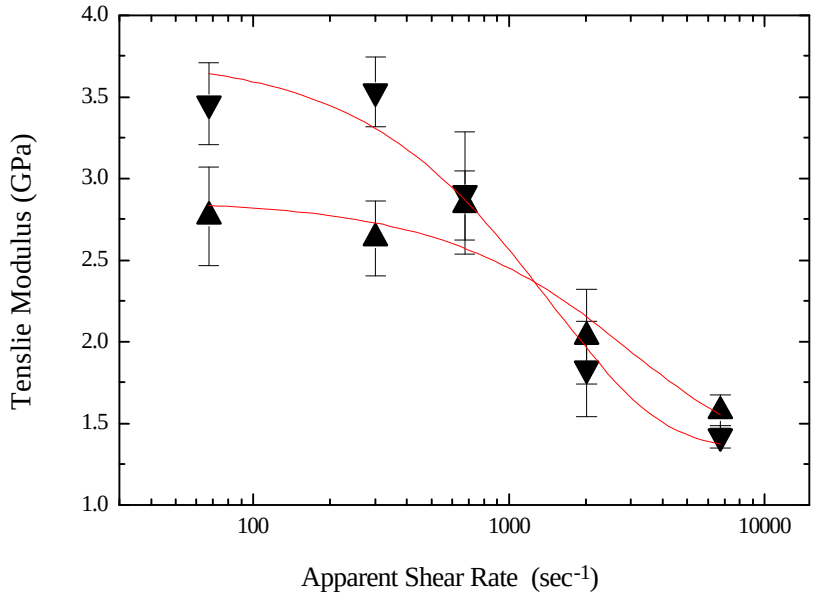

Figure 3.7 : Tensile modulus of Vectra A/PP (28/72 wt%) composite monofilaments as a function of apparent shear rate extruded through a 0.7 mm diameter capillary at 180°C where L/D=12.5 (▲) and L/D=18.5 (▼).

The effects of the apparent shear rate on the tensile strength of the monofilament were also examined using dies 3 and 4. In Figure 3.8, the tensile strength of Vectra A/PP (28/72 wt%) composite monofilaments is presented as a function of apparent shear rate. The decrease in tensile strength of the monofilaments with increasing apparent shear rate was found to be analogous to that of the tensile moduli of the monofilaments extruded under the same processing conditions. The maximum strength of the monofilament, 44 MPa, was observed when processed at the lowest shear rate through die 4. Monofilaments extruded through both dies demonstrated relatively constant tensile strengths at low apparent shear rates, and at the higher shear rates the strengths of the monofilaments showed a steady decrease. Also, at higher shear rates the tensile strengths of the monofilaments extruded through the two dies were similar, eliminating the advantage of increased monofilament strength when extruded through the die with a larger L/D.

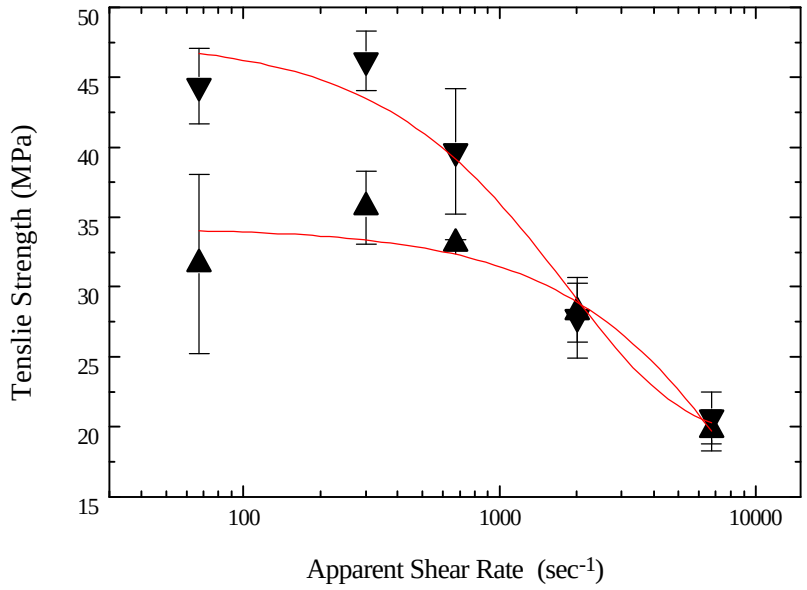

Figure 3.8 : Tensile strength of Vectra A/PP (28/72 wt%) composite monofilaments as a function of apparent shear rate extruded through a 0.7 mm diameter capillary at 180°C where L/D=12.5 (▲) and L/D=18.5 (▼).

The effect of apparent shear rate was also examined on the tensile modulus and the tensile strength of the Vectra A/PP (28/72 wt%) composites extruded through dies 1 and 2. In Figure 3.9, the effect of apparent shear rate on the tensile moduli of the monofilaments is shown. In both cases the moduli were somewhat constant at the lower apparent shear rates, less than 100 sec^{-1}, and at the higher shear rates, greater than 100 sec^{-1}, the moduli decreased. When extruded at the highest apparent shear rate, the moduli of the monofilaments extruded through the dies were similar. In Figure 3.10, the dependence of the tensile strength of the monofilament on the apparent shear rate is shown. Similar to the moduli of the monofilaments, the strengths were somewhat constant at low apparent shear rates for both dies, less than 100 sec^{-1}, and when extruded at higher apparent shear rates, greater than 100 sec^{-1}, the strengths of the monofilaments decreased. When processed using the highest apparent shear rate, the moduli and the strengths of the monofilaments extruded through both dies were similar. Thus, the advantage of extruding through higher L/D dies was not observed at higher shear rates.

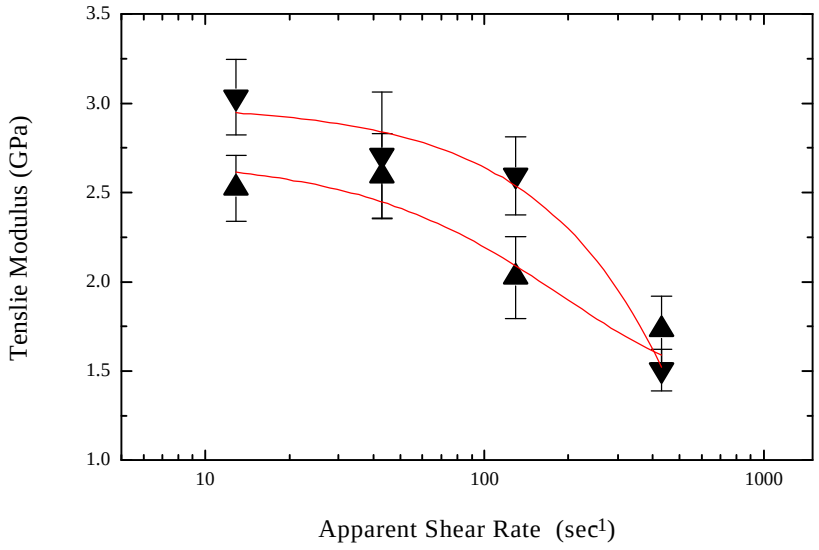

Figure 3.9 : Tensile modulus of Vectra A/PP (28/72 wt%) composite monofilaments as a function of apparent shear rate extruded through a 1.8 mm diameter capillary at 180°C where L/D=7.8 (▲) and L/D=14.2 (▼).

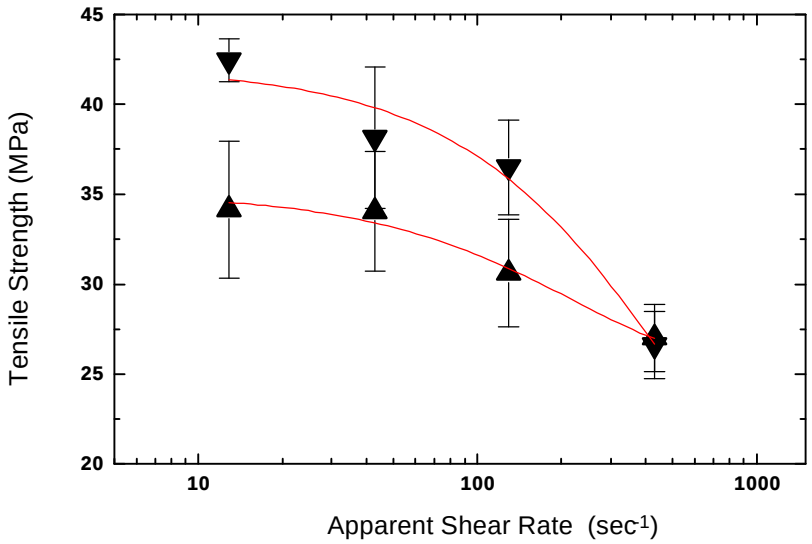

Figure 3.10 : Tensile strength of Vectra A/PP (28/72 wt%) composite monofilaments as a function of apparent shear rate extruded through a 1.8 mm diameter capillary at 180°C where L/D=12.5 (▲) and L/D=18.5 (▼).

In Figure 3.11, a micrograph of the cross section of a monofilament is shown where the monofilament was extruded through die 4 with a constant temperature of 180°C and at the highest apparent shear rate. The sides of the fibrils were visible in the micrograph indicating that the fibrils were not aligned in the direction parallel to the monofilament, nor were they necessarily aligned in the same direction as the adjacent fibrils. Contours in the matrix formed from fibril pullout appear as troughs in the micrograph indicating that the fibrils were embedded in the matrix at angles almost perpendicular to the direction of the monofilament. Many of the fibrils were curved and a few were also twisted, resulting in lower effective aspect ratio and reinforcing potential. The reduction in properties is believed to be due to a decrease in the alignment of the reinforcing fibrils, as a result of increased shear rates in the capillary.

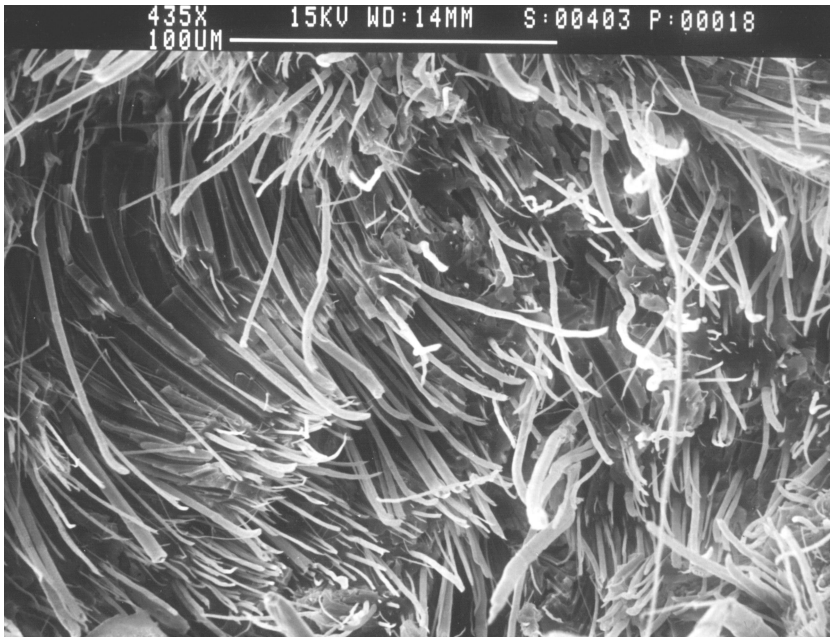

Figure 3.11 : Scanning electron micrograph of the cross section of Vectra A/PP (28/72 wt%) composite monofilaments extruded through the capillary rheometer at 180°C. The monofilament was extruded through a capillary die with a diameter of 0.7 mm and L/D of 18.5 at an extrusion rate of 230 mg/sec.

The effects of temperature at which the composite strands were re-extruded through the capillary rheometer on tensile properties of the monofilaments was examined. The Vectra A/PP (28/72 wt%) strands were extruded through die 4 at an apparent shear rate of 2.3 mg/sec and at a temperature of 180°C, 210°C, and 240°C. In Figure 3.12, the tensile modulus and strength are shown as a function of processing temperature. Clear trends were not evident because the tensile properties were not statistically different at different processing temperatures. The maximum modulus, 4.0 GPa, was observed when processed at 240°C while the maximum strength of 44 MPa was observed at 180ºC. A micrograph of the cross section of a monofilament processed at 210°C did not reveal any obvious differences in the contour of the reinforcing fibrils or in the alignment of the fibrils as compared to the monofilament extruded at 180° C (Figure 3.5a). The reason the tensile properties appear to be independent of temperature is not clear.

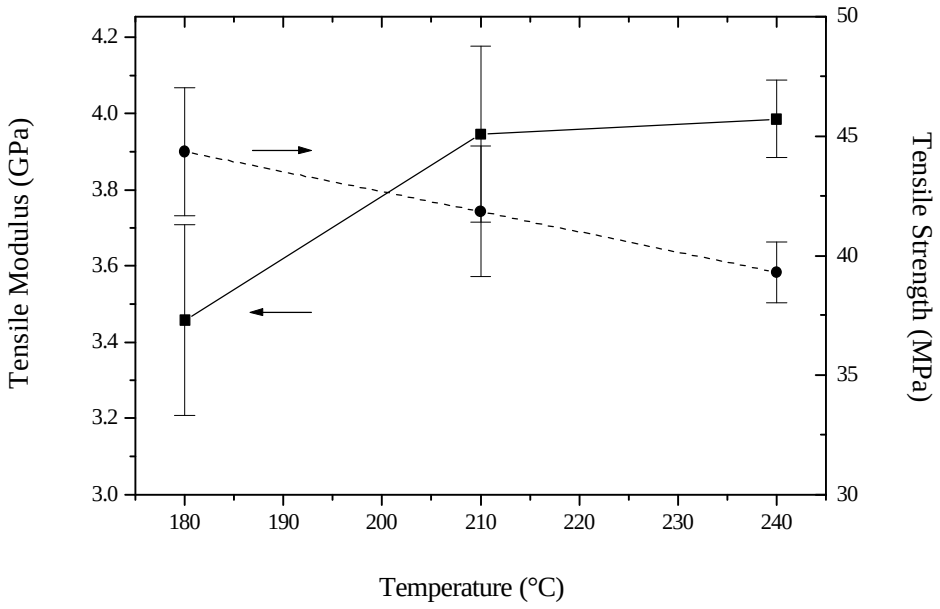

Figure 3.12 : Tensile modulus (—■—) and strength (- -●- -) of Vectra A/PP (28/72 wt%) composites monofilaments as a function post-processing temperature extruded through a 0.7 mm capillary with an L/D of 18.5 and an apparent shear rate of 67 sec^{-1}.

The tensile properties of the monofilaments produced via post-processing of the composite strands in a capillary rheometer were lower than those of the strands from the dual extrusion process. The Vectra A/PP (28/72 wt%) composite strands from the dual extrusion process had a tensile modulus of 14.0 GPa. The effects of thermal history in a quiescent environment were assumed to reduce the modulus by approximately 20%. After an imposed thermal history during consolidation of the composite strands into cartridges, the modulus of the composites was calculated to be approximately 11 GPa. The maximum modulus of the composite after extrusion through the capillary rheometer system was 4.0 GPa, resulting in a significant decrease in modulus. The low tensile properties were probably due to several reasons. Micrographs indicated that the fibrils were not fully aligned parallel to the direction of the monofilament. Micrographs also showed that the fibrils were curved and twisted which caused a decrease in the effective aspect ratio and thus decrease the reinforcing potential of the fibrils.

The tensile properties of the long fiber reinforced composites were compared to the tensile properties of previously fabricated short fiber reinforced Vectra A prototypes. In our previous work it was shown that the maximum tensile modulus and strength of the short fiber Vectra A/PP (40/60 wt%) composites, fabricated uniaxially in the machine direction via FDM, were 2.7 GPa and 37 MPa, respectively [12, 21]. The maximum tensile properties of Vectra A/PP (28/72 wt%) long fiber monofilaments were 4.0 GPa and 46 MPa, respectively. Therefore, the tensile properties of the long fiber composite monofilaments were greater than those of the TLCP short fiber reinforced composite prototypes fabricated via FDM, while the long fiber composites had lower Vectra A concentrations. Thus, a plunger actuated FDM system would enable the fabrication of long fiber reinforced prototypes with excellent tensile properties, and the tensile properties of these composites are far greater than those of most commercially available materials used in FDM applications.

3.4 Conclusions

TLCP long fiber reinforced composite monofilaments were generated via a plunger driven extrusion system. This extrusion system has the potential to be implemented in a FDM rapid prototyping system which can fabricate long fiber reinforced prototypes with tensile properties similar to those of long fiber reinforced monofilaments. The tensile properties of the monofilaments generated using this extrusion system, and potentially those of prototypes fabricated from a similar FDM system, have greater mechanical properties than those of previous fabricated prototypes reinforced with short TLCP fibers.

It was found that the tensile properties of the composite monofilaments were less than those of the composite strands, and this was attributed to the thermal and deformation history imposed during post-processing. It was found that the thermal history imposed during consolidation of 20 wt% and 40 wt% Vectra A composite strands at 180°C resulted in approximately a 20% reduction in the tensile moduli of both materials. This reduction in tensile

moduli was potentially due to a decrease in orientation of the Vectra A reinforcement as a result of molecular relaxation or as a result of poor strand alignment during consolidation

It was determined that the deformation history during re-extrusion of the composite strands affected the mechanical properties of the long fiber reinforced monofilaments. It was shown that the capillary L/D, the capillary diameter, and the apparent shear rate in the capillary affected the properties of the composite monofilament when processed at 180°C. It was determined, for the post-processing conditions considered, that smaller diameter capillary dies and lower apparent shear rates resulted in greater tensile properties of the composite monofilament. It was also determined, for the post-processing conditions studied, that a critical L/D was necessary in order to obtain the optimal mechanical properties in the monofilaments.

3.5 Acknowledgments

This research was supported by the Army Research Office (Grant No. DAAH04-94-G-0282), and the Naval Surface Warfare Center, Dahlgren Division and Armstrong Laboratory, Brooks AFB under contract N60921-89-D-A239, Order 0059. Also, we would like to thank G. L. Wilkes, M. A. McLeod and B. D. Kaushiva.

---

1 R. W. Gray IV, D. G. Baird, J. H. Bøhn, *Rap. Proto. J.*, in preparation (1997).
2 A. I. Isayev, in Liquid-Crystalline Polymer Systems Technological Advances, ed. A. I. Isayev, T. Kyu, and S. Z. D. Cheng, American Chemical Society, Washington D. C. 1996.
3 D. G. Baird, in Polymeric Materials Encyclopedia, ed. J. C. Salamone, CRC Press, Boca Raton 1996.
4 A. A. Handlos and D. G. Baird, *J. Macromol. Sci.-Rev. in Macromol. Chem. and Phy.*, C35, 183 (1995).
5 E. A. Sabol, A. A. Handlos, and D. G. Baird, *Polym. Comp.*, 16, 330 (1995).
6 Himont Profax Bulletin AP-002, Himont U. S. A., Inc. (1990).
7 K. G. Blizard and D. G. Baird, *Polym. Eng. And Sci.*, 27, 653 (1987).
8 R. A. Weiss, W. Hun, and L. Nicolais, *Polym. Eng. And Sci.*, 27, 673 (1987).
9 D. G. Baird and A. Sukhadia, U.S. Patent 5,225,488 (1993).
10 E. A. Sabol, M. S. Thesis, Virginia Polytechnic Institute and State University (1994).
11 S. M. Guskey and H. H. Winter, *J. Rheol.*, 35, 1191 (1991).
12 R. W. Gray IV, M. S. Thesis, Virginia Polytechnic Institute and State University (1997).
13 C. R. Robertson, M. S. Thesis, Virginia Polytechnic Institute and State University (1994).
14 C. G. Robertson and D. G. Baird, *Intern. Polym. Proc.*, in press (1996).
15 R. K. Krishnaswamy and D.G. Baird, *Polym. Comp.*, in press (1997).
16 C. G. Robertson, J. P. de Souza, and D. G. Baird, Recent Advances in Liquid Crystalline Polymers, A. I. Isayev, T. Kyu, and S. Z. D. Cheng eds., ACS Books, Washington D. C. (1996).

17 A. A. Handlos and D. G. Baird, *Intern. Polym. Proc.*, XI, 82 (1996).
18 A. A. Handlos and D. G. Baird, *Polym. Comp.*, 17, 73 (1996).
19 A. A. Handlos and D. G. Baird, *Polym. Eng. and Sci.*, 36, 378 (1996).
20 R. K. Krishnaswamy, J. Xue, and D. G. Baird, *SAMPE J.*, in preparation (1997).
21 R. W. Gray IV, D. G. Baird, J. H. Bøhn, in preparation (1997).
22 M. Y. Cao and B. Wunderlich, *J. Polym. Sci.: Polym. Phy. Ed.*, 23, 521 (1985).
23 Amoco Polypropylene Homopolymers Bulletin PP-8, Amoco Polymers, Inc. (1996).
24 G. Crevecoeur and G. Groeninckx, *Polym. Eng. and Sci.*, 30, 532 (1990).
25 J. C. Halpin, *Polym. Eng. and Sci.*, 16, 344 (1976).
26 H. N. Yoon, L. F. Charbonneau, and G. W. Calundann, *Adv. Mater.*, 3, 206 (1992).
27 Y. G. Lin and H. H. Winter, *Macromol.*, 21, 2439 (1988).

4.0 Recommendations

• Develop TLCP composites with very high TLCP loading, and use a carrier with an extremely low viscosity for FDM applications. This has the potential of increasing the mechanical properties of the composite by using greater quantities of TLCP. The viscosity ratio between the two phases could develop a sheath core morphology (e.g., a low viscosity polyphenylenesulfide PPS and Vectra B). Thus, the sheath region could serve to provide adhesion between adjacent roads and layers. These high TLCP concentration composites could be processed both above and below the melting point of the TLCP. The strength of the prototypes could be enhanced if the sheath material could be cross-linked after fabrication.

• Design a die to be used in FDM rapid prototyping applications that is able to develop orientation in the reinforcing phase. The die should be designed considering the conclusions made concerning die geometry for long fiber reinforced systems. This has the potential to increase fibril alignment in prototypes fabricated from composites where the reinforcement was developed in the dual extrusion process. A second die should be designed to develop strong extensional stress that could better orient TLCPs in the melt state, thus generating the reinforcement in situ.

• Design a FDM rapid prototyping system that is more robust than the system used in this research. The new system should be able to extrude resin in pellet and powder form and be able to generate and withstand pressures that are typically present during polymer processing. The new extrusion system should also be designed such that it could easily be cleaned, allowing many materials to be used in the system. The system should also be designed to withstand the temperatures required for processing engineering thermoplastics. If the purpose if the rapid prototyping system is to fabricate parts from composites generated using the dual extrusion system, a ram extrusion system should be used. If the purpose of the system, however, is to fabricate prototypes using unfilled resins, a screw extrusion system should be implemented.

• It was shown that long fiber composites extruded through a die had better mechanical properties than those of short fiber composites. It would be beneficial if long fiber monofilaments could be generated by consolidating several strands from the dual extrusion process to form a monofilament using a continuous process. This could be accomplished by passing the strands through rollers where a desired cross-section had been removed from the rollers' surface. This

could be used to produce monofilaments for FDM applications, or the monofilaments could be pelletized for post-processing using conventional processing equipment.

Appendix A :

Rheology Data

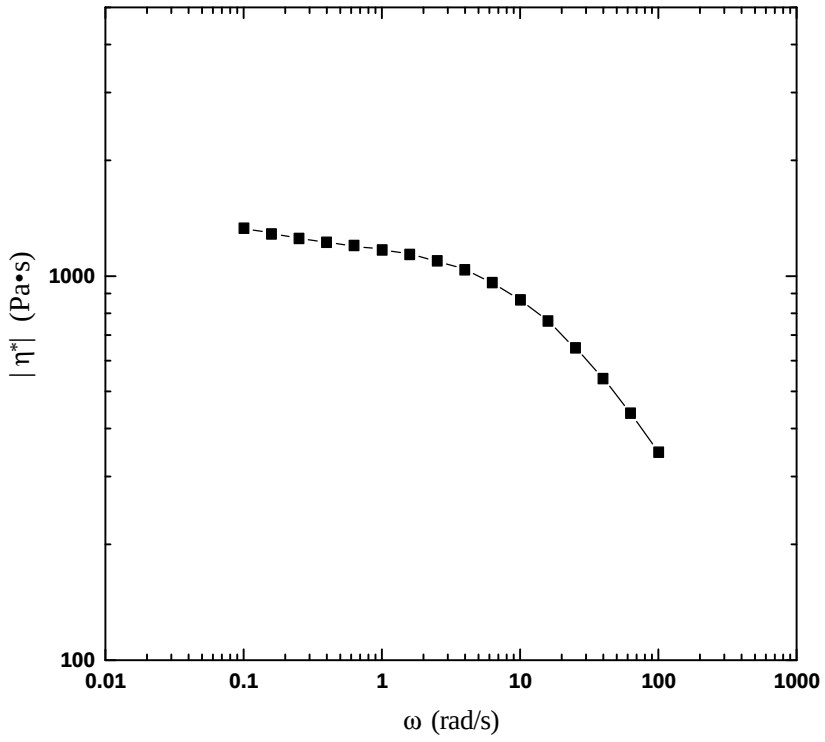

Figure A.1: | η*| (—■—) as a function of frequency for ABS used in the FDM 1600 rapid prototyping system at 270°C and at 5% strain.

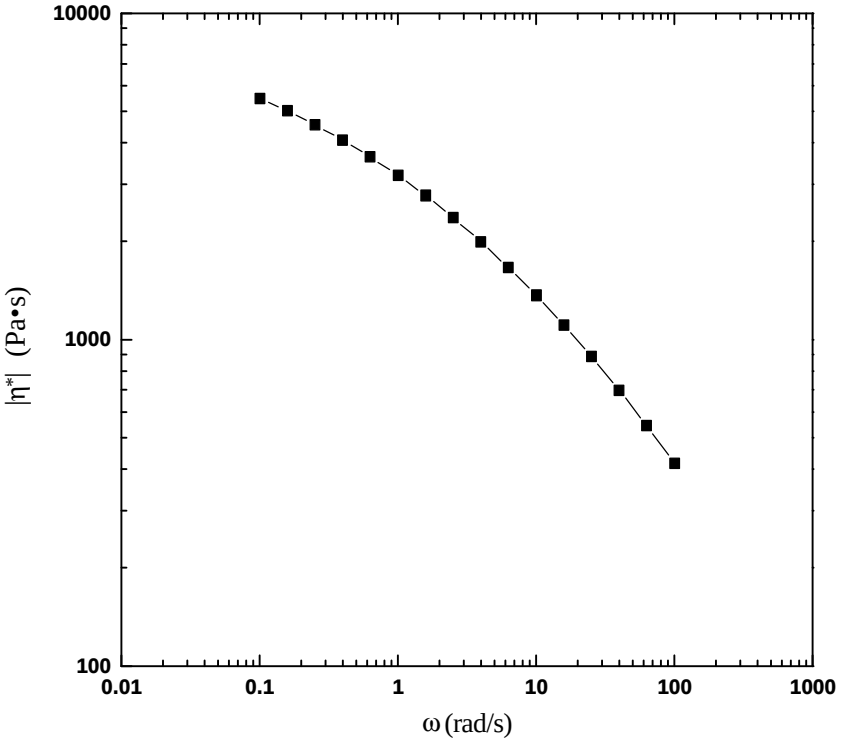

Figure A.2 : $|\eta^*|$ (—■—) as a function of frequency for 4018 grade PP at 183 °C and at 10% strain.

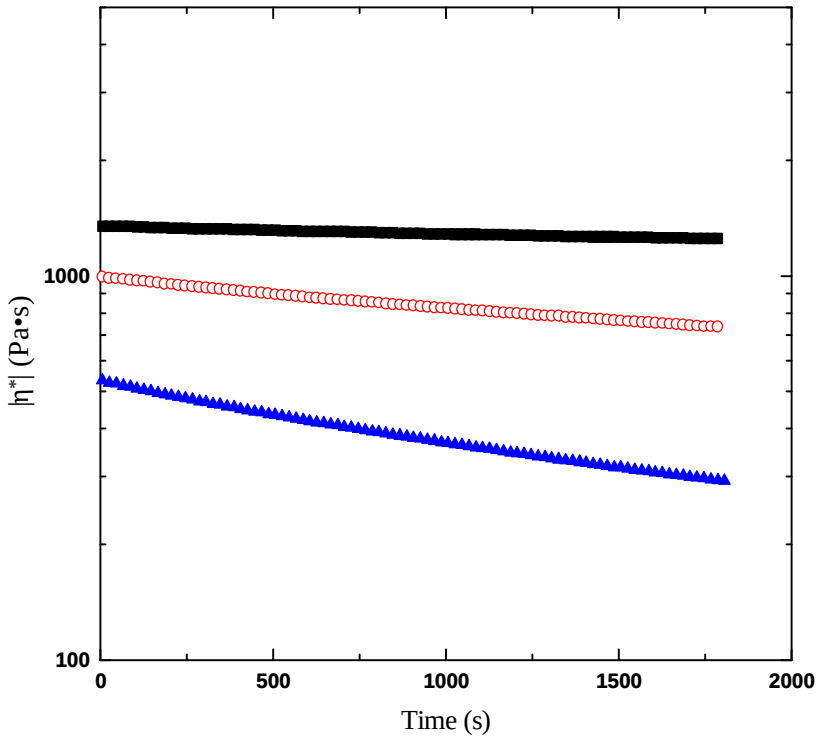

Figure A.3 : |η*| as a function of time for Amaco 4018 grade PP at an angular frequency of 1 rad/s and at 10% strain for three temperature 242°C (—■—), 262°C (—○—), and 282°C(—▲—).

Appendix B :

DMTA Data

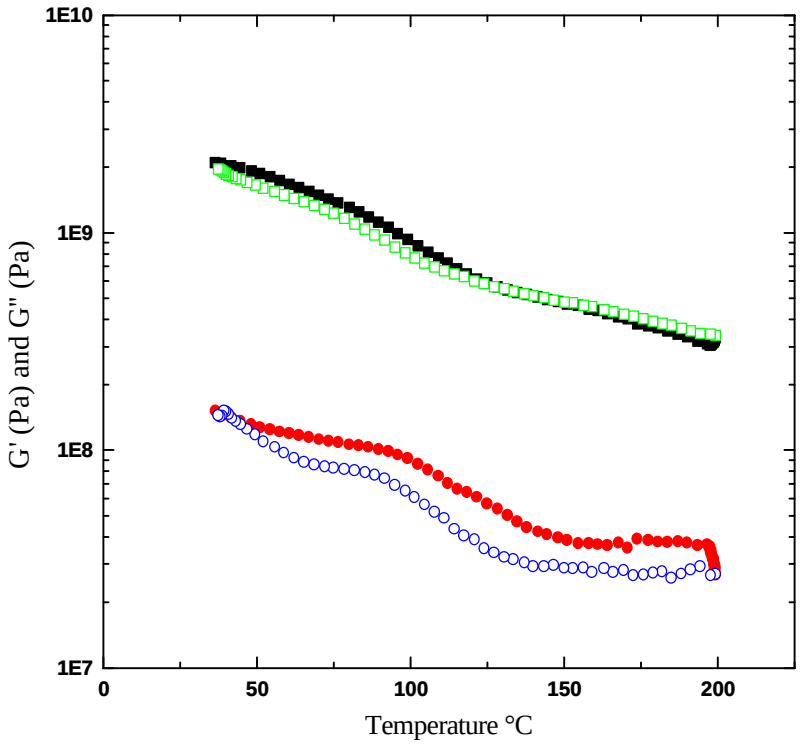

Figure B.1 : G' [heating (—■—) cooling (—□—)] and G" [heating (—●—) cooling (—○—)] as a function of time where a neat Vectra A injection molded plaque was heated at a rate of 10°C/min until it reached 200°C. It was held at temperature for 10 minutes and then cooled at the same rate at a frequency of 1 (rad/sec), and at 0.1% strain. The plaque was 1.1mm thick.

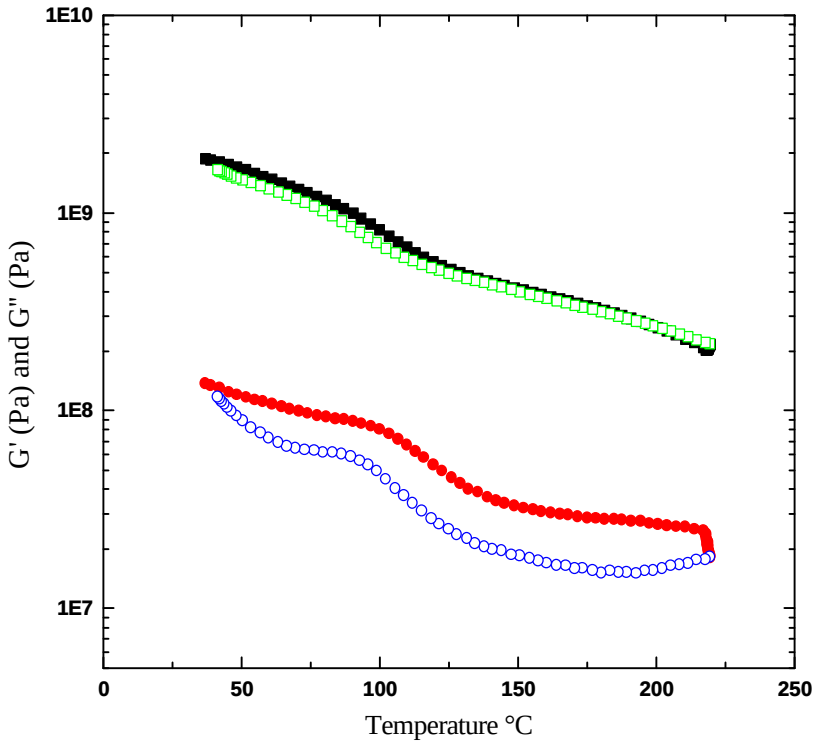

Figure B.2 : G' [heating (—■—) cooling (—□—)] and G" [heating (—●—) cooling (—○—)] as a function of time where a neat Vectra A injection molded plaque was heated at a rate of 10°C/min until it reached 220°C. It was held at temperature for 10 minutes and then cooled at the same rate at a frequency of 1 (rad/sec), and at 0.1% strain. The plaque was 1.1mm thick.

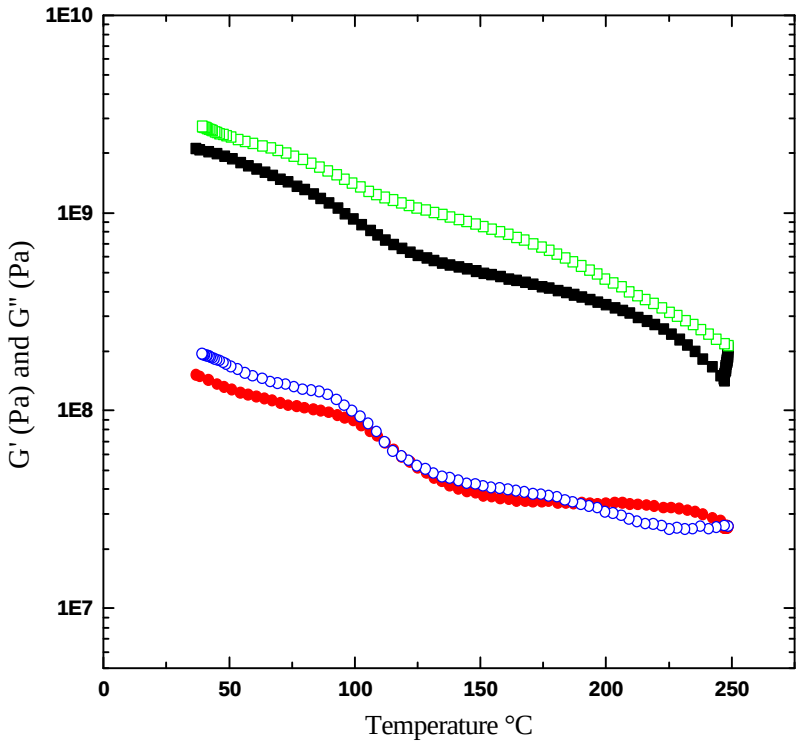

Figure B.3 : G' [heating (—■—) cooling (—□—)] and G" [heating (—●—) cooling (—○—)] as a function of time where a neat Vectra A injection molded plaque was heated at a rate of 10°C/min until it reached 200°C. It was held at temperature for 10 minutes and then cooled at the same rate at a frequency of 1 (rad/sec), and at 0.1% strain. The plaque was 1.1mm thick.

Appendix C :

Micrographs

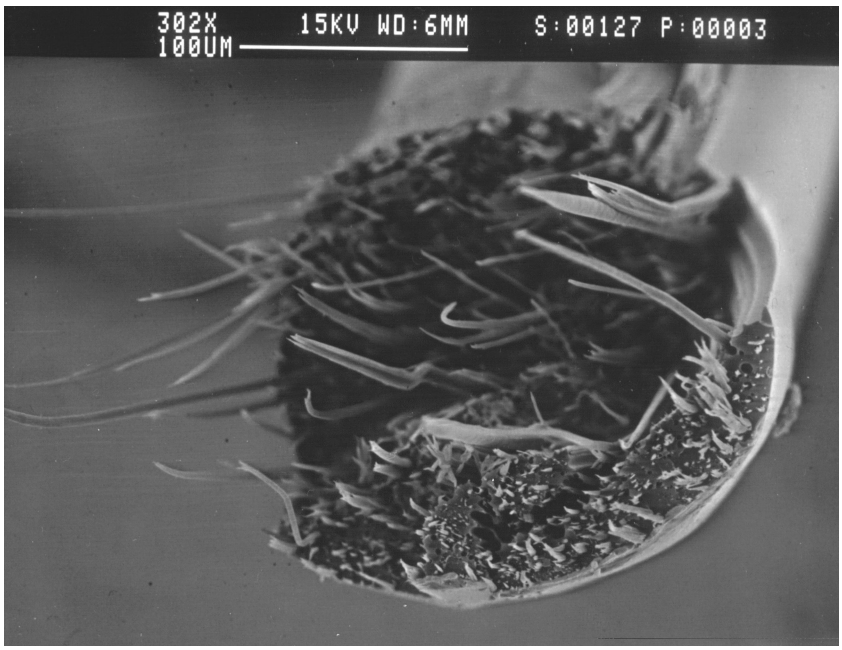

Figure C.1 : Scanning election micrograph of the cross-section of a Vectra A/PP (40/60 wt%) strand spun via the dual extrusion system using a capillary die having a diameter of 1.8 mm and L/D=1 and taken up at draw to ratios greater than 70.

Figure C.2 : Scanning election micrograph of the cross-section of a Vectra A/PP (40/60 wt%) plaque consolidated from uniaxially aligned strands spun via the dual extrusion system using a capillary die having a diameter of 1.8 mm and L/D=1 and taken up at draw to ratios greater than 70.

Appendix D :

FDM 1600 Operating Procedure

When using the FDM 1600 rapid prototyping system, the following protocol should be used. The protocol is divided into two sections: software and hardware. The software provides the series of directions necessary to the hardware, so that it can perform the necessary tasks to fabricate a particular prototype.

D.1 : A *.sml* file must be created containing specific instructions for part fabrication. It can be created using two different methods.

- Software packages can be employed to generated this file. First, the CAD system I-DEAS is employed to generate a mesh of the proposed part. This is then saved as a *.stl* file. This software is found in the Virginia Tech Computer Aided Design Laboratory along with the manuals. The *.stl* file can then be loaded into QuickSlice, a software package that generates the *.sml* file. The *.sml* file is a series of instructions containing the tool path and the extrusion rates necessary to fabricate a particular prototype. This application and manuals are also found in the Virginia Tech CAD Laboratory.
- The *.sml* file can also be generated by writing a computer program that writes *.sml* files. The C++ program used in this research along with a representative *.sml* file are shown in Appendix E.

D.2 : Before the part can be built a series of hardware procedures must be completed.

- The proper head with the proper material must be installed in the FDM 1600 rapid prototyping system. The procedures for the these two steps are described in detail in the FDM System Documentation in the FDM Hardware Section entitled FDM 1600 Manual Release 2.0 on pages F16-18 through F16-28 (5OCT95).
- The liquefier head must then be positioned before each part is fabricated. This is described on pages F16-32 and F16-33 (5OCT95) of the afore-mentioned section. It is also described in the Training Section of the manual entitled QuickSlice Training Manual Release 4.0 pages T-12 and T-13 (12AUG96).
- To fabricate a part, the *.sml* is then sent to the FDM 1600 rapid prototyping system from the Silicon Graphics workstation, following the procedure in the Training Section of the manual entitled QuickSlice Training Manual Release 4.0 pages T-11 (12AUG96). The UNIX command "ssend" is also described in the Utilities Section entitled Utilities Manual Release 4.0 pages U-9 and U-10 (20DEC96).
- The tips of the two liquefier dies on the head must be calibrated with respect their relative position to each other. The procedure for this is found on pages F16-13 through F16-18 (5OCT95) of the FDM Hardware Section. This needs to by performed every time the dies are adjusted.
- If a new material is being used, the extrusion rate of the material needs to be calibrated. This is explained in Appendix D.3.
- Before removing the head, the liquefier needs to be purged. This process is described in detail in Appendix D.4.

D.3 : The line speed of the monofilament feed stock needs to be calibrated for every material and for the same material having a different diameter feed stock. The *.sml* file specifies the

monofilament line speed. Thus a change in feed stock diameter changes the volumetric flow rate. The line speed is specified in the command

PD.08,41;MM;MM0,53;MM006,100;MM-70,175;SR800;AC5;

The line is described in detail in the Utilities Section of the manual entitled Utilities Manual on pages U-2 and U-3 (20DEC96). The C++ code in Appendix E defines this line as "const char parameter_string []". The line can easily be changed by: changing the string in the C++ program, compiling the code, and generating a new *sml* file. To calibrate the command line for a new material where the C++ code is used to generate the *sml* file:

- Determine the desired cross-sectional area of the road in mil^2 (1 mil = 0.001 inches = 0.025 mm).
- Find this number in the DEF file in Appendix E under the column titled "Flow Area."
- Find the corresponding DO number (digital output number).
- In the C++ code insert the DO number into the "const char parameter_string []" as indicated.

  PD.08,41;MM;MM0,53;MM006**100**;MM-70,175;SR800;AC5;
- Save the C++ code, and compile the file by typing "make". (The make file is shown in Appendix E).
- Build a simple part such as a rectangular prism.
- Measure the part dimensions and determine if too much or not enough material was used.
- Adjust the "const char parameter_string []" as necessary and repeat until the dimensions of the final part are similar to that expected.

D. 4 : If the liquefier is not dedicated to a specific material, it is import to purge the liquefier after each use.

- A suitable purge material must be chosen. The purge material and the modeling should have similar processing temperatures, and neither should degrade at the processing temperature of the other. In this research ABS was used as the purge material.
- Unload the modeling material from the head.
- Adjust the liquefier temperature to the processing temperature of the purge material.
- Load the purge material.
- Purge the using the "Load" button in the front of the FDM 1600 system, until all of the model material has been removed. {If some material cannot be removed using this method remove the liquefier from the head by removing the screws that secure the liquefier in the head. Then remove the insulation and heater from the liqufier. Place it in a furnace to carbonize the material. The carbon can be removed from the liquefier by placing in an ultrasonic bath. (Avoid removing the liquefier if possible!)}
- Remove the head using the procedure previously referenced.

Appendix E :

C++ Code

The FDM 1600 rapid prototyping system requires a series of directions that position the liquefier head and dictate the extrusion rate of both the support and model material. Because some of the materials used in this research could not easily separate from the die upon the completion of a road, it was necessary that the part be built from exactly one continuos road. However, the existing software, QuickSlice, was unable to develop a tool path for a part consisting of a single continuos road. Therefore, the following C++ code was developed to generate *.sml* files that were used to build rectangular prisms with a continuous road via the FDM 1600 rapid prototyping system operating with QuickSlice 2.0.

This program can easily be altered to generate parts of varying dimensions, lay-down patterns, and materials. The dimensions of the part are specified by the global variables and can easily be changed. The lay-down pattern used during part fabrication can also be dictated. This is done by placing remark commands in front of all of the subroutines whose name starts with "plaq" in the main routine except the subroutine of the lay-down pattern to be used. Varying materials can also be used. The processing temperature of the material must be specified manually using the controllers on the front of the FDM 1600 rapid prototyping system. The mass rate of the material is adjusted by changing the linear speed of the monofilament feed stock. This is specified by the "const char parameter_string []", and is discussed in Appendix D.3.

The C++ program accesses an existing *sml* file named "t12_2plaq.sml" in order to build the base. The base fabricated by this *sml* file is a constant size and thus does not change with the prototype size.

The "const char parameter_string []" was calibrated by Stratasys, Inc. for ABS plastic. The QuickSlice software accesses this calibration table, "DEF", while generating the *sml* file. This table is used as a first approximation when calibrating the monofilament line speed for new materials

Summary of Files Listed in Appendix E

C++ code : Creates *.sml* files

```
// Robert Gray
// tensile bar sample generator
// Jan. 1997
//_______________________________


#include <math.h>
#include <fstream.h>
#include <iostream.h>
#include <stdio.h>
#include <stdlib.h>

const float height = 80;              // part height in mil(height/roadhei=int);
const float width  = 300;             // part width in mil(width/roadwi/2=int);
const float length = 3000;            // part length in mil(length/roadwi/2=int);
const float road_height = 10;         // road height in mil;
const float road_width = 30;          // road width in mil;
const int start_XX = 150;             // start postion of the part in the X direction in mils;
const int start_YY = 100;             // start postion of the part in the Y direction in mils;
const int num_of_plaques = 8;         // number of plaques to be built
const int lay_pattern = 3;            // lay down pattern
                                      // 1 = machine direction
                                      // 2 = transverse direction
                                      // 3 = zero ninty
const char parameter_string[]= "PD.151,47;MM;MM0,33;MM50,178;MM-83,161;SR800;AC5;WA0.;#ORD:34
Z:0.0400 S:0.0400\n";//material parameters
const char my_file[] = "com100a.sml";    // file to write sml code to Va/4018 20/80 chopped mono
const char my_support[] = "t12_2plaq.sml";  // file to read support from_  two layers of fine
ofstream OFile;

void Initialisation();
void OrigineSetup();
void MaterialInit();
void InsertSupportCode();
void plaq_machine_direction(int, int);
void plaq_machine_layer(int, int);
void plaq_transverse_direction(int, int);
void plaq_transverse_layer(int, int);
void plaq_zero_ninty(int, int);
void plaq_several(int, int);
void SetEndWork();


int main()
{
        OFile.open(my_file);
        Initialisation();
        OrigineSetup();
        MaterialInit();
        OFile.close();
        InsertSupportCode(); // try to use system command to add support.structure my_support
        OFile.open(my_file, ios::out|ios::app);

//      plaq_machine_direction(start_XX, start_YY);
//      plaq_transverse_direction(start_XX, start_YY);
      plaq_zero_ninty(start_XX, start_YY);
//      plaq_several(start_XX, start_YY);

        SetEndWork();
        OFile.close();
        return 0;
}


//
//
//
void
```

```
Initialisation() {
        OFile << " .K;;;;; .J;;;;; .R\n";
        OFile << " .I;;17:\n";
        OFile << " .N10;19:\n";
        OFile << " .M10;;;;;:\n";
        OFile << " .E;;;;;;\n";
        OFile << "# Date           : 09/28/96   23:32:29\n";
        OFile << "# File           : /usr2/research/chem/rogray/plaq/plaq3.sml\n";
        OFile << "# QuickSlice     : 2.0a 03-Apr-96 (qsqk) ---------------- units = inc    h\n";
        OFile << "# Modeler        : FDM1600\n";
        OFile << "# Material       : ABS_P400 and PP VA microcomposites\n";
        OFile << "IN;\n";
        OFile << "CD129;WA1;CD0; # alt-tip off, enable operator alt mat change\n";
        OFile << "# CF;\n";
        OFile << "# VC100;OF;\n";
        OFile << "# V*100,1.;#Xshrinkage\n";
        OFile << "# V*101,1.;#Yshrinkage\n";
        OFile << "# CF@100,@101;\n";
        OFile << "# CZ100;\n";
        OFile << "MZ1200;\n";
        OFile << "FH;XD210;FZ;\n";
        OFile << "MZ1200;\n";
        OFile << "MA1200,500;    # take this out if res  tarting a model\n";
        OFile << "# MA@102,@103; # put this in if restarting a model\n";
        OFile << "XD121;#TW\n";
        OFile << "#\n";
        OFile << "# The toolpath units are in inches.\n";
        OFile << "# ORD HEADER # normal\n";
        OFile << "# ORD list is all possible curve types, whether used or not.\n";
        OFile << "#                                                  Wait (once per Z, next Z)\n";
        OFile << "#       Pre                 Main  Shut Roll        |    \n";
        OFile << "#       Delay  Start-flow    Flow   off back    Speed  |     Setname, Type\n";
        OFile << "#         |    |        |       |     |  |     |    | \n";
        OFile << "#ORD: 1 PD.118,79;MM;MM0,25;MM60,122;MM-70,175;SR800;AC5;WA0.;#DEFAULT,Open\n";
        OFile << "# height = " << height << "  all values are in mils\n";
        OFile << "# width  = " << width  << " \n";
        OFile << "# length = " << length << " \n";
        OFile << "# road_height = " << road_height <<  " \n";
        OFile << "# road_width = " << road_width <<  " \n";
        OFile << "# start_XX = " << start_XX <<  " \n";
        OFile << "# start_YY = " << start_YY <<  " \n";
        OFile << "# num_of_plaques = " << num_of_plaques << " \n";
        OFile << "# lay_pattern  = " << lay_pattern  << " \n";
        OFile << "# parameter_string = " << parameter_string <<  " \n";
        OFile << "# my_file = " << my_file << " \n";
        OFile << "# my_support = " << my_support << " \n";
        OFile << "# road width max 60 mil min 30 mil for 25 mil tip:height 10 mil\n";
        OFile << "# road width max 30 mil min 12 mil for 12 mil tip:height 10 mil\n";
}

//
//
//
//

void
OrigineSetup() {
        OFile << "MZ0;  # FOAM HEIGHT FACTOR HERE \n";
        OFile << "PS;WA0;VC102;OA;SO@102,@103;VC104;OZ;MR0,0;\n";
        OFile << "VS110,@102;VS111,@103;VS112,@104;\n";
        OFile << "V+110,@121;V+111,@122;\n";
        OFile << "AM0;\n";
}

//
//
//
//

void
```

```
MaterialInit() {
        OFile << "########## MATERIAL INITIALIZATION\n";
        OFile << "CD129;WA1; # alt-tip off\n";
        OFile << "CD135; # RB RNG ABS\n";}
//
//
//
//

void
InsertSupportCode() {
  char line[100];
        sprintf(line,"cat %s >> %s",my_support,my_file);
        system(line);

}

//
//
//
//

void
SetEndWork() {


        OFile << "# TAIL #\n";
        OFile << "VM7;\n";
        OFile << "MZ20;\n";
        OFile << "CD129;WA1;CD0; # alt-tip off\n";
        OFile << "#\n";
        OFile << "# dz=0.010 co=0.0060 dp=0.0010 ct=0.0006 alt=0 ff=0.1200 u=inch\n";
        OFile << "#\n";
        OFile << "XD211;\n";
        OFile << "####.....................................................................\n";
        OFile << "# Date           : 01/02/97\n";
        OFile << "# File           : /usr2/research/chem/rogray/plaq/\n";
        OFile << "# Qui ckSlice     : 2.0a 03-Apr-96 (qsqk)\n";
        OFile << "# Modeler        : FDM1600\n";
        OFile << "# Material       : ABS_P400 and vectra A / PP blends\n";
        OFile << "# Shrinkage  XY  : 1.008\n";
        OFile << "#             Z  : 1\n";
        OFile << "# Applied        : yes\n";
        OFile << "# Road width min :  inch\n";
        OFile << "#            max : \n";
        OFile << "# Tip            : 0.025\n";
        OFile << "# Envelope    X  : 9.4 inch\n";
        OFile << "#             Y  : 10\n";
        OFile << "#             Z  : 10\n";
        OFile << "# Wip e interval  : no wipe\n";
        OFile << "#.....................................................................\n";
        OFile << "# Estimated values......\n";
        OFile << "# Modeling time  :      hours    (approx)\n";
        OFile << "# Filament usage : \n";
        OFile << "#   main         : \n";
        OFile << "#   support      : \n";
        OFile << "####.....................................................................\n";

}

////////////////////////////////////////////////////////////////
//The part building procedures                                //
//                                                            //
////////////////////////////////////////////////////////////////

//////////////////
//machine
//
//////////////////
```

```
void
plaq_machine_direction(int X,int Y) {// X and Y are the absolute points of the corner were the
part will start to build from

    int JJ;

                OFile << "#######\n\n";
                OFile << "## build material \n\n";
                OFile << "#######\n\n";
                OFile << "\n XD129;  #alt-tip off\n";
                OFile << "MA" << (.5*road_width+X) << "," << (.5*road_width+Y) << ";#start
position \n";
                for ( JJ=1; JJ<=(height/road_height/2); JJ++)
                      {plaq_machine_layer(X, Y);}

                       }



void
plaq_machine_layer(int XX,int YY) {//XX and YY are the absolute value of the cornerwere the layer
is started from

    int II,l;


                      OFile << "MZ" << (road_height*2) << "; #next layer\n";
                      OFile << parameter_string;
                      OFile << "AS1;VM4;BC;#st  art flow  begin series of movements\n";

                      for ( II=1; II<=(width/road_width/2); II++)
                            { for ( l=1 ;l<=5;l++)
                                {if (II==(48*l))
                                   {OFile << "EC;VM3;WA2;   #curve length break up\n";
                                     OFile << parameter_string;
                                     OFile << "AS1; VM4; BC; #re start\n";
                                     OFile << "MA" << (.5*road_width+XX) << "," <<
(.5*road_width)+(road_width*(2*II-3))+YY << ";\n";
                                   }
                              }

                            OFile << "MA" << (.5*road_width+XX) <<   "," <<
(.5*road_width)+(road_width*(2*II-2))+YY << ";\n";
                            OFile << "MA" << (length-(.5*road_width)+XX) << "," <<
(.5*road_width)+(road_width*(2*II-2))+YY << ";\n";
                            OFile << "MA" << (length-(.5*road_width)+XX) << "," <<
(.5*road_width)+(road_width*(2*II-1))+YY << ";\n";
                            OFile << "MA" << (.5*road_width+XX) << "," <<
(.5*road_width)+(road_width*(2*II-1))+YY << ";\n";
                            }
                      OFile << "EC; VM3;#end series of movements   end flow\n";
                      OFile << "XD209; # capture postion FC\n";
                      OFile << "MZ" << (road_height*2) << ";#next layer\n";
                      OFile << parameter_string;
                      OFile << "AS1;VM4;BC;# start flow begin series of movements\n";

                      for ( II=(width/road_width/2); II>=1 ; II--)
                             { for ( l=1 ;l<=5;l++)
                                 {if (II==(48*l))
                                   {OFile << "EC;VM3;WA2;   #curve length break up\n";
                                     OFile << parameter_string;
                                     OFile << "AS1; VM4; BC; #re start\n";
                                     OFile << "MA" << (.5*road_wid  th+XX) << "," <<
(.5*road_width)+(road_width*(2*II))+YY << ";\n";
                                   }
                              }
                            OFile << "MA" << (.5*road_width+XX) << "," <<
(.5*road_width)+(road_width*(2*II-1))+YY << ";\n";
                            OFile << "MA" << (length-(.5*road_width)+XX) << "," <<
(.5*road_width)+(road_width*(2*II-1))+YY << ";\n";
```

```
                          OFile << "MA" << (length-(.5*road_width)+XX) << "," <<
(.5*road_width)+(road_width*(2*II-2))+YY << ";\n";
                          OFile << "MA" << (.5*road_width+XX) << "," <<
(.5*road_width)+(road_width*(2*II-2))+YY << ";\n";
                          }

                     OFile << "EC; VM3;#end flow end series of movements \n";
                     OFile << "XD209; #capture postion FC\n";

                     }

////////////////////
//transverse
//
////////////////////

void
plaq_transverse_direction(int X, int Y) {// X and Y are the absolute points of the corner were
the part will be started from
    int JJ ;


               OFile << "#######\n\n";
               OFile << "## build material \n\n";
               OFile << "#######\n\n";
               OFile << "XD129;   #alt-tip off\n";
               OFile << "MA" << ((.5*road_width)+X) << "," << ((.5*road_width)+Y) << ";#start
postion\n";
               for ( JJ=1; JJ<=(height/road_height/2); JJ++)
                     {plaq_transverse_layer(X, Y);}

                     }



void
plaq_transverse_layer(int XX, int YY) {// XX and YY are the absolute points of the corner were
the layer will start and end at

    int II,l;


                     OFile << "MZ" << (road_height*2) << ";#next layer\n";
                     OFile << parameter_string;
                     OFile << "AS1;VM4;BC;#begin   flow  begin series of movements\n";

                     for ( II=1; II<=(length/road_width/2); II++)
                           { for ( l=1 ;l<=5;l++)
                               {if (II==(48*l))
                                  {OFile << "EC;VM3;WA2;   #curve length break up\n";
                                    OFile << parameter_string;
                                    OFile << "AS1; VM4; BC; #re start\n";
                                   OFile << "MA" << (.5*road_width)+(road_width*(2*II-3))+XX  <<
","  <<  (.5*road_width+YY) << ";\n";
                                  }
                              }
                          OFile << "MA" << (.5*road_width)+(road  _width*(2*II-2))+XX  <<  ","  <<
(.5*road_width+YY) << ";\n";
                          OFile << "MA" << (.5*road_width)+(road_width*(2*II-2))+XX  <<  ","  <<
(width-(.5*road_width))+YY << ";\n";
                          OFile << "MA" << (.5*road_width)+(road_width*(2*II-1))+XX  <<  ","  <<
(width-(.5*road_width))+YY <<
";\n";
                          OFile << "MA" << (.5*road_width)+(road_width*(2*II-1))+XX  <<  ","  <<
(.5*road_width+YY) << ";\n";

                          }
                     OFile << "EC; VM3;#end series of movements\n";
                     OFile << "XD209; # capture position   FC\n";
                     OFile << "MZ" << (road_height*2) << ";#next layer\n";
```

```
                    OFile << parameter_string;
                    OFile << "AS1;VM4;BC;# begin flow begin series of movements\n";

                    for ( II=(length/road_width/2); II>=1 ; II--)
                          { for ( l=1 ;l<=5;l++)
                              {if (II==(48*l))
                                 {OFile << "EC;VM3;WA2;   #curve length break up\n";
                                  OFile << parameter_string;
                                  OFile << "AS1; VM4; BC; #re start\n";
                                  OFile << "MA" << (.5*roa  d_width)+(road_width*(2*II))+XX  <<
","  <<  (.5*road_width)+YY << ";\n";
                                 }
                             }

                            OFile << "MA" << (.5*road_width)+(road_width*(2*II-1))+XX  <<  ","  <<
(.5*road_width)+YY << ";\n";
                            OFile << "MA" << (.5*road_width)+(road_width*(2*II-1))+XX  <<  ","  <<
(width-(.5*road_width))+YY << ";\n";
                            OFile << "MA" << (.5*road_width)+(road_width*(2*II-2))+XX  <<  ","  <<
(width-(.5*road_width))+YY << ";\n";
                            OFile << "MA" << (.5*road_width)+(road_width*(2*II-2))+XX  <<  ","     <<
(.5*road_width)+YY << ";\n";

                            }

                    OFile << "EC; VM3;# end flow end series of movements\n";
                    OFile << "XD209; # capture postionFC\n";

                    }

//////////////////
// Zero Ninty
//
//////////////////

void
plaq_zero_ninty(int X, int Y) {// X and Y are the absolute points of the corner of the part

    int JJ;

              OFile << "XD129;  #alt-tip off\n";
              OFile << "MA" << (X) << "," << (Y) << ";#start postion\n";
              for ( JJ=1; JJ<=(height/road_height/4); JJ++)
                    {plaq_transverse_layer(X, Y);
                    plaq_machine_layer(X, Y);}
                 }


////////////////////////////
// several plaques are made
// of a particular lay down
// pattern
////////////////////////////

void
plaq_several(int XX, int YY) {// XX and YY are the absolute corner of the first part

    int KK,xx,yy;
      xx = XX;
      yy = YY;

      for ( KK=1; KK<= (num_of_plaques); KK++)
        {
          if (lay_pattern == 1) plaq_machine_direction(xx, yy);
          if (lay_pattern == 2) plaq_transverse_direction(  xx, yy);
          if (lay_pattern == 3) plaq_zero_ninty(xx, yy);
          yy=yy+width+200;
        }
}
```

DEF : Contains calibrations to build ABS parts with differing road size

```
# $Id: DEF,v 1.18 1997/01/07 20:10:08 phopkins Exp $
# File: strata/modelers/1600/P400/T25/Z10/DEF
#-------------------------------------------------------------------------#

#-------------------------------------------------------------------------#
# WARNING:   Preset values defined by Stratasys Inc.
#   Any changes made to this file are at your own risk.
#   Stratasys Inc. will not support any non-Stratasys changes to this file.
#-------------------------------------------------------------------------#

IDENT $Revision: 1.18 $

FILEUNITS INCH    # units for commands in current file only   { INCH | MM }

MODELER 1600 {9.4 10.0 10.0} {.1 .1 .0} {1.2 .5 .0} 0.026

MATERIAL P400 {1.007 1.0} 52

TIP T25 {.010 .020} {.025 .08} {1.5 4.0}

ACCELERATION 5
DEFL_ANGLE 30 70 110
ZIGZAG 0.06 6
TIP_WIPE 2 "XD121;#TW"
ROLLBACK_M "CD135;#ABS RB_SF"
DENSITY 1.05
SHORT 0.20
BASE_BOTTOM_Z .015 .030

P1 20
PO 0.25

# PURGE ----------------------------------------------------------------#
##        idle time between tip use      (table gives purge time in seconds)
##       0  1  10  20  30  40  50  60 +  (minutes)
PV  1    0  1  1   1   5   5   5   5    # very dry material  0     - 0.249
PV  2    1  1  1   2   5   5   5   5    # medium dry         0.25  - 0.499
PV  3    1  1  2   2   5   5   5   5    # medium             0.50  - 0.749
PV  4    1  1  2   2   5   5   5   7    # medium wet         0.75  - 0.999
PV  5    2  2  2   2   5   5   5  10    # very wet material  1.0   - greater
# PURGE END ------------------------------------------------------------#


# SETS START ------------------------------------------------------------#
G 0 DEFAULT  DACBa0 NO In-Out MOD 45 -45 .000 .000 .050 RED 0 0.0 \
.028  OFF    .999 99 99 99 999 -99 999 999 99 FORW  .10 SOLID \
.028  IN     .999 99 99 99 999 -99 999 999 99 START .10 SOLID \
.028  .000   .999 99 99 99 999 -99 999 999 99 FORW  .10 SOLID YES \
.028  .000   .999 99 99 99 999 -99 999 999 99 START .10 SOLID

G 1 Part     DACBa0 NO In-Out MOD 45 -45 .000 .000 .050 RED 0 0.0 \
.028  OFF    .999 99 99 99 999 -99 999 999 99 FORW  .10 SOLID \
.028  IN     .999 99 99 99 999 -99 999 999 99 START .10 SOLID \
.028  .000   .999 99 99 99 999 -99 999 999 99 FORW  .10 SOLID YES \
.028  .000   .999 99 99 99 999 -99 999 999 99 START .10 SOLID

G 3 PartFast DCABa1 NO In-Out MOD 45 -45 .000 -.002 .050 LIGHT-RED 2 0.0 \
.028  OFF    .999 99 99 99 999 -99 999 999 99 FORW  .10 SOLID \
.028  IN     .999 99 99 99 999 -99 999 999 99 START .10 SOLID \
.056  .000   .999 99 99 99 999 -99 999 999 99 FORW  .10 SOLID YES \
.028  .000   .999 99 99 99 999 -99 999 999 99 START .10 SOLID

G 5 SupportFace DACBa0 NO  In-Out ALT -22 -22 .005 .000 .050 LIGHT-GREEN 0 0.0 \
.028  OFF    .999 99 99 99 999 -99 999 999 99 FORW  .10 SOLID \
.028  OFF    .999 99 99 99 999 -99 999 999 99 START .10 SOLID \
.028  .000   .999 99 99 99 999 -99 999 999 99 FORW  .10 SOLID YESA \
.028  .000   .999 99 99 99 999 -99 999 999 99 START .10 SOLID
```

```
G 6 Support  DACBa0 NO  In-Out ALT  68  68 .005 .000 .050 LIGHT-YELLOW 0 0.0 \
.028  OFF    .999 99 99 99 999 -99 999 999 99 FORW  .10 SOLID \
.028  OFF    .999 99 99 99 999 -99 999 999 99 START .10 SOLID \
.028  .035   .999 99 99 99 999 -99 999 999 99 FORW  .10 SOLID YESA \
.028  .000   .999 99 99 99 999 -99 999 999 99 START .10 SOLID

G 7 SupportFast DACBa1 NO  In-Out ALT -22 -22 .005 .000 .050 DARK-GRAY 1 0.0 \
.028  OFF    .999 99 99 99 999 -99 999 999 99 FORW  .10 SOLID \
.028  OFF    .999 99 99 99 999 -99 999 999 99 START .10 SOLID \
.028  .250   .999 99 99 99 999 -99 999 999 99 FORW  .10 SOLID YESA \
.028  .000   .999 99 99 99 999 -99 999 999 99 START .10 SOLID

G 8 BaseTop  DACBa0 NO  In-Out ALT -32 -32 .000 .000 .050 BLUE 0 0.0 \
.028  OFF    .999 99 99 99 999 -99 999 999 99 FORW  .10 SOLID \
.028  OFF    .999 99 99 99 999 -99 999 999 99 START .10 SOLID \
.028  -.004  .999 99 99 99 999 -99 999 999 99 FORW  .10 SOLID YESA \
.028  .000   .999 99 99 99 999 -99 999 999 99 START .10 SOLID

G 9 BaseFast DACBa1 NO  In-Out ALT 68 68 .000 .000 .050 LIGHT-BLUE 0 0.0 \
.028  OFF    .999 99 99 99 999 -99 999 999 99 FORW  .10 SOLID \
.028  OFF    .999 99 99 99 999 -99 999 999 99 START .10 SOLID \
.028  .050   .999 99 99 99 999 -99 999 999 99 FORW  .10 SOLID YESA \
.028  .000   .999 99 99 99 999 -99 999 999 99 START .10 SOLID
# SET END ----------------------------------------------------------------#

# PDMM START -------------------------------------------------------------#

#------ CURVES -----------------------------------------------------------#
# Flow  D   Pre   Pre  Start Start Shut Roll
# Area  O   Delay Flow Flow  Dis.  Off  Back Speed
# xxxx  xxx .xxx  xxx  xxx   xxx   xxx  xxx  xxxxx

PDMM
   30   2   .065   47   13    50    15   139   800
   31   4   .066   47   13    50    16   139   800
   32   6   .067   47   13    50    17   139   800
   33   8   .068   47   13    50    18   139   800
   34  10   .069   47   15    50    19   139   800
   35  12   .070   47   15    50    20   139   800
   36  14   .071   47   15    50    21   139   800
   37  16   .072   47   15    50    22   139   800
   38  18   .073   47   17    50    23   139   800
   40  20   .074   47   17    50    24   139   800
   41  22   .075   47   17    50    25   139   800
   42  24   .076   47   17    50    26   139   800
   44  26   .077   47   17    50    27   141   800
   45  28   .078   47   17    50    28   141   800
   46  30   .079   47   17    50    29   141   800
   48  32   .080   47   19    50    30   141   800
   49  34   .081   47   19    50    31   141   800
   51  36   .082   47   19    50    32   141   800
   53  38   .083   47   19    50    33   143   800
   54  40   .084   47   19    50    34   143   800
   56  42   .085   47   19    50    35   143   800
   58  44   .086   47   19    50    36   143   800
   60  46   .087   47   19    50    37   143   800
   62  48   .088   47   21    50    38   143   800
   64  50   .089   47   21    50    39   145   800
   66  52   .090   47   21    50    40   145   800
   68  54   .091   47   21    50    41   145   800
   70  56   .092   47   21    50    42   145   800
   72  58   .093   47   21    50    43   145   800
   74  60   .094   47   21    50    44   145   800
   77  62   .095   47   21    50    45   147   800
   79  64   .096   47   21    50    46   147   800
   82  66   .097   47   23    50    47   147   800
   85  68   .098   47   23    50    48   147   800
   87  70   .099   47   23    50    49   147   800
   90  72   .100   47   23    50    50   147   800
   93  74   .101   47   23    50    51   149   800
```

96	76	.102	47	25	50	52	149	800
99	78	.103	47	25	50	53	149	800
102	80	.104	47	25	50	54	149	800
106	82	.105	47	25	50	55	149	800
109	84	.106	47	25	50	56	149	800
113	86	.107	47	25	50	57	149	800
116	88	.108	47	25	50	58	151	800
120	90	.109	47	25	50	59	151	800
124	92	.110	47	25	50	60	151	800
128	94	.111	47	27	50	61	151	800
132	96	.112	47	27	50	62	151	800
136	98	.113	47	27	50	63	151	800
141	100	.114	47	27	50	64	151	800
146	102	.115	47	27	50	65	151	800
150	104	.116	47	27	50	66	153	800
155	106	.117	47	29	50	67	153	800
160	108	.118	47	29	50	68	153	800
166	110	.119	47	29	50	69	153	800
171	112	.120	47	29	50	70	153	800
177	114	.121	47	29	50	71	153	800
182	116	.122	47	29	50	72	153	800
188	118	.123	47	29	50	73	155	800
195	120	.124	47	29	50	74	155	800
201	122	.125	47	29	50	75	155	800
208	124	.126	47	29	50	75	155	800
214	126	.127	47	29	50	75	155	800
221	128	.128	47	31	50	75	155	800
229	130	.129	47	31	50	75	157	800
236	132	.130	47	31	50	75	157	800
244	134	.131	47	31	50	75	157	800
252	136	.131	47	33	50	75	159	800
260	138	.133	47	33	50	75	159	800
269	140	.136	47	33	50	77	159	800
277	142	.139	47	33	50	79	159	800
287	144	.143	47	33	50	81	161	800
296	146	.147	47	33	50	81	161	800
306	148	.151	47	33	50	83	161	800
316	150	.156	47	35	50	83	161	800
326	152	.162	47	35	50	83	163	800
337	154	.166	47	35	50	83	163	800
348	156	.172	47	37	50	83	163	800
359	158	.178	47	37	50	83	163	800
371	160	.182	47	37	50	83	165	800
383	162	.186	47	39	50	83	165	800
396	164	.190	47	39	50	83	165	800
409	166	.199	47	41	50	83	167	800
422	168	.208	47	41	50	83	167	800
436	170	.214	47	41	50	83	167	800
450	172	.220	47	43	50	83	169	800
465	174	.227	47	43	50	83	169	800
481	176	.233	47	45	50	83	169	800
496	178	.239	47	45	50	83	171	800
513	180	.246	47	45	50	83	171	800
530	182	.253	47	47	50	83	171	800
547	184	.260	47	47	50	83	173	800
565	186	.265	47	47	50	83	173	800
584	188	.270	47	49	50	83	173	800
603	190	.275	47	49	50	83	173	800
623	192	.280	47	49	50	83	175	800
643	194	.285	47	51	50	83	175	800
664	196	.290	47	51	50	83	175	800
686	198	.294	47	51	50	83	175	800
709	200	.298	47	51	50	83	177	800
732	202	.302	47	53	50	83	177	800
756	204	.306	47	53	50	83	177	800
781	206	.311	47	53	50	83	177	800
807	208	.316	47	53	50	83	179	800
833	210	.318	47	53	50	83	179	800
861	212	.321	47	55	50	83	179	800
889	214	.324	47	55	50	83	181	800

```
  918  216  .326   47   55    50    83   181   800
  949  218  .328   47   55    50    83   181   800
  980  220  .331   47   57    50    83   181   800
 1012  222  .333   47   57    50    83   183   800
 1046  224  .336   47   57    50    85   183   800
 1080  226  .338   47   59    50    85   185   800
 1116  228  .340   47   59    50    87   185   800
 1153  230  .342   47   59    50    87   185   800
 1191  232  .344   47   61    50    87   187   800
 1230  234  .346   47   61    50    89   187   800
 1270  236  .348   47   63    50    89   189   800
 1312  238  .351   47   63    50    90   189   800
 1356  240  .353   47   65    50    91   191   800
 1400  242  .356   47   67    50    92   193   800
 1446  244  .359   47   69    50    94   195   800
 1494  246  .361   47   71    50    95   197   800
 1543  248  .364   47   73    50    97   199   800
 1594  250  .375   47   75    50    98   201   800
 1647  252  .380   47   77    50    99   203   800
 1701  254  .385   47   79    50   100   205   800
END PDMM
# PDMM END ------------------------------------------------------------------#
```

MAKEFILE : Compiles and links all programs

```
DIR2        = /usr/lpp/xlC/include
DIR3        = /usr/include
CFLAGS      = -I$(DIR2) -I$(DIR3) -g
LIBRARIES   = -lm
OBJECTS     = gen3.o
CC          = xlC

main: $(OBJECTS)
        $(CC) -o main $(OBJECTS) $(LIBRARIES)

.C.o:
        $(CC) $(CFLAGS) -c $<
```

t12_2plaq.sml : File containing directions for building the base

```
###
###
# HEADER #               ### BEGIN FIRST SLICE ###
# Z = 0.0090 S = 0.00900 ### NEW Z-LEVEL ###
# tip 12 mil ; one plaque
###
###
MZ52; # up off deck
XD131; # alt-tip on
PD.1,79;MM;MM0,19;MM60,146;MM-68,167;SR500;AC5;XD210;AS1;VM4;BC; # purge flow values
MR-250,0;MR250,0;EC;VM3;#purging of material
XD121;#Tip wipe
MA3146,64;#move to start
#MZ20;#new layer
MZ-52;#down to deck
# object 0 - Raster Fill - alt mat on - road width: 0.0200
PD.118,79;MM;MM0,25;MM60,122;MM-70,175;SR800;AC5;WA0.;#ORD:31 Z:0.0090 S:0.0090# support flow
values
AS1;#
VM4;#start flow
BC;#begin flow commands
MA3146,64;
MA3168,117;
MA3168,306;
MA3067,58;
MA2991,58;
MA3146,440;
MA3137,444;
MA3125,446;
MA3072,446;
MA2915,58;
MA2839,58;
MA2996,446;
MA2920,446;
MA2763,58;
MA2687,58;
MA2844,446;
MA2768,446;
MA2611,58;
MA2535,58;
MA2692,446;
MA2615,446;
MA2459,58;
MA2383,58;
MA2539,446;
MA2463,446;
MA2306,58;
MA2230,58;
MA2387,446;
MA2311,446;
MA2154,58;
MA2078,58;
MA2235,446;
MA2159,446;
MA2002,58;
MA1926,58;
MA2083,446;
MA2007,446;
MA1850,58;
MA1774,58;
MA1931,446;
MA1854,446;
MA1698,58;
MA1622,58;
MA1778,446;
MA1702,446;
MA1545,58;
```

```
MA1469,58;
MA1626,446;
MA1550,446;
MA1393,58;
MA1317,58;
MA1474,446;
MA1398,446;
MA1241,58;
MA1165,58;
MA1322,446;
MA1246,446;
MA1089,58;
MA1013,58;
MA1170,446;
MA1093,446;
MA937,58;
MA861,58;
MA1017,446;
MA941,446;
MA784,58;
MA708,58;
MA865,446;
MA789,446;
MA632,58;
MA556,58;
MA713,446;
MA637,446;
MA480,58;
MA404,58;
MA561,446;
MA485,446;
MA328,58;
MA252,58;
MA408,446;
MA332,446;
MA176,58;
MA100,58;
MA256,446;
MA180,446;
MA58,144;
MA58,332;
MA104,446;
EC;VM3;#end movement and end flow
XD209;#lock panel end flow locate position unlock panel
MA142,539;#break line
# Z = 0.0190 S = 0.01900 ### NEW Z-LEVEL ###
MZ52;# up off deck
MA3146,64;# new location
MZ20;#next layer
MZ-52;# down on deck
# object 0 - Raster Fill - alt mat on - road width: 0.0200
PD.118,79;MM;MM0,25;MM60,122;MM-70,175;SR800;AC5;WA0.;#ORD:31 Z:0.0190 S:0.0190# flow values
AS1;VM4;BC;#start flow
MA3146,64;
MA3168,117;
MA3168,306;
MA3067,58;
MA2991,58;
MA3146,440;
MA3137,444;
MA3125,446;
MA3072,446;
MA2915,58;
MA2839,58;
MA2996,446;
MA2920,446;
MA2763,58;
MA2687,58;
MA2844,446;
MA2768,446;
```

```
MA2611,58;
MA2535,58;
MA2692,446;
MA2615,446;
MA2459,58;
MA2383,58;
MA2539,446;
MA2463,446;
MA2306,58;
MA2230,58;
MA2387,446;
MA2311,446;
MA2154,58;
MA2078,58;
MA2235,446;
MA2159,446;
MA2002,58;
MA1926,58;
MA2083,446;
MA2007,446;
MA1850,58;
MA1774,58;
MA1931,446;
MA1854,446;
MA1698,58;
MA1622,58;
MA1778,446;
MA1702,446;
MA1545,58;
MA1469,58;
MA1626,446;
MA1550,446;
MA1393,58;
MA1317,58;
MA1474,446;
MA1398,446;
MA1241,58;
MA1165,58;
MA1322,446;
MA1246,446;
MA1089,58;
MA1013,58;
MA1170,446;
MA1093,446;
MA937,58;
MA861,58;
MA1017,446;
MA941,446;
MA784,58;
MA708,58;
MA865,446;
MA789,446;
MA632,58;
MA556,58;
MA713,446;
MA637,446;
MA480,58;
MA404,58;
MA561,446;
MA485,446;
MA328,58;
MA252,58;
MA408,446;
MA332,446;
MA176,58;
MA100,58;
MA256,446;
MA180,446;
MA58,144;
MA58,332;
```

```
MA104,446;
EC;VM3;#end flow
XD209;# capture postion
MA142,539;#break line
# Z = 0.0290 S = 0.02900 ### NEW Z-LEVEL ###
MZ52;#up off deck
XD121;#TW
MA3146,64;#new start position
MZ20;#next layer
MZ-52;#down on deck
# object 0 - Raster Fill - alt mat on - road width: 0.0200
PD.118,79;MM;MM0,25;MM60,122;MM-70,175;SR800;AC5;WA0.;#ORD:31 Z:0.0290 S:0.0290
AS1;VM4;BC;#begin flow
MA3146,64;
MA3168,117;
MA3168,306;
MA3067,58;
MA2991,58;
MA3146,440;
MA3137,444;
MA3125,446;
MA3072,446;
MA2915,58;
MA2839,58;
MA2996,446;
MA2920,446;
MA2763,58;
MA2687,58;
MA2844,446;
MA2768,446;
MA2611,58;
MA2535,58;
MA2692,446;
MA2615,446;
MA2459,58;
MA2383,58;
MA2539,446;
MA2463,446;
MA2306,58;
MA2230,58;
MA2387,446;
MA2311,446;
MA2154,58;
MA2078,58;
MA2235,446;
MA2159,446;
MA2002,58;
MA1926,58;
MA2083,446;
MA2007,446;
MA1850,58;
MA1774,58;
MA1931,446;
MA1854,446;
MA1698,58;
MA1622,58;
MA1778,446;
MA1702,446;
MA1545,58;
MA1469,58;
MA1626,446;
MA1550,446;
MA1393,58;
MA1317,58;
MA1474,446;
MA1398,446;
MA1241,58;
MA1165,58;
MA1322,446;
MA1246,446;
```

```
MA1089,58;
MA1013,58;
MA1170,446;
MA1093,446;
MA937,58;
MA861,58;
MA1017,446;
MA941,446;
MA784,58;
MA708,58;
MA865,446;
MA789,446;
MA632,58;
MA556,58;
MA713,446;
MA637,446;
MA480,58;
MA404,58;
MA561,446;
MA485,446;
MA328,58;
MA252,58;
MA408,446;
MA332,446;
MA176,58;
MA100,58;
MA256,446;
MA180,446;
MA58,144;
MA58,332;
MA104,446;
EC;VM3;#end flow
XD209;#capture position
MA142,539;#break line
# Z = 0.0390 S = 0.03900 ### NEW Z-LEVEL ###
MZ52;#up off deck
MA3146,64;#new start position
MZ20;#next layer
MZ-52;#down on deck
# object 0 - Raster Fill - alt mat on - road width: 0.0200
PD.118,79;MM;MM0,25;MM60,122;MM-70,175;SR800;AC5;WA0.;#ORD:31 Z:0.0390 S:0.0390
AS1;VM4;BC;# start flow
MA3146,64;
MA3168,117;
MA3168,306;
MA3067,58;
MA2991,58;
MA3146,440;
MA3137,444;
MA3125,446;
MA3072,446;
MA2915,58;
MA2839,58;
MA2996,446;
MA2920,446;
MA2763,58;
MA2687,58;
MA2844,446;
MA2768,446;
MA2611,58;
MA2535,58;
MA2692,446;
MA2615,446;
MA2459,58;
MA2383,58;
MA2539,446;
MA2463,446;
MA2306,58;
MA2230,58;
MA2387,446;
```

```
MA2311,446;
MA2154,58;
MA2078,58;
MA2235,446;
MA2159,446;
MA2002,58;
MA1926,58;
MA2083,446;
MA2007,446;
MA1850,58;
MA1774,58;
MA1931,446;
MA1854,446;
MA1698,58;
MA1622,58;
MA1778,446;
MA1702,446;
MA1545,58;
MA1469,58;
MA1626,446;
MA1550,446;
MA1393,58;
MA1317,58;
MA1474,446;
MA1398,446;
MA1241,58;
MA1165,58;
MA1322,446;
MA1246,446;
MA1089,58;
MA1013,58;
MA1170,446;
MA1093,446;
MA937,58;
MA861,58;
MA1017,446;
MA941,446;
MA784,58;
MA708,58;
MA865,446;
MA789,446;
MA632,58;
MA556,58;
MA713,446;
MA637,446;
MA480,58;
MA404,58;
MA561,446;
MA485,446;
MA328,58;
MA252,58;
MA408,446;
MA332,446;
MA176,58;
MA100,58;
MA256,446;
MA180,446;
MA58,144;
MA58,332;
MA104,446;
EC;VM3;#end flow
XD209;#capture postion
MA142,539;#break line
# Z = 0.0490 S = 0.04900 ### NEW Z-LEVEL ###
MZ52;# up off deck
XD121;#TW
MA59,97;#new start postion
MZ20;# next layer
MZ-52;# down on deck
# object 0 - Raster Fill - alt mat on - road width: 0.0200
```

```
PD.118,79;MM;MM0,25;MM60,122;MM-70,175;SR800;AC5;WA0.;#ORD:27 Z:0.0490 S:0.0490
AS1;VM4;BC;# start flow
MA59,97;
MA120,58;
MA151,58;
MA58,116;
MA58,135;
MA181,58;
MA211,58;
MA58,154;
MA58,173;
MA242,58;
MA272,58;
MA58,192;
MA58,211;
MA303,58;
MA333,58;
MA58,230;
MA58,249;
MA364,58;
MA394,58;
MA58,268;
MA58,287;
MA424,58;
MA455,58;
MA58,306;
MA58,325;
MA485,58;
MA516,58;
MA58,344;
MA58,363;
MA546,58;
MA577,58;
MA58,382;
MA58,401;
MA607,58
MA638,58;
MA61,418;
MA64,425;
MA70,432;
MA668,58;
MA698,58;
MA84,442;
MA91,445;
MA102,446;
MA108,446;
MA729,58;
MA759,58;
MA138,446;
MA169,446;
MA790,58;
MA820,58;
MA199,446;
MA230,446;
MA851,58;
MA881,58;
MA260,446;
MA291,446;
MA911,58;
MA942,58;
MA321,446;
MA351,446;
MA972,58;
MA1003,58;
MA382,446;
MA412,446;
MA1033,58;
MA1064,58;
MA443,446;
MA473,446;
```

```
MA1094,58;
MA1125,58;
MA504,446;
MA534,446;
MA1155,58;
MA1185,58;
MA565,446;
MA595,446;
MA1216,58;
MA1246,58;
MA625,446;
MA656,446;
MA1277,58;
MA1307,58;
MA686,446
MA717,446;
MA1338,58;
MA1368,58;
MA747,446;
MA778,446;
MA1398,58;
MA1429,58;
MA808,446;
MA838,446;
MA1459,58;
MA1490,58;
MA869,446;
MA899,446;
MA1520,58;
MA1551,58;
MA930,446;
MA960,446;
MA1581,58;
MA1611,58;
MA991,446;
MA1021,446;
MA1642,58;
MA1672,58;
MA1051,446;
MA1082,446;
MA1703,58;
MA1733,58;
MA1112,446;
MA1143,446;
MA1764,58;
MA1794,58;
MA1173,446;
MA1204,446;
MA1825,58;
MA1855,58;
MA1234,446;
MA1265,446;
MA1885,58;
MA1916,58;
MA1295,446;
MA1325,446;
MA1946,58;
MA1977,58;
MA1356,446;
MA1386,446;
MA2007,58;
MA2038,58;
MA1417,446;
MA1447,446;
MA2068,58;
MA2098,58;
MA1478,446;
MA1508,446;
MA2129,58;
MA2159,58;
```

```
MA1538,446;
MA1569,446;
MA2190,58;
MA2220,58;
MA1599,446;
MA1630,446;
MA2251,58;
MA2281,58;
MA1660,446;
MA1691,446;
MA2312,58;
MA2342,58;
MA1721,446;
MA1752,446;
MA2372,58;
MA2403,58;
MA1782,446;
MA1812,446;
MA2433,58;
MA2464,58;
MA1843,446;
MA1873,446;
MA2494,58;
MA2525,58;
MA1904,446;
MA1934,446;
MA2555,58;
MA2585,58;
MA1965,446;
MA1995,446;
MA2616,58;
MA2646,58;
MA2025,446;
MA2056,446;
MA2677,58;
MA2707,58;
MA2086,446;
MA2117,446;
MA2738,58;
MA2768,58;
EC;VM3;WA2;  # Curve Length Breakup end flow
PD.118,79;MM;MM0,25;MM60,122;MM-70,175;SR800;AC5;WA0.;#ORD:27 Z:0.0490 S:0.0490
AS1;VM4;BC; #restart flow
MA2768,58;
MA2147,446;
MA2178,446;
MA2798,58;
MA2829,58;
MA2208,446;
MA2238,446;
MA2859,58;
MA2890,58;
MA2269,446;
MA2299,446;
MA2920,58;
MA2951,58;
MA2330,446;
MA2360,446;
MA2981,58;
MA3012,58;
MA2391,446;
MA2421,446;
MA3042,58;
MA3072,58;
MA2452,446;
MA2482,446;
MA3103,58;
MA3124,58;
MA3132,59;
MA2512,446;
```

```
MA2543,446;
MA3150,67;
MA3154,70;
MA3161,78;
MA2573,446;
MA2604,446;
MA3167,94;
MA3168,101;
MA3168,113;
MA2634,446;
MA2665,446;
MA3168,132;
MA3168,151;
MA2695,446;
MA2725,446;
MA3168,170;
MA3168,189;
MA2756,446;
MA2786,446;
MA3168,208;
MA3168,227;
MA2817,446;
MA2847,446;
MA3168,246;
MA3168,265;
MA2878,446;
MA2908,446;
MA3168,284;
MA3168,303;
MA2939,446;
MA2969,446;
MA3168,322;
MA3168,341;
MA2999,446;
MA3030,446;
MA3168,360;
MA3168,379;
MA3060,446;
MA3091,446;
MA3168,398;
MA3168,402;
MA3166,413;
MA3164,419;
MA3121,446;
EC;VM3;# end flow
XD209;#capture postion
MA142,539;#break line
# Z = 0.0490 S = 0.04900 ### NEW Z-LEVEL ###
MZ52;# up off deck
XD121;#TW
MA59,97;#new start postion
MZ20;# next layer
MZ-52;# down on deck
# object 0 - Raster Fill - alt mat on - road width: 0.0200
PD.118,79;MM;MM0,25;MM60,122;MM-70,175;SR800;AC5;WA0.;#ORD:27 Z:0.0490 S:0.0490
AS1;VM4;BC;# start flow
MA59,97;
MA120,58;
MA151,58;
MA58,116;
MA58,135;
MA181,58;
MA211,58;
MA58,154;
MA58,173;
MA242,58;
MA272,58;
MA58,192;
MA58,211;
MA303,58;
```

```
MA333,58;
MA58,230;
MA58,249;
MA364,58;
MA394,58;
MA58,268;
MA58,287;
MA424,58;
MA455,58;
MA58,306;
MA58,325;
MA485,58;
MA516,58;
MA58,344;
MA58,363;
MA546,58;
MA577,58;
MA58,382;
MA58,401;
MA607,58;
MA638,58;
MA61,418;
MA64,425;
MA70,432;
MA668,58;
MA698,58;
MA84,442;
MA91,445;
MA102,446;
MA108,446;
MA729,58;
MA759,58;
MA138,446;
MA169,446;
MA790,58;
MA820,58;
MA199,446;
MA230,446;
MA851,58;
MA881,58;
MA260,446;
MA291,446;
MA911,58;
MA942,58;
MA321,446;
MA351,446;
MA972,58;
MA1003,58;
MA382,446;
MA412,446;
MA1033,58;
MA1064,58;
MA443,446;
MA473,446;
MA1094,58;
MA1125,58;
MA504,446;
MA534,446;
MA1155,58;
MA1185,58;
MA565,446;
MA595,446;
MA1216,58;
MA1246,58;
MA625,446;
MA656,446;
MA1277,58;
MA1307,58;
MA686,446;
MA717,446;
```

```
MA1338,58;
MA1368,58;
MA747,446;
MA778,446;
MA1398,58;
MA1429,58;
MA808,446;
MA838,446;
MA1459,58;
MA1490,58;
MA869,446;
MA899,446;
MA1520,58;
MA1551,58;
MA930,446;
MA960,446;
MA1581,58;
MA1611,58;
MA991,446;
MA1021,446;
MA1642,58;
MA1672,58;
MA1051,446;
MA1082,446;
MA1703,58;
MA1733,58;
MA1112,446;
MA1143,446;
MA1764,58;
MA1794,58;
MA1173,446;
MA1204,446;
MA1825,58;
MA1855,58;
MA1234,446;
MA1265,446;
MA1885,58;
MA1916,58;
MA1295,446;
MA1325,446;
MA1946,58;
MA1977,58;
MA1356,446;
MA1386,446;
MA2007,58;
MA2038,58;
MA1417,446;
MA1447,446;
MA2068,58;
MA2098,58;
MA1478,446;
MA1508,446;
MA2129,58;
MA2159,58;
MA1538,446;
MA1569,446;
MA2190,58;
MA2220,58;
MA1599,446;
MA1630,446;
MA2251,58;
MA2281,58;
MA1660,446;
MA1691,446;
MA2312,58;
MA2342,58;
MA1721,446;
MA1752,446;
MA2372,58;
MA2403,58;
```

```
MA1782,446;
MA1812,446;
MA2433,58;
MA2464,58;
MA1843,446;
MA1873,446;
MA2494,58;
MA2525,58;
MA1904,446;
MA1934,446;
MA2555,58;
MA2585,58;
MA1965,446;
MA1995,446;
MA2616,58;
MA2646,58;
MA2025,446;
MA2056,446;
MA2677,58;
MA2707,58;
MA2086,446;
MA2117,446;
MA2738,58;
MA2768,58;
EC;VM3;WA2;  # Curve Length Breakup end flow
PD.118,79;MM;MM0,25;MM60,122;MM-70,175;SR800;AC5;WA0.;#ORD:27 Z:0.0490 S:0.0490
AS1;VM4;BC; #restart flow
MA2768,58;
MA2147,446;
MA2178,446;
MA2798,58;
MA2829,58;
MA2208,446;
MA2238,446;
MA2859,58;
MA2890,58;
MA2269,446;
MA2299,446;
MA2920,58;
MA2951,58;
MA2330,446;
MA2360,446;
MA2981,58;
MA3012,58;
MA2391,446;
MA2421,446;
MA3042,58;
MA3072,58;
MA2452,446;
MA2482,446;
MA3103,58;
MA3124,58;
MA3132,59;
MA2512,446;
MA2543,446;
MA3150,67;
MA3154,70;
MA3161,78;
MA2573,446;
MA2604,446;
MA3167,94;
MA3168,101;
MA3168,113;
MA2634,446;
MA2665,446;
MA3168,132;
MA3168,151;
MA2695,446;
MA2725,446;
MA3168,170;
```

```
MA3168,189;
MA2756,446;
MA2786,446;
MA3168,208;
MA3168,227;
MA2817,446;
MA2847,446;
MA3168,246;
MA3168,265;
MA2878,446;
MA2908,446;
MA3168,284;
MA3168,303;
MA2939,446;
MA2969,446;
MA3168,322;
MA3168,341;
MA2999,446;
MA3030,446;
MA3168,360;
MA3168,379;
MA3060,446;
MA3091,446;
MA3168,398;
MA3168,402;
MA3166,413;
MA3164,419;
MA3121,446;
EC;VM3;# end flow
XD209;#capture postion
MA3036,500;# break line
##
#end of support
##
XD129; # alt-tip off
PD.1,79;MM;MM0,19;MM60,250;MM-68,167;SR500;AC5;XD210;AS1;VM4;BC; # purge
MR-1750,0;MR1750,0;
MR-1750,0;MR1750,0;
MR-1750,0;MR1750,0;
MR-1750,0;MR1750,0;
#MR-1750,0;MR1750,0;
#MR-1750,0;MR1750,0;
#MR-1750,0;MR1750,0;
#MR-1750,0;MR1750,0;
#MR-1750,0;MR1750,0;
#MR-1750,0;MR1750,0;
#MR-1750,0;MR1750,0;
#MR-1750,0;MR1750,0;

EC;VM3;
XD121;#TW
XD131; #alt-tip on
##
#end of purge of support
##
```

.sml file : sample file generated by the C++ code

```
 .K;;;; .J;;;;; .R
 .I;;17
 .N10;19
 .M10;;;;;
 .E;;;;;;
# Date           : 09/28/96   23:32:29
# File           : /usr2/research/chem/rogray/plaq/plaq3.sml
# QuickSlice     : 2.0a 03-Apr-96 (qsqk) ----------------- units = inch
# Modeler        : FDM1600
# Material       : ABS_P400 and PP VA microcomposites
IN;
CD129;WA1;CD0; # alt-tip off, enable operator alt mat change
# CF;
# VC100;OF;
# V*100,1.;#Xshrinkage
# V*101,1.;#Yshrinkage
# CF@100,@101;
# CZ100;
MZ1200;
FH;XD210;FZ;
MZ1200;
MA1200,500;    # take this out if restarting a model
# MA@102,@103; # put this in if restarting a model
XD121;#TW
#
# The toolpath units are in inches.
# ORD HEADER # normal
# ORD list is all possible curve types, whether used or not.
#                                                 Wait (once per Z, next Z)
#       Pre                 Main  Shut Roll        |
#       Delay  Start-flow    Flow   off back Speed  |     Setname, Type
#         |    |         |       |     |  |     |    |
#ORD: 1 PD.118,79;MM;MM0,25;MM60,122;MM-70,175;SR800;AC5;WA0.;#DEFAULT,Open
# height = 80  all values are in mils
# width  = 300
# length = 3000
# road_height = 10
# road_width = 30
# start_XX = 100
# start_YY = 100
# num_of_plaques = 8
# lay_pattern  = 1
# parameter_string = PD.151,47;MM;MM0,33;MM50,172;MM-83,161;SR800;AC5;WA0.;#ORD:34 Z:0.0400
S:0.0400

# my_file = ma40a.sml
# my_support = t12_1plaq.sml
# road width max 60 mil min 30 mil for 25 mil tip:height 10 mil
# road width max 30 mil min 12 mil for 12 mil tip:height 10 mil
MZ0;    # FOAM HEIGHT FACTOR HERE
PS;WA0;VC102;OA;SO@102,@103;VC104;OZ;MR0,0;
VS110,@102;VS111,@103;VS112,@104;
V+110,@121;V+111,@122;
AM0;
########## MATERIAL INITIALIZATION
CD129;WA1; # alt-tip off
CD135; # RB RNG ABS
###
###
# HEADER #               ### BEGIN FIRST SLICE ###
# Z = 0.0090 S = 0.00900 ### NEW Z-LEVEL ###
# tip 12 mil ; one plaque
###
###
MZ52; # up off deck
XD131; # alt-tip on
PD.1,79;MM;MM0,19;MM60,146;MM-68,167;SR500;AC5;XD210;AS1;VM4;BC; # purge flow values
```

```
MR-250,0;MR250,0;EC;VM3;#purging of material
XD121;#Tip wipe
MA3146,64;#move to start
MZ20;#new layer
MZ-52;#down to deck
# object 0 - Raster Fill - alt mat on - road width: 0.0200
PD.118,79;MM;MM0,25;MM60,122;MM-70,175;SR800;AC5;WA0.;#ORD:31 Z:0.0090 S:0.0090# support flow
values
AS1;#
VM4;#start flow
BC;#begin flow commands
MA3146,64;
MA3168,117;
MA3168,306;
MA3067,58;
MA2991,58;
MA3146,440;
MA3137,444;
MA3125,446;
MA3072,446;
MA2915,58;
MA2839,58;
MA2996,446;
MA2920,446;
MA2763,58;
MA2687,58;
MA2844,446;
MA2768,446;
MA2611,58;
MA2535,58;
MA2692,446;
MA2615,446;
MA2459,58;
MA2383,58;
MA2539,446;
MA2463,446;
MA2306,58;
MA2230,58;
MA2387,446;
MA2311,446;
MA2154,58;
MA2078,58;
MA2235,446;
MA2159,446;
MA2002,58;
MA1926,58;
MA2083,446;
MA2007,446;
MA1850,58;
MA1774,58;
MA1931,446;
MA1854,446;
MA1698,58;
MA1622,58;
MA1778,446;
MA1702,446;
MA1545,58;
MA1469,58;
MA1626,446;
MA1550,446;
MA1393,58;
MA1317,58;
MA1474,446;
MA1398,446;
MA1241,58;
MA1165,58;
MA1322,446;
MA1246,446;
MA1089,58;
MA1013,58;
```

```
MA1170,446;
MA1093,446;
MA937,58;
MA861,58;
MA1017,446;
MA941,446;
MA784,58;
MA708,58;
MA865,446;
MA789,446;
MA632,58;
MA556,58;
MA713,446;
MA637,446;
MA480,58;
MA404,58;
MA561,446;
MA485,446;
MA328,58;
MA252,58;
MA408,446;
MA332,446;
MA176,58;
MA100,58;
MA256,446;
MA180,446;
MA58,144;
MA58,332;
MA104,446;
EC;VM3;#end movement and end flow
XD209;#lock panel end flow locate position unlock panel
MA142,539;#break line
# Z = 0.0190 S = 0.01900 ### NEW Z-LEVEL ###
MZ52;# up off deck
MA3146,64;# new location
MZ20;#next layer
MZ-52;# down on deck
# object 0 - Raster Fill - alt mat on - road width: 0.0200
PD.118,79;MM;MM0,25;MM60,122;MM-70,175;SR800;AC5;WA0.;#ORD:31 Z:0.0190 S:0.0190# flow values
AS1;VM4;BC;#start flow
MA3146,64;
MA3168,117;
MA3168,306;
MA3067,58;
MA2991,58;
MA3146,440;
MA3137,444;
MA3125,446;
MA3072,446;
MA2915,58;
MA2839,58;
MA2996,446;
MA2920,446;
MA2763,58;
MA2687,58;
MA2844,446;
MA2768,446;
MA2611,58;
MA2535,58;
MA2692,446;
MA2615,446;
MA2459,58;
MA2383,58;
MA2539,446;
MA2463,446;
MA2306,58;
MA2230,58;
MA2387,446;
MA2311,446;
MA2154,58;
```

```
MA2078,58;
MA2235,446;
MA2159,446;
MA2002,58;
MA1926,58;
MA2083,446;
MA2007,446;
MA1850,58;
MA1774,58;
MA1931,446;
MA1854,446;
MA1698,58;
MA1622,58;
MA1778,446;
MA1702,446;
MA1545,58;
MA1469,58;
MA1626,446;
MA1550,446;
MA1393,58;
MA1317,58;
MA1474,446;
MA1398,446;
MA1241,58;
MA1165,58;
MA1322,446;
MA1246,446;
MA1089,58;
MA1013,58;
MA1170,446;
MA1093,446;
MA937,58;
MA861,58;
MA1017,446;
MA941,446;
MA784,58;
MA708,58;
MA865,446;
MA789,446;
MA632,58;
MA556,58;
MA713,446;
MA637,446;
MA480,58;
MA404,58;
MA561,446;
MA485,446;
MA328,58;
MA252,58;
MA408,446;
MA332,446;
MA176,58;
MA100,58;
MA256,446;
MA180,446;
MA58,144;
MA58,332;
MA104,446;
EC;VM3;#end flow
XD209;# capture postion
MA142,539;#break line
# Z = 0.0290 S = 0.02900 ### NEW Z-LEVEL ###
MZ52;#up off deck
XD121;#TW
MA3146,64;#new start position
MZ20;#next layer
MZ-52;#down on deck
# object 0 - Raster Fill - alt mat on - road width: 0.0200
PD.118,79;MM;MM0,25;MM60,122;MM-70,175;SR800;AC5;WA0.;#ORD:31 Z:0.0290 S:0.0290
AS1;VM4;BC;#begin flow
```

MA3146,64;
MA3168,117;
MA3168,306;
MA3067,58;
MA2991,58;
MA3146,440;
MA3137,444;
MA3125,446;
MA3072,446;
MA2915,58;
MA2839,58;
MA2996,446;
MA2920,446;
MA2763,58;
MA2687,58;
MA2844,446;
MA2768,446;
MA2611,58;
MA2535,58;
MA2692,446;
MA2615,446;
MA2459,58;
MA2383,58;
MA2539,446;
MA2463,446;
MA2306,58;
MA2230,58;
MA2387,446;
MA2311,446;
MA2154,58;
MA2078,58;
MA2235,446;
MA2159,446;
MA2002,58;
MA1926,58;
MA2083,446;
MA2007,446;
MA1850,58;
MA1774,58;
MA1931,446;
MA1854,446;
MA1698,58;
MA1622,58;
MA1778,446;
MA1702,446;
MA1545,58;
MA1469,58;
MA1626,446;
MA1550,446;
MA1393,58;
MA1317,58;
MA1474,446;
MA1398,446;
MA1241,58;
MA1165,58;
MA1322,446;
MA1246,446;
MA1089,58;
MA1013,58;
MA1170,446;
MA1093,446;
MA937,58;
MA861,58;
MA1017,446;
MA941,446;
MA784,58;
MA708,58;
MA865,446;
MA789,446;
MA632,58;

```
MA556,58;
MA713,446;
MA637,446;
MA480,58;
MA404,58;
MA561,446;
MA485,446;
MA328,58;
MA252,58;
MA408,446;
MA332,446;
MA176,58;
MA100,58;
MA256,446;
MA180,446;
MA58,144;
MA58,332;
MA104,446;
EC;VM3;#end flow
XD209;#capture position
MA142,539;#break line
# Z = 0.0390 S = 0.03900 ### NEW Z-LEVEL ###
MZ52;#up off deck
MA3146,64;#new start position
MZ20;#next layer
MZ-52;#down on deck
# object 0 - Raster Fill - alt mat on - road width: 0.0200
PD.118,79;MM;MM0,25;MM60,122;MM-70,175;SR800;AC5;WA0.;#ORD:31 Z:0.0390 S:0.0390
AS1;VM4;BC;# start flow
MA3146,64;
MA3168,117;
MA3168,306;
MA3067,58;
MA2991,58;
MA3146,440;
MA3137,444;
MA3125,446;
MA3072,446;
MA2915,58;
MA2839,58;
MA2996,446;
MA2920,446;
MA2763,58;
MA2687,58;
MA2844,446;
MA2768,446;
MA2611,58;
MA2535,58;
MA2692,446;
MA2615,446;
MA2459,58;
MA2383,58;
MA2539,446;
MA2463,446;
MA2306,58;
MA2230,58;
MA2387,446;
MA2311,446;
MA2154,58;
MA2078,58;
MA2235,446;
MA2159,446;
MA2002,58;
MA1926,58;
MA2083,446;
MA2007,446;
MA1850,58;
MA1774,58;
MA1931,446;
MA1854,446;
```

```
MA1698,58;
MA1622,58;
MA1778,446;
MA1702,446;
MA1545,58;
MA1469,58;
MA1626,446;
MA1550,446;
MA1393,58;
MA1317,58;
MA1474,446;
MA1398,446;
MA1241,58;
MA1165,58;
MA1322,446;
MA1246,446;
MA1089,58;
MA1013,58;
MA1170,446;
MA1093,446;
MA937,58;
MA861,58;
MA1017,446;
MA941,446;
MA784,58;
MA708,58;
MA865,446;
MA789,446;
MA632,58;
MA556,58;
MA713,446;
MA637,446;
MA480,58;
MA404,58;
MA561,446;
MA485,446;
MA328,58;
MA252,58;
MA408,446;
MA332,446;
MA176,58;
MA100,58;
MA256,446;
MA180,446;
MA58,144;
MA58,332;
MA104,446;
EC;VM3;#end flow
XD209;#capture postion
MA142,539;#break line
# Z = 0.0490 S = 0.04900 ### NEW Z-LEVEL ###
MZ52;# up off deck
XD121;#TW
MA59,97;#new start postion
MZ20;# next layer
MZ-52;# down on deck
# object 0 - Raster Fill - alt mat on - road width: 0.0200
PD.118,79;MM;MM0,25;MM60,122;MM-70,175;SR800;AC5;WA0.;#ORD:27 Z:0.0490 S:0.0490
AS1;VM4;BC;# start flow
MA59,97;
MA120,58;
MA151,58;
MA58,116;
MA58,135;
MA181,58;
MA211,58;
MA58,154;
MA58,173;
MA242,58;
MA272,58;
```

```
MA58,192;
MA58,211;
MA303,58;
MA333,58;
MA58,230;
MA58,249;
MA364,58;
MA394,58;
MA58,268;
MA58,287;
MA424,58;
MA455,58;
MA58,306;
MA58,325;
MA485,58;
MA516,58;
MA58,344;
MA58,363;
MA546,58;
MA577,58;
MA58,382;
MA58,401;
MA607,58;
MA638,58;
MA61,418;
MA64,425;
MA70,432;
MA668,58;
MA698,58;
MA84,442;
MA91,445;
MA102,446;
MA108,446;
MA729,58;
MA759,58;
MA138,446;
MA169,446;
MA790,58;
MA820,58;
MA199,446;
MA230,446;
MA851,58;
MA881,58;
MA260,446;
MA291,446;
MA911,58;
MA942,58;
MA321,446;
MA351,446;
MA972,58;
MA1003,58;
MA382,446;
MA412,446;
MA1033,58;
MA1064,58;
MA443,446;
MA473,446;
MA1094,58;
MA1125,58;
MA504,446;
MA534,446;
MA1155,58;
MA1185,58;
MA565,446;
MA595,446;
MA1216,58;
MA1246,58;
MA625,446;
MA656,446;
MA1277,58;
```

```
MA1307,58;
MA686,446;
MA717,446;
MA1338,58;
MA1368,58;
MA747,446;
MA778,446;
MA1398,58;
MA1429,58;
MA808,446;
MA838,446;
MA1459,58;
MA1490,58;
MA869,446;
MA899,446;
MA1520,58;
MA1551,58;
MA930,446;
MA960,446;
MA1581,58;
MA1611,58;
MA991,446;
MA1021,446;
MA1642,58;
MA1672,58;
MA1051,446;
MA1082,446;
MA1703,58;
MA1733,58;
MA1112,446;
MA1143,446;
MA1764,58;
MA1794,58;
MA1173,446;
MA1204,446;
MA1825,58;
MA1855,58;
MA1234,446;
MA1265,446;
MA1885,58;
MA1916,58;
MA1295,446;
MA1325,446;
MA1946,58;
MA1977,58;
MA1356,446;
MA1386,446;
MA2007,58;
MA2038,58;
MA1417,446;
MA1447,446;
MA2068,58;
MA2098,58;
MA1478,446;
MA1508,446;
MA2129,58;
MA2159,58;
MA1538,446;
MA1569,446;
MA2190,58;
MA2220,58;
MA1599,446;
MA1630,446;
MA2251,58;
MA2281,58;
MA1660,446;
MA1691,446;
MA2312,58;
MA2342,58;
MA1721,446;
```

```
MA1752,446;
MA2372,58;
MA2403,58;
MA1782,446;
MA1812,446;
MA2433,58;
MA2464,58;
MA1843,446;
MA1873,446;
MA2494,58;
MA2525,58;
MA1904,446;
MA1934,446;
MA2555,58;
MA2585,58;
MA1965,446;
MA1995,446;
MA2616,58;
MA2646,58;
MA2025,446;
MA2056,446;
MA2677,58;
MA2707,58;
MA2086,446;
MA2117,446;
MA2738,58;
MA2768,58;
EC;VM3;WA2;  # Curve Length Breakup end flow
PD.118,79;MM;MM0,25;MM60,122;MM-70,175;SR800;AC5;WA0.;#ORD:27 Z:0.0490 S:0.0490
AS1;VM4;BC; #restart flow
MA2768,58;
MA2147,446;
MA2178,446;
MA2798,58;
MA2829,58;
MA2208,446;
MA2238,446;
MA2859,58;
MA2890,58;
MA2269,446;
MA2299,446;
MA2920,58;
MA2951,58;
MA2330,446;
MA2360,446;
MA2981,58;
MA3012,58;
MA2391,446;
MA2421,446;
MA3042,58;
MA3072,58;
MA2452,446;
MA2482,446;
MA3103,58;
MA3124,58;
MA3132,59;
MA2512,446;
MA2543,446;
MA3150,67;
MA3154,70;
MA3161,78;
MA2573,446;
MA2604,446;
MA3167,94;
MA3168,101;
MA3168,113;
MA2634,446;
MA2665,446;
MA3168,132;
MA3168,151;
```

```
MA2695,446;
MA2725,446;
MA3168,170;
MA3168,189;
MA2756,446;
MA2786,446;
MA3168,208;
MA3168,227;
MA2817,446;
MA2847,446;
MA3168,246;
MA3168,265;
MA2878,446;
MA2908,446;
MA3168,284;
MA3168,303;
MA2939,446;
MA2969,446;
MA3168,322;
MA3168,341;
MA2999,446;
MA3030,446;
MA3168,360;
MA3168,379;
MA3060,446;
MA3091,446;
MA3168,398;
MA3168,402;
MA3166,413;
MA3164,419;
MA3121,446;
EC;VM3;# end flow
XD209;#capture postion
MA3036,500;# break line
##
#end of support
##
XD129; # alt-tip off
PD.1,79;MM;MM0,19;MM60,146;MM-68,167;SR500;AC5;XD210;AS1;VM4;BC; # purge
MR-1750,0;MR1750,0;
#MR-1750,0;MR1750,0;
#MR-1750,0;MR1750,0;
EC;VM3;
XD121;#TW
XD131; #alt-tip on
##
#end of purge of support
#########

## build material

#######


 XD129;  #alt-tip off
MA115,115;#start position
MZ20; #next layer
PD.151,47;MM;MM0,33;MM50,172;MM-83,161;SR800;AC5;WA0.;#ORD:34 Z:0.0400 S:0.0400
AS1;VM4;BC;#start flow  begin series of movements
MA115,115;
MA3085,115;
MA3085,145;
MA115,145;
MA115,175;
MA3085,175;
MA3085,205;
MA115,205;
MA115,235;
MA3085,235;
MA3085,265;
```

```
MA115,265;
MA115,295;
MA3085,295;
MA3085,325;
MA115,325;
MA115,355;
MA3085,355;
MA3085,385;
MA115,385;
EC; VM3;#end series of movements   end flow
XD209; # capture postion FC
MZ20;#next layer
PD.151,47;MM;MM0,33;MM50,172;MM-83,161;SR800;AC5;WA0.;#ORD:34 Z:0.0400 S:0.0400
AS1;VM4;BC;# start flow begin series of movements
MA115,385;
MA3085,385;
MA3085,355;
MA115,355;
MA115,325;
MA3085,325;
MA3085,295;
MA115,295;
MA115,265;
MA3085,265;
MA3085,235;
MA115,235;
MA115,205;
MA3085,205;
MA3085,175;
MA115,175;
MA115,145;
MA3085,145;
MA3085,115;
MA115,115;
EC; VM3;#end flow end series of movements
XD209; #capture postion FC
MZ20; #next layer
PD.151,47;MM;MM0,33;MM50,172;MM-83,161;SR800;AC5;WA0.;#ORD:34 Z:0.0400 S:0.0400
AS1;VM4;BC;#start flow  begin series of movements
MA115,115;
MA3085,115;
MA3085,145;
MA115,145;
MA115,175;
MA3085,175;
MA3085,205;
MA115,205;
MA115,235;
MA3085,235;
MA3085,265;
MA115,265;
MA115,295;
MA3085,295;
MA3085,325;
MA115,325;
MA115,355;
MA3085,355;
MA3085,385;
MA115,385;
EC; VM3;#end series of movements   end flow
XD209; # capture postion FC
MZ20;#next layer
PD.151,47;MM;MM0,33;MM50,172;MM-83,161;SR800;AC5;WA0.;#ORD:34 Z:0.0400 S:0.0400
AS1;VM4;BC;# start flow begin series of movements
MA115,385;
MA3085,385;
MA3085,355;
MA115,355;
MA115,325;
MA3085,325;
```

```
MA3085,295;
MA115,295;
MA115,265;
MA3085,265;
MA3085,235;
MA115,235;
MA115,205;
MA3085,205;
MA3085,175;
MA115,175;
MA115,145;
MA3085,145;
MA3085,115;
MA115,115;
EC; VM3;#end flow end series of movements
XD209; #capture postion FC
MZ20; #next layer
PD.151,47;MM;MM0,33;MM50,172;MM-83,161;SR800;AC5;WA0.;#ORD:34 Z:0.0400 S:0.0400
AS1;VM4;BC;#start flow  begin series of movements
MA115,115;
MA3085,115;
MA3085,145;
MA115,145;
MA115,175;
MA3085,175;
MA3085,205;
MA115,205;
MA115,235;
MA3085,235;
MA3085,265;
MA115,265;
MA115,295;
MA3085,295;
MA3085,325;
MA115,325;
MA115,355;
MA3085,355;
MA3085,385;
MA115,385;
EC; VM3;#end series of movements   end flow
XD209; # capture postion FC
MZ20;#next layer
PD.151,47;MM;MM0,33;MM50,172;MM-83,161;SR800;AC5;WA0.;#ORD:34 Z:0.0400 S:0.0400
AS1;VM4;BC;# start flow begin series of movements
MA115,385;
MA3085,385;
MA3085,355;
MA115,355;
MA115,325;
MA3085,325;
MA3085,295;
MA115,295;
MA115,265;
MA3085,265;
MA3085,235;
MA115,235;
MA115,205;
MA3085,205;
MA3085,175;
MA115,175;
MA115,145;
MA3085,145;
MA3085,115;
MA115,115;
EC; VM3;#end flow end series of movements
XD209; #capture postion FC
MZ20; #next layer
PD.151,47;MM;MM0,33;MM50,172;MM-83,161;SR800;AC5;WA0.;#ORD:34 Z:0.0400 S:0.0400
AS1;VM4;BC;#start flow  begin series of movements
MA115,115;
```

```
MA3085,115;
MA3085,145;
MA115,145;
MA115,175;
MA3085,175;
MA3085,205;
MA115,205;
MA115,235;
MA3085,235;
MA3085,265;
MA115,265;
MA115,295;
MA3085,295;
MA3085,325;
MA115,325;
MA115,355;
MA3085,355;
MA3085,385;
MA115,385;
EC; VM3;#end series of movements   end flow
XD209; # capture postion FC
MZ20;#next layer
PD.151,47;MM;MM0,33;MM50,172;MM-83,161;SR800;AC5;WA0.;#ORD:34 Z:0.0400 S:0.0400
AS1;VM4;BC;# start flow begin series of movements
MA115,385;
MA3085,385;
MA3085,355;
MA115,355;
MA115,325;
MA3085,325;
MA3085,295;
MA115,295;
MA115,265;
MA3085,265;
MA3085,235;
MA115,235;
MA115,205;
MA3085,205;
MA3085,175;
MA115,175;
MA115,145;
MA3085,145;
MA3085,115;
MA115,115;
EC; VM3;#end flow end series of movements
XD209; #capture postion FC
# TAIL #
VM7;
MZ20;
CD129;WA1;CD0; # alt-tip off
#
# dz=0.010 co=0.0060 dp=0.0010 ct=0.0006 alt=0 ff=0.1200 u=inch
#
XD211;
####.....................................................................
# Date           : 01/02/97
# File           : /usr2/research/chem/rogray/plaq/
# QuickSlice     : 2.0a 03-Apr-96 (qsqk)
# Modeler        : FDM1600
# Material       : ABS_P400 and vectra A / PP blends
# Shrinkage  XY  : 1.008
#             Z  : 1
# Applied        : yes
# Road width min :  inch
#            max :
# Tip            : 0.025
# Envelope    X  : 9.4 inch
#             Y  : 10
#             Z  : 10
# Wipe interval  : no wipe
```

```
#.................................................................
# Estimated values......
# Modeling time  :      hours    (approx)
# Filament usage :
#   main         :
#   support      :
####.............................................................
```

Vita

Robert W. Gray IV

The author was raised on a family farm in Waynesboro Virginia. Upon the completion of his secondary education, the author attended the Massachusetts Institute of Technology, where he was awarded a Bachelor of Science in Chemical Engineering in 1995. His undergraduate education was supplemented by several years of undergraduate research under the advisement of Professor R. E. Cohen. He then received a Master's of Science under the advisement of Prof. D. G. Baird at Virginia Polytechnic Institute and State University in 1997. He was offered and accepted a position at Du Pont.